Interactive comment on "Vertical distribution of chlorophyll in dynamically distinct regions of the southern Bay of Bengal" by Venugopal Thushara et al.

Reply to comments by Referee 1

(Referee's comments are given in blue and the response to comments are in black.)

Based on an observational campaign in the southern Bay of Bengal authors have tried to document the bio-physical interactions, particularly for the evolution of surface/subsurface chlorophyll blooms, in this region during the summer monsoon. They have also used an OGCM to explain the dynamical processes relating to the nitrate limitations for the chl concentration. Considering the data sparsity in the Bay of Bangal, particularly for the biogeochemical data, this manuscript certainly contributes to enhance the existing literature of this region. However, I often find statements made in this manuscript are not well supported by the figures. Below, I have listed some of them.

The referee has made a constructive review on the manuscript which has helped to improve the analysis and presentation of results. We thank the referee for the comments and we have addressed each of them below.

Also, I have serious doubt about the application of the model, particularly because spin-up time for the biogeochemical model is only 10 years, which is way too small for the nutrient levels to be stabilized. I believe, for such a basin scale TOPAZ, a minimum 30-50 years of spin-up is needed to stabilize the climatological nutrient levels, which will ultimately determine the surface chl concentration. Authors may plot the climatological simulation for the subsurface nitrate to see if that is stabilized. However, as this manuscript described the processes for a month long only and therefore, the results presented here might be unaffected by the slow drift in the nutrient levels of the model during the initial spin-up. But even then, a proper spin-up would be a good choice. Further, what about using open boundary conditions for the biogeochemical variables?

Thanks to the referee for the suggestion. The time evolution of biological variables obtained from the ecosystem model shows that the spin up period of 10 years is fairly sufficient to address the processes that we are curretly looking at. Time series of chlorophyll and nitrate at different depth ranges in the southern Bay of Bengal from the

model spin up is shown in Fig. R1. Chlorophyll and nutrient levels show a stable annual cycle after 5-7 years of the spin up. Any model drift in the deep ocean circulation or nutrients is unlikely to affect the upper ocean bloom dynamics in the given time scale of interest. For the biogeochemical variables, no-flux condition has been applied at the open boundaries in the south and east. Open boundaries in the present model configuration are away from the study region and these boundaries have little impact on the model results for the timescale of our interest.

Page15, line 7-10: "The hydrodynamics of the region suggests that the triggering mechanism for bloom generation is open ocean Ekman pumping forced by positive wind stress curl (Vinayachandran et al., 2004; Wijesekera et al., 2016a), favouring vertical transport of nutrients to the surface sunlit layers."

The authors relied too much on referencing. It is not difficult to calculate Ekman Pumping for the specific period. Authors are encouraged show that indeed the Ekman pumping is the primary driver. What about instability? This region exhibits one of the strongest barotropic/baroclinic instability of the north Indian Ocean.

Thanks to the referee for pointing out this. We agree with the referee's comment on processes other than Ekman pumping in controlling the bloom dynamics in the region of the Sri Lanka Dome (SLD). Ekman pumping was calculated using ASCAT winds as shown in Fig. R2. Time series over the location of SG579 shows upwelling tendencies during most of the observational period (Fig. R2a). Pumping velocities peaked to about 2-3 m day^{-1} by mid-June. Time series of minimum SLA shows that SLD attained its peak by the end of June (Fig. R2a), coinciding with the observed bloom at SG579. Ekman pumping remained to be upwelling favourable (0.4-0.7 m day^{-1}) during the period of surface bloom (30 June-02 July), though the magnitudes were relatively weaker. Strong upwelling in the second half of June, prior to the bloom event, is presumed to provide a favourable pre-conditioning by lifting the nitracline towards the surface. (This is explained below using the ecosystem model). Spatial distribution of mean Ekman pumping averaged for the BoBBLE observational period (24 June – 23 July) indicates widespread upwelling in the southern BoB (Fig. R2b).

During the decaying phase of the SLD in July, Ekman pumping velocities were positive, with peak values of about 2 m day^{-1} (Fig. R2a). This indicates that the influence of remote

effects propagating from the eastern boundary of the BoB were dominant during this period (Vinayachandran and Yamagata 1998; Shankar et al., 2002; Wijesekera et al. 2016; Burns et al., 2017; Webber et al., 2018). Time-longitude hovmoller diagram of SLA from AVISO during May-July along 8°N, between 80-100°E is shown in Fig. R3. The decay period of SLD coincides with the arrival of positive SLA anomalies from east, representing the westward propagation of downwelling Rossby waves (Webber et al., 2018). This shows that, despite the positive Ekman pumping, remote forcings from the east contributed to the weakening of the SLD. The dynamics of the BoB is also characterised by instability effects associated with barotropic and baroclinic energy conversions (Vinayachandran and Yamagata, 1998; Kurien et al., 2010; Cheng et al., 2017). A complete energy analysis to examine the role of instability is beyond the scope of this paper. As far as the surface bloom generation is concerned, the proximity of nutricline to the surface (as well as the light availability, which will be explained in the following sections) is of primary concern. Hence we relied on the ecosystem model to identify the dominant forcing controlling the vertical displacement of nitracline.

The modelled SLD peaked on 28 June, two days prior to the observed peak. The developing phase of the simulated SLD (14-28 July) was characterised by the shoaling of nitracline. The shoaling rate of nitracline increased to about 1.0 m day^{-1} by mid-June and closely followed the Ekman pumping velocities (Fig. R4). This shows that the vertical supply of nutrients to the surface layers during the developing phase of the SLD can be largely attributed to Ekman pumping. During the peak phase of the SLD, both Ekman pumping velocities and nitracline shoaling rates weakened. However, the larger shoaling rates during the preceeding week indicate a favourable pre-conditioning for bloom generation during the peak phase of the SLD. Later, during the decaying phase of the SLD in July, Ekman pumping gradually increased. However, the corresponding nitracline variability (with deepening tendencies) was not consistent with the pumping velocities, indicating the effect of remote forcings. These additional explanations will be added in Section 3.2.1 of the manuscript and Figures R2, R3 and R4 will be included.

Page 15, line no. 15: "The decay of surface bloom after 02 July (Fig. 5) followed the weakening of the dome (Fig. 3)." Not vary clear

Time series of minimum SLA in the region of the dome is shown in Fig. R2a. Sea level

anomalies decreased to about -0.3 m on 30 June. Intensification of the SLD coincided with the observed surface bloom at SG579. The dome weakened afterwards as indicated by the weakening of negative SLA. The bloom decay after 02 July followed the weakening of the dome. This will be clarified in Section 3.2.1 of the manuscript and Fig. R2 will be included.

Page 15, lines 17-21: "CTD observations within the dome until 29 June, when the ship was at TSW, show that the subsurface chlorophyll concentrations were weak (< 0.5 mg m −3) just before the surface bloom event (Fig. 4e). This indicates that the vertical redistribution of subsurface phytoplankton does not have significant contribution in enhancing the surface chlorophyll. The generation of surface blooms is presumed to be dominantly controlled by the vertical transport of subsurface nutrients to the euphotic zone."

The mixed layer in SG579 does not seems shallowed considerably during the initial phase, but the chl concentration enhanced significantly in the mixed layer. The clear sky might be the major factor for this surface bloom as the authors said that the monsoon was active and therefore had considerable cloud cover in the previous week. It is possible that as the sky became clear it enhance the available light and thus marked by enhanced Chl. However, as the surface nutrients get consumed in few days the Chl concentration decreases again in spite of the persistence clear sky. How, authors can discard this possibility?

We thank the referee for pointing out this possibility. Photosynthetically available radiation (PAR) from MODIS/VIIRS merged product along 8° N from June to July is shown in Fig. R5. The study region was under the influence of an active phase of the monsoon until the third week of June. This indicates light limitation on phytoplankton growth during this period. The active phase was followed by a convectively suppressed phase by the last week of June, one week prior to the glider deployment. In the region of SLD, PAR levels increased from about 12 E m^{-2} day^{-1} on 22 June to 50 E m^{-2} day^{-1} on 26 June. This shows that the transition from active to supressed phase favoured enhanced light availability for bloom generation. The glider data sampling began on 30 June, after the commencement of the suppressed phase and coinciding with the peak phase of the SLD. This restricts the identification of the relative importance of light and nutrient limitations on

the generation of blooms at SG579. It may be noted that high radiation levels persisted till mid-July, however, the surface layers exhibited oligotrophic conditions after the bloom decay. Surface chlorophyll dropped to levels below 0.1 mg m^{-3} after 02 July (Fig 4a in the manuscript). This implies nutrient depletion in the surface layers resulting from phytoplankton consumption during the bloom event. The above details will be included in Section 3 of the manuscript. The shoaling of MLD is not so evident in the glider data, probably because the sampling period of SG579 starts on 30 June, when the SLD was already at its peak (Fig. R2a).

Page 16, lines 13-15: "Subsequent deepening of the mixed layer (~70 m, Fig. 4d) suggests the role of mixing and entrainment in triggering the surface blooms."
What happens after 7th July when the MLD shallowed again in spite of increased wind speed? This does not explain authors hypothesis that the MLD deepens due to increased winds.

Mixed layer shoaling after 07 July, despite the increase in wind speed, can be attributed to surface freshening. Surface salinity decreased by about 0.8 psu from 07 July to 10 July, inducing strong near-surface stratification (Fig. 6 in the manuscript). The resultant shoaling of mixed layer and the barrier layer formation (Fig. 7 in the manuscript) reveal the dominant role of freshwater over wind forcing in controlling the near-surface stratification and hence the surface blooms.

Deepening of mixed layer on 06 July occured between two freshening events; the first during 04-05 July and the second during 07-10 July (Fig. 6 in the manuscript). Surface salinity stratification was relatively weaker in between these events, providing conditions favourable for wind induced mixing. Taking into account the dynamic nature of the region, any impact of lateral transport of salinity on mixed layer deepening cannot be ignored. The quantification of lateral transport, however, is not feasible without estimates of advection and hence is outside the scope of the paper.

"The decay period of the bloom (08–10 July) coincided with the development of a freshening event. Surface salinity decreased by about 0.8 psu from 06 July to 10 July (Fig. 6) and the corresponding decrease in surface chlorophyll was about 0.27 mg m −3 (Fig. 5)."

The decrease of salinity during 6-10 July is of same order as seen during 4-5 July. This is only due to the fact that MLD shallows again and thereby inhibits the subsurface mixing of salinity. It may not be linked with lateral advection of fresh water and more to do with dynamics behind deepening of MLD during 5-7 July, which is not quite explained by the authors.

Later, in Figure 7 authors nicely explained the formation of barrier layer which inhibits surface Chl. However, yet to convincingly explain why MLD deepens during 6-7 July. It may also help to extend the Figure 7 from 3rd July to see the barrier layer evolution.

The decrease in surface salinity cannot be completely attributed to mixed layer shoaling and inhibition of subsurface mixing of salinity. In the absence of an external freshwater source, mixed layer shoaling will not cause any further freshening in the surface layers as observed in the glider data. Since there was no local precipitation, the dominant mechanism which leads to surface freshening is presumed to be lateral advection. Impact of surface freshening on MLD and the barrier layer formation is evident from the profiles before and after the freshening event (Fig. 7 in the manuscript). Inhibition of mixing will finally limit the availability of nutrients in the surface layers and hence the surface bloom decays. Note that the shoaling of mixed layer occurs slightly later at the CTD location (Fig. 4e) and the surface bloom persists for longer here.

Figure 7 has been modifed by including selected daily mean profiles starting from 03 July till 10 July from SG620 (Fig. R6a-e). The barrier layer formation due to surface freshening can be observed during both the freshening events (Vinayachandran et al., 2018). Initial drop in surface salinity during the freshening events were of the same order (~0.4 psu; 04 July and 07 July in Fig. 6 of the manuscript). However, the first event was relatively shorter (04-05 July) and the second event lasted for a longer time period (07-10 July). Inhibition of surface blooms and the intensification of the DCM in the presence of surface salinity stratification can be observed during both the freshening events (Fig. R6b and R6d-e). Vertical profiles obtained from CTD at TSE for the same period are given in Figure R6f-j. CTD data shows both the freshening events, the associated development of barrier layers, the resultant decline in surface chlorophyll and the intensification of DCM, consistent with the glider observations (Fig. R6g and R6i-j). Above details and the modified Fig. 7 will be included in the manuscript.

Page 29, line 11: " Hence NO 3 was preferred over PO 4 and Fe (SiO4 does not limit growth in TOPAZ)" I think this statement is not true. In TOPAZv1 large phytoplankton limitation term is dependent on Silicate. Please verify.

Thanks to the reviewer for the correction. SiO4 limits the growth of large phytoplankton in the model, but not considered in the case of small phytoplankton and diazotrophs. The text will be modified accordingly.

Figure 14: This figure is very confusing. It would help to overlay the weekly mean currents over the tendency terms. Many a times statements are made on vortices, SMC and its consequences on the NO3 budget, but without showing the mean currents it is very difficult to follow as a reader.

For example, authors said "Along the path of SMC, a clear patch of increased nitrate levels was evident (Fig. 14i), which extended from the southern tip of India up to about 85E. This indicates horizontal advection of coastally upwelled nutrients from the southern coasts of India and Sri Lanka (Fig. 14k) into the southern BoB by the SMC"

To me the NO3 show a negative tendency in the core of the SMC (east of SriLanka) and the positive patch may be along the edges. However, I can not make a concrete conclusions without any information of currents.

Thanks to the reviewer for the suggestion. Weekly mean currents are overlayed over the tendency terms (Fig. R7). Horizontal advection of coastally upwelled nutrients from the southern coasts of India and Sri Lanka can be seen along the path of SMC (Fig. R7i and R7k).

Further, authors claimed that Ekman pumping is the primary mechanism of surface Chl bloom, which I think is not well supported. Also, what about entrainment? At least SG620 show a clear signature of entrainment during 6-7 July.

Observations from SG579, in the region of SLD, shows no significant deepening of mixed layer during the period of surface blooms (Fig. 4a in the manuscript). This indicates that entrainment was relatively weaker here. Ouside the region of SLD, at TSE, SG620 shows deepening of mixed layer by about 20-30 m during 3rd and 6th July. This indicates a

significant contribution of entrainment in the vertical supply of nutrients and hence the surface bloom formation. Quantification of entrainment, however, requires additional information on the vertical gradient of nutrients.

Finally, what will be the effect of Rossby wave radiations from the eastern boundary of the Bay Bengal. Since, 8N is very close to the equatorial region, Rossby waves can travel pretty fast (~20-25 cm/s ?) which means a Rossby wave front can cover about 2 degrees during the observation period and therefore, can implicate the east-west contrast between TSW and TSE.

We thank the referree for the suggestion. Rossby waves propagating from the eastern boundary of the BoB can influence the depth of thermocline (nitracline) and hence the bloom activity. The east-west contrast between TSW and TSE is largely dependent on the spatial extent and strength of SMC and SLD, which is attributed to the combined effect of local as well as remote forcings. Observations of currents and sea level anomalies reveal that the location and intensity of SMC and SLD varied during the observational period (Fig. 3 in the manuscript). Using geostrophic velocities obtained from satellite data, Webber et al. (2018) showed that the SMC moved westward during the BoBBLE observational period. They related the westward shift of SMC to the westward propagation of downwelling Rossby waves from the eastern boundary of the BoB. The strength and spatial extend of SLD also varied accordingly. The decay period of the SLD coincided with the arrival of westward propagating high in sea level anomalies associated with the Rossby wave propagation (Fig. R3). The above explanations will be included in the manuscript.

References

Burns, J. M., B. Subrahmanyam, and V. S. N. Murty, (2017), On the dynamics of the Sri Lanka Dome in the Bay of Bengal, J. Geophys. Res. Oceans, 122, 7737–7750, doi:10.1002/2017JC012986.

Cheng, X., J. P. McCreary, B. Qiu, Y. Qi, and Y. Du, (2017), Intraseasonal-to-semiannual variability of sea-surface height in the astern, equatorial Indian Ocean and southern Bay of Bengal, J. Geophys. Res. Oceans, 122, doi:10.1002/2016JC012662.

Prescilla Kurien, Motoyoshi Ikeda and Vinu K. Valsala, (2010), Mesoscale Variability along the East Coast of India in Spring as Revealed from Satellite Data and OGCM Simulations, Journal of Oceanography, 66, 273–289

Shankar, D., Vinayachandran, P., and Unnikrishnan, A., (2002), The monsoon currents in the north Indian Ocean, Progress in Oceanography, 52, 63–120.

Vinayachandran, P. N. and Yamagata, T., (1998), Monsoon Response of the Sea around Sri Lanka: Generation of Thermal Domes and Anticyclonic Vortices, J. Phys. Oceanogr., 28, 1946–1960.

Vinayachandran, P. N., and Coauthors, (2018), BoBBLE (Bay of Bengal Boundary Layer Experiment): Ocean–atmosphere interaction and its impact on the South Asian monsoon. *Bull. Amer. Meteor. Soc.*,99, 1569–1587, https://doi.org/10.1175/BAMS-D-16-0230.1.

Webber, B. G. M., Matthews, A. J., Vinayachandran, P. N., Neema, C. P., Sanchez-Franks, A., Vijith, V., Amol, P., and Baranowski, D. B., (2018), The dynamics of the Southwest Monsoon current in 2016 from high-resolution in situ observations and models, Journal of Physical Oceanography, 48, 2259-2282.

Wijesekera, H. W., Shroyer, E., Tandon, A., Ravichandran, M., Sengupta, D., Jinadasa, S. U. P., Fernando, H. J. S., Agarwal, N., and Coauthors, (2016), "ASIRI: An Ocean–Atmosphere Initiative for Bay of Bengal", Bull. Am. Meteorol. Soc., 97, 1859–1884, https://doi.org/10.1175/BAMS-D-14-00197.1.

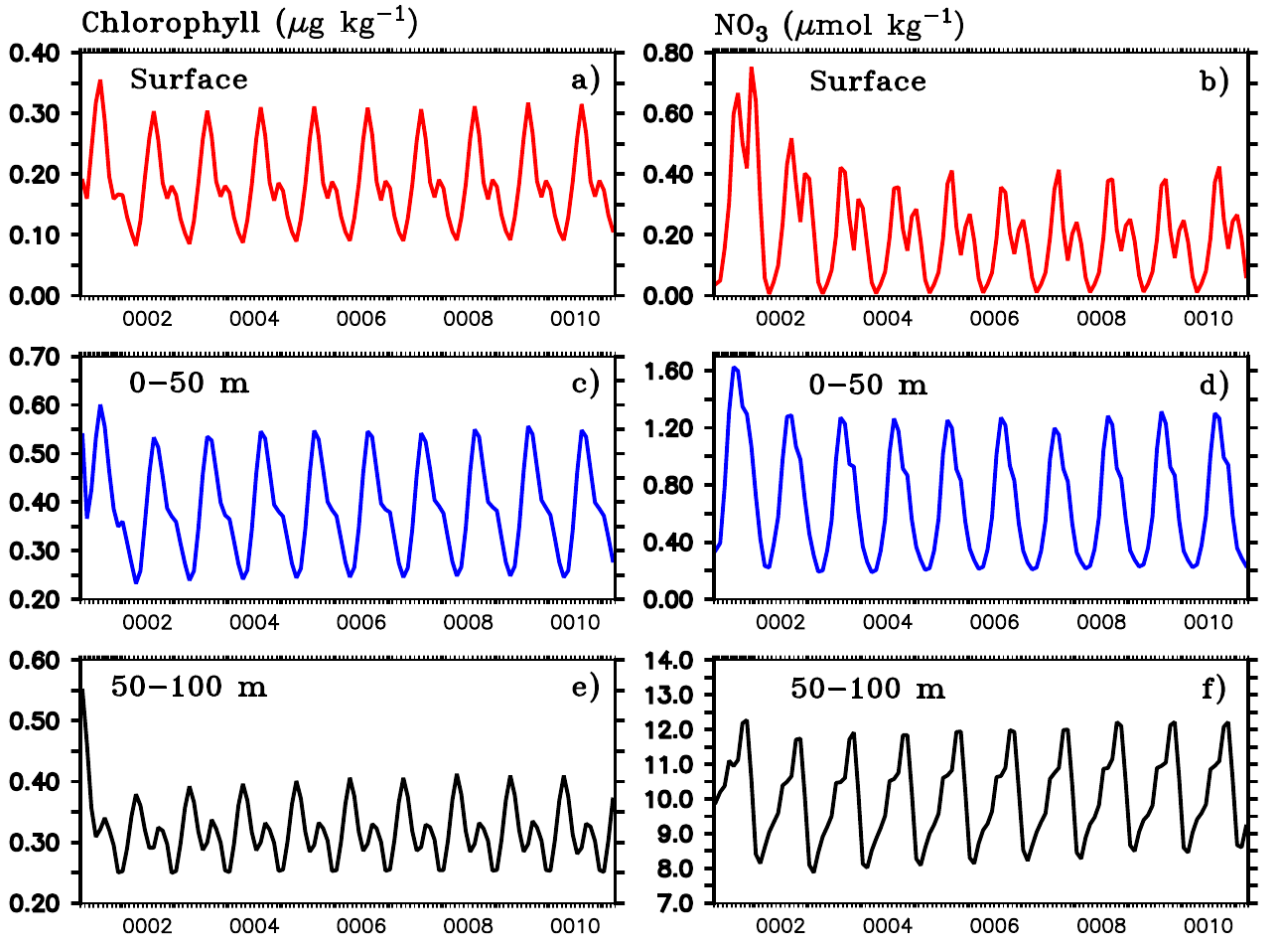

Figure R1. Time evolution of simulated chlorophyll (left panels) and nitrate (right panels) at the surface (top panels), 0-50 m (middle panels) and 50-100 m (bottom panels) for 10 years of the model spin up.

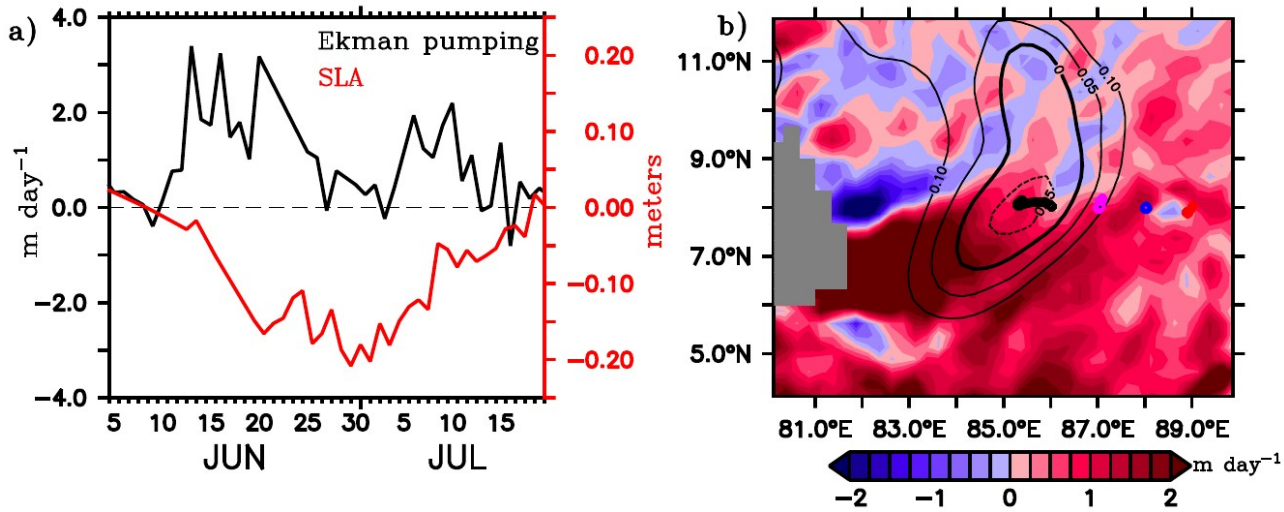

Figure R2. a) Time series of Ekman pumping (m day^{-1}; black) calculated from ASCAT winds around the location of SG579 (85-86° E, 7.5-8.5° N) and the minimum SLA (m; red) in the region of the Sri Lanka Dome (SLD) from 05 June to 20 July. b) Mean Ekman pumping averaged for the BoBBLE observational period (24 June – 23 July) in the southern BoB. Contours of SLA are overlayed.

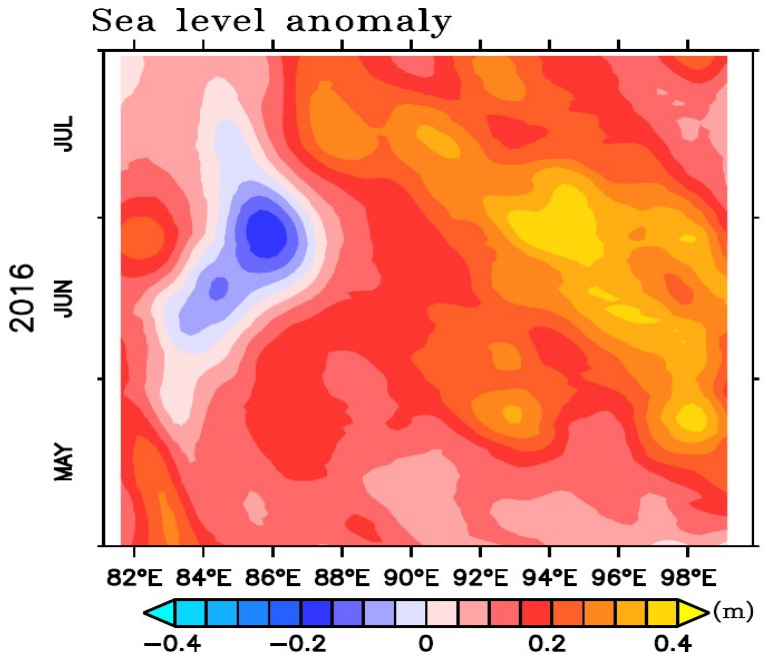

Figure R3. Time-longitude hovmoller diagram of SLA (m) along 8°N between 81-100°E from May to July 2016.

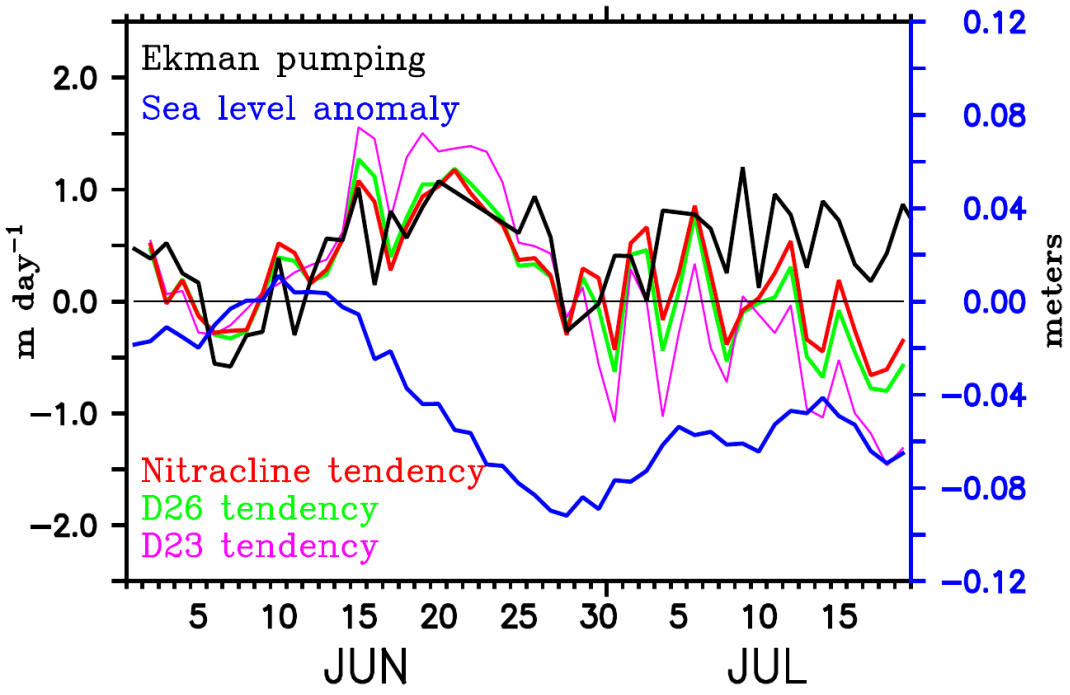

Figure R4. Ekman pumping (m day^{-1}; black) and tendencies of nitracline (m day^{-1}; red), D26 (m day^{-1}; green) and D23 (m day^{-1}; magenta) averaged over the region of the modelled Sri Lanka Dome. Note that the tendency terms are reversed in sign so that positive (negative) values indicate shoaling (deepening). Nitracline is defined as the depth of 2 µmol kg^{-1} nitrate isoline. Minimum sea level anomaly (m; blue) in the region of SLD is overlayed.

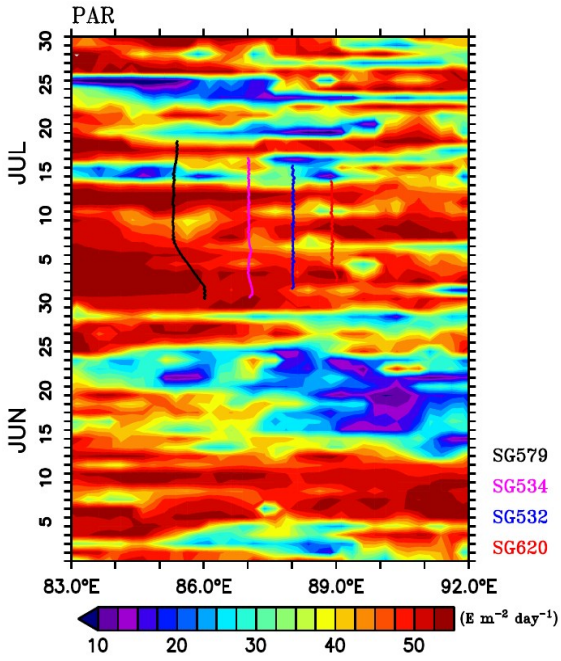

Figure R5: Photosynthetically available radiation (PAR; E m^{-2} day^{-1}) along 8° N, between 83-92° E from June-July, 2016. The glider tracks during the BoBBLE field program are overlayed.

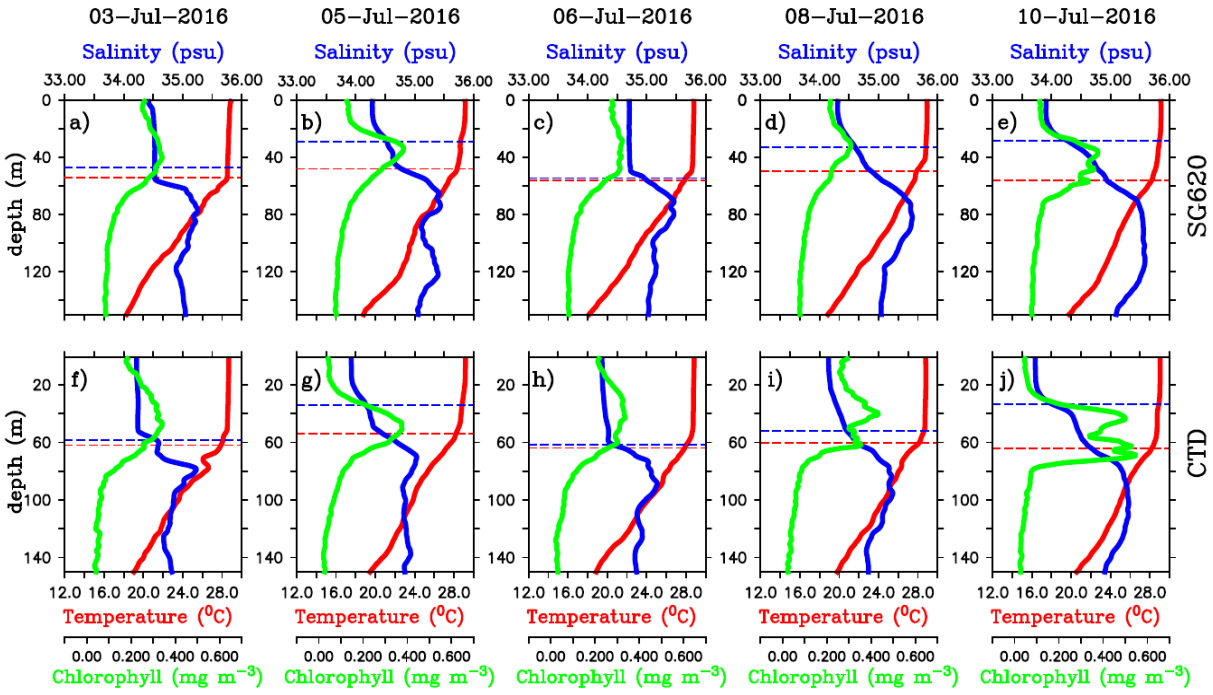

Figure R6. Daily mean vertical profiles of temperature (°C; red), salinity (psu; blue) and chlorophyll (mg m^{-3}; green) from (a-e) SG620 and (f-j) CTD at TSE location for selected days. The blue dashed line indicates the mixed layer depth, which is calculated as the depth where density is equal to the sea surface density plus an increase in density equivalent to 0.8°C. The red dashed line indicates isothermal layer depth (ILD) which is calculated as the depth where the temperature is cooler than SST by 0.8° C. The region between the MLD and ILD represents the barrier layer.

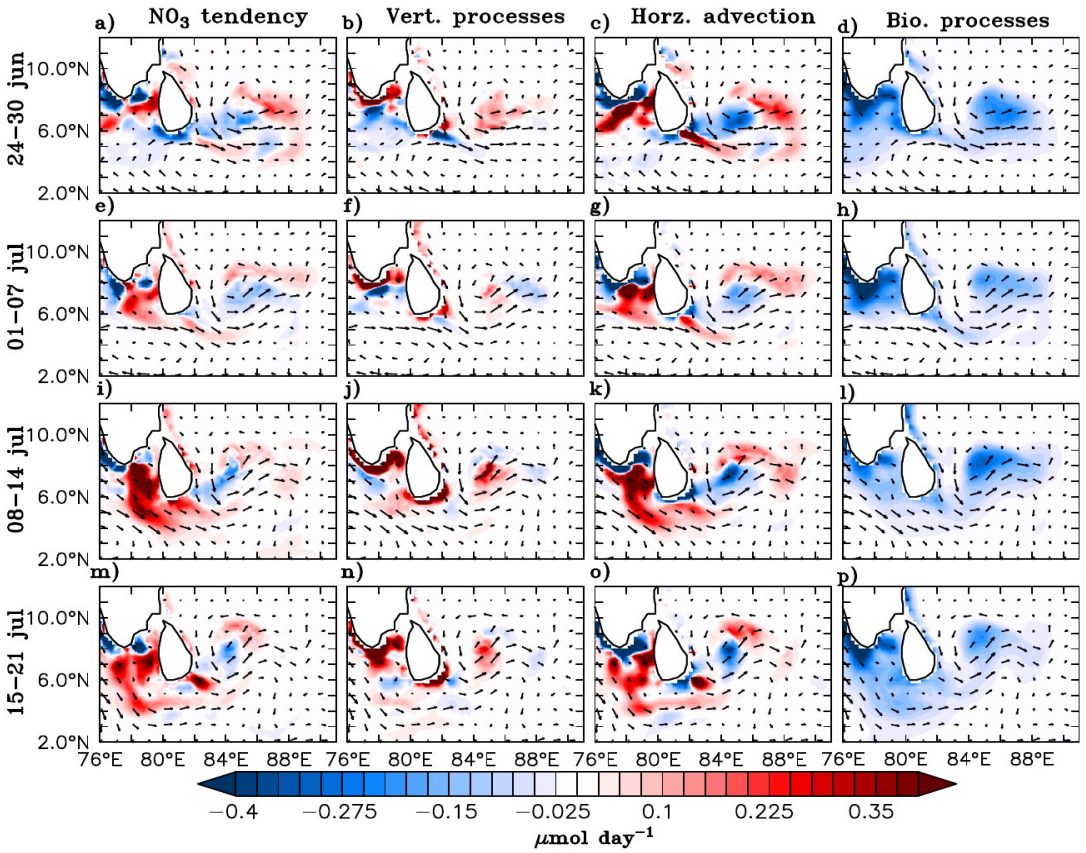

Figure R7. Model nitrate budget averaged over the mixed layer. Nitrate tendency (first column), vertical processes (second column), horizontal advection (third column) and the biological processes (fourth column) in μmol day^{-1} are shown for 7-day averages starting from 24 June to 21 July 2016, marked on the left side of the corresponding panels. Vertical processes include vertical advection and mixing, and biological processes include source (nitrification) and sink (denitrification and uptake by the phytoplankton) terms for the model nitrate. Surface current (ms^{-1}) vectors are overlayed.

Interactive comment on "Vertical distribution of chlorophyll in dynamically distinct regions of the southern Bay of Bengal" by Venugopal Thushara et al.

Reply to comments by E. Boss (Referee)

(Referee's comments are given in blue and the response to comments are in black.)

This paper is concerned with the dynamics of chlorophyll concentration in the Bay of Bengal, and uses observations from glider, a ship, satellite and a numerical model to describe it and attempt to understand it.
The paper's English is good. However, the English used is often not clear when it comes to the description of phytoplankton and their evolution. Bloom is never defined, sometime it seems to mean a relatively elevated chlorophyll concentration while in other time it denote a positive change in time.
The paper may be of interest to readers of BG but I feel that it could be of significant more value if the authors addressed the following. I am also returning an annotated PDF (I stopped towards the end due to exasperation. Sorry.). I think addressing these will do a lot to make this paper significantly more useful.

We thank Dr. E. Boss for carefully reading the manuscript and offering the comments and suggestions. The term 'bloom' was used to refer to a condition of elevated chlorophyll concentration which is clearly distinguishable in space and time. During the study period, satellite observations of ocean color showed patches of high chlorophyll (0.3-0.7 mg m^{-3}) in the regions of the Sri Lanka Dome (SLD) and the summer monsoon current (SMC), whereas the surrounding regions, outside the influence of these features, exhibited lower surface chlorophyll levels (< 0.2 mg m^{-3}). These details will be included in the revised manuscript. The term bloom will be replaced by increase in chlorophyll appropriately.

1. The author adopt the classical view that phytoplankton dynamics are all determined by nutrients and light with physics modulating their availability. This view is not consistent with the fact that phytoplankton do not double in concentration daily even though they, on average, divide daily in most of the oceans (see review in ARMS by Ed Laws). This bottom up view is understandable given the lack of measurements to constrain losses, but the author should be very careful in their interpretation of temporal dynamics. In fact, in the

height of the bloom, the maximal concentration, is when loss = growth. The recent paper by Behrenfeld and Boss, 2017, may make this point of view clearer to the writers. Yes, productivity=growth rate x biomass, and hence when there is more chlorophyll there is likely more productivity.

Yes, chlorophyll distribution is determined by both physical and biological processes. In the present study, our main objective is to document the physical controls on the chlorophyll distribution, associated with the monsoon dynamics. In the southern BoB, high chlorophyll concentrations were observed in the regions of strong dynamics, including the SLD and the SMC, indicating that the distribution of chlorophyll is largely dependent on the upper ocean dynamics. The biological controls are equally important. However, lack of observations on loss terms including mortality and sinking rates, and grazing by different zooplankton groups restricts a detailed investigation on their relative importance with respect to the physical processes during different stages of the chlorophyll bloom evolution. These limitations will be mentioned in the revised manuscript.

2. The issue of photoaclimation is very important in stratified waters as chl/C can vary by factors as high as 5. The fact that the glider measure bbp as well as chlorophyll could be use to study this question. Similarly, the model you use should have variable Chl/C, unless you use bbp to estimate C_phyto (e.g. Graff et al., 2015)

We agree that photoacclimation is important. Considering the variability in available light as a function of depth, the physiological adaptation of phytoplankton through photoacclimation has a significant control on the chlorophyll concentration. The observed vertical distribution of chlorophyll does not necessarily represent the phytoplankton biomass distribution, since the chlorophyll to carbon ratio (Chl/C) can vary. The relation between chlorophyll and bbp has been examined using observations from SG620 at the time series location (Fig. R1). This shows a linear relationship between chlorophyll and bbp, which indicates that the Chl:C ratio did not vary much in the region during the observational period.

The ecosystem model incorporates the effect of photoacclimation on the simulated chlorophyll distribution (Dunne et al., 2010). The model calculates a variable Chl:C which is dependent on light availability following Geider et al. (1997).

3. If Fcdom is available (not clear what the 3rd channel of the triplet is) it could also be useful to understand light availability to phytoplankton.

Fcdom is not available at the time series location.

4. Chlorophyll is a limited descriptor of biology (we don't know the species and the associated ecosystem from it). Limiting the text to describe its dynamics rather than talking about the 'biology' will make your text more palatable to some. In addition, the value you are estimating for it based on 'factory calibration' is likely biased by a factor of 2 (e.g. Roesler et al., 2017).

Thanks to the referee for the suggestion. The text will be modified accordingly in the revised manuscript.

5. The term 'bloom activity' is used over and over. What does that mean? Changes in chlorophyll concentrations? Try to be more precise.

The term bloom activity was used indicate elevated levels of chlorophyll that is clearly identifiable in space and evolving in time. Generally, the surface layers of the southern Bay of Bengal exhibit oligotrophic conditions with chlorophyll concentrations below 0.2 mg m^{-3}. During the summer monsoon, patches of enhanced chlorophyll concentrations (0.3-0.7 mg m^{-3}) are observed in the dynamically active regions of the SLD and the SMC. By the end of the summer monsoon, chlorophyll levels decrease considerably. For clarity, the term 'bloom' will be replaced by 'chlorophyll' appropriately in the revised manuscript.

6. Phytoplankton primary productivity is driven by PAR, which means they care about absorbing a photon in the visible but not about the energy of the photon (blue photons have about twice as much as red one). Your light model should be in PAR not W mˆ-2 and should take CDOM into account ('compete' with phytoplankton by absorbing blue photons).

We agree with the referee that PAR is the appropriate parameter to explain primary productivity. At the time series location (89°E, 8°N), in situ observations of the vertical distribution of PAR is not available. Spatial and temporal coverage of attenuation coefficients derived from satellite data are also insufficient during the study period. The light model presented in the analysis (Morel and Antoine, 1994 and Manizza et al., 2005)

uses surface irradiance as input, instead of PAR. Hence, we preferred using the observed irradiance from the shipboard measurements to calculate the light penetration. The model considers light partioning into infrared and visible bands. Attenuation coefficients in the visible range were calculated seperately for two averaged wavelength bands (red and blue/green) at each depth levels as functions of chlorophyll profiles obtained from the glider (SG620), following Morel (1988). The vertically varying attenuation coefficients in the visible band will take into account the self-shading effect caused by the presence of phytoplankton in modulating the penetrative radiation into the subsurface layers, thereby influencing the DCM distribution.

PAR (E m^{-2} s^{-1}) was estimated from the calculated penetrative radiation using the conversion,

$$PAR_{(z)} = I\_vis_{(z)} * 2.75e18 / 6.023e23,$$

where $I\_vis_{(z)}$ is the penetrative radiation (W m^{-2}) in the visible range at depth z calculated using the light model, 2.75e18 quanta s^{-1} W^{-1} is the conversion factor obtained from Morel and Smith (1974), and 6.023e23 quanta E^{-1} is the number of photons corresponding to one mole. The depth of euphotic zone (Z_{eu}) was calculated as the depth at which light reduces to 1% of the surface PAR value. Considering the fact that phytoplankton sees the absolute light level and not the percentage (Banse, 2004), the depth of threshold isolume ($Z_{0.415}$), taken as the depth where PAR is 0.415 E m^{-2} day^{-1} below which light is insufficient to support photosynthesis (Letelier et al., 2004; Boss and Behrenfeld, 2010), is also shown (Figure R2).

Both Z_{eu} and $Z_{0.415}$ decreased during days with elevated surface chlorophyll (06-07 July) and deepened during days with weaker surface chlorophyll levels. This shows enhanced (reduced) light availability in the subsurface layers during days with low (high) surface chlorophyll, consistent with our results. Figure 10 in the manuscript and the corresponding text in Section 3.2.3. will be modifed in the revised manuscript following the above calculations. The location of study region is away from the coastal ocean indicating less turbidity and relatively lower concentrations of CDOM, except those associated with the phytoplankton blooms. Hence we believe that exclusion of CDOM effect in the present light model will not affect the results significantly.

References

Banse, K., (2004), Should we continue to use the 1% light depth convention for estimating the compensation depth of phytoplankton for another 70 years?, Limnology and Oceanography Bulletin 13, 49–51.

Behrenfeld, M. J. and E. S. Boss (2017), Student's tutorial on bloom hypotheses in the context of phytoplankton annual cycles, *Global Change Biology*,1–23 doi:10.1111/gcb.13858

Boss E. and Behrenfeld M., (2010), In situ evaluation of the initiation of the North Atlantic phytoplankton bloom, Geophysical Research Letters, 37, L18603, doi:10.1029/2010GL044174.

Dunne, J. P., Gnanadesikan, A., Sarmiento, J. L., and Slater, R. D., (2010), Technical description of the prototype version (v0) of Tracers of Phytoplankton with Allometric Zooplankton (TOPAZ) ocean biogeochemical model as used in the Princeton IFMIP model, Biogeosciences, 7 (Suppl.), 3593, https://doi.org/10.5194/bg-7-3593-2010.

Geider, R. J., MacIntyre, H. L., and Kana, T. M., (1997), Dynamic model of phytoplankton growth and acclimation: responses of the balanced growth rate and the chlorophyll a:carbon ratio to light, nutrient-limitation and temperature, Marine Ecology, 148, 187–200.

Letelier, R.M., Karl, D.M., Abbott, M.R., Bidigare, R.R., (2004). Light driven seasonal patterns of chlorophyll and nitrate in the lower euphotic zone of the North Pacific Subtropical Gyre. Limnology and Oceanography 49, 508–519.

Manizza, M., Quere, C. L., Watson, A. J., and Buitenhuis, E. T., (2005), Bio-optical feedbacks among phytoplankton, upper ocean physics and sea-ice in a global model, Geophys. Res. Lett, 32, L05 603, https://doi.org/10.1029/2004GL020778.

Morel A, and Raymond C. Smith, (1974), Relation between total quanta and total energy for aquatic photosynthesis, 19, 591-600, https://doi.org/10.4319/lo.1974.19.4.0591.

Morel, A., (1988), Optical modelling of the upper ocean in relation to its biogenous matter content (case I waters), J. Geophys. Res., 93, 10,749 – 10,768.

Morel, A. and Antoine, D., (1994), Heating rate within the upper ocean in relation to its bio-optical state, J. Phys. Oceanogr., 24, 1652–1665.

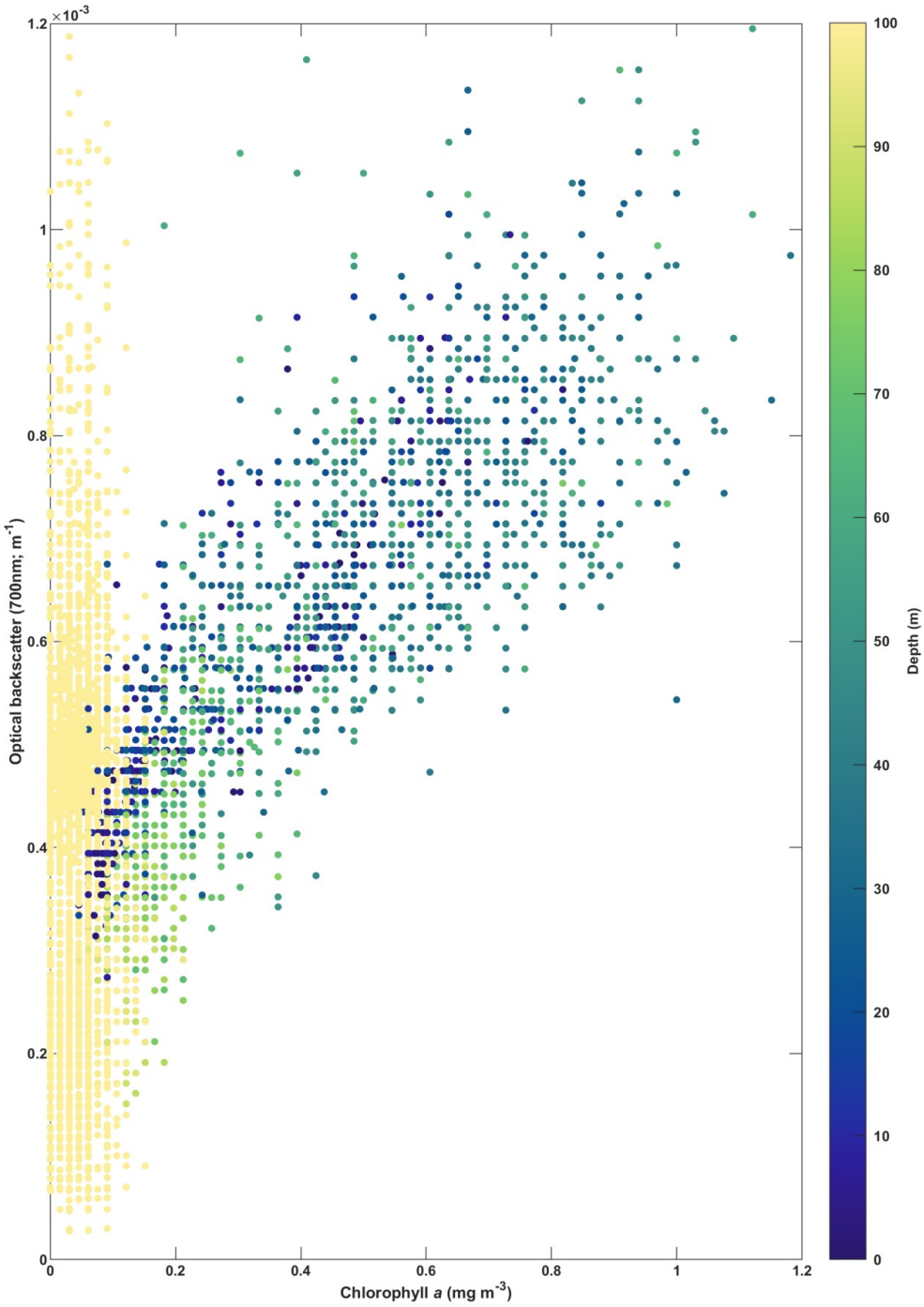

Figure R1. Relation between chlorophyll (mg m^{-3}) and optical backscatter (m^{-1}) obtained from SG620 at TSE (89°E, 8°N). The color bar shows the depth ranges.

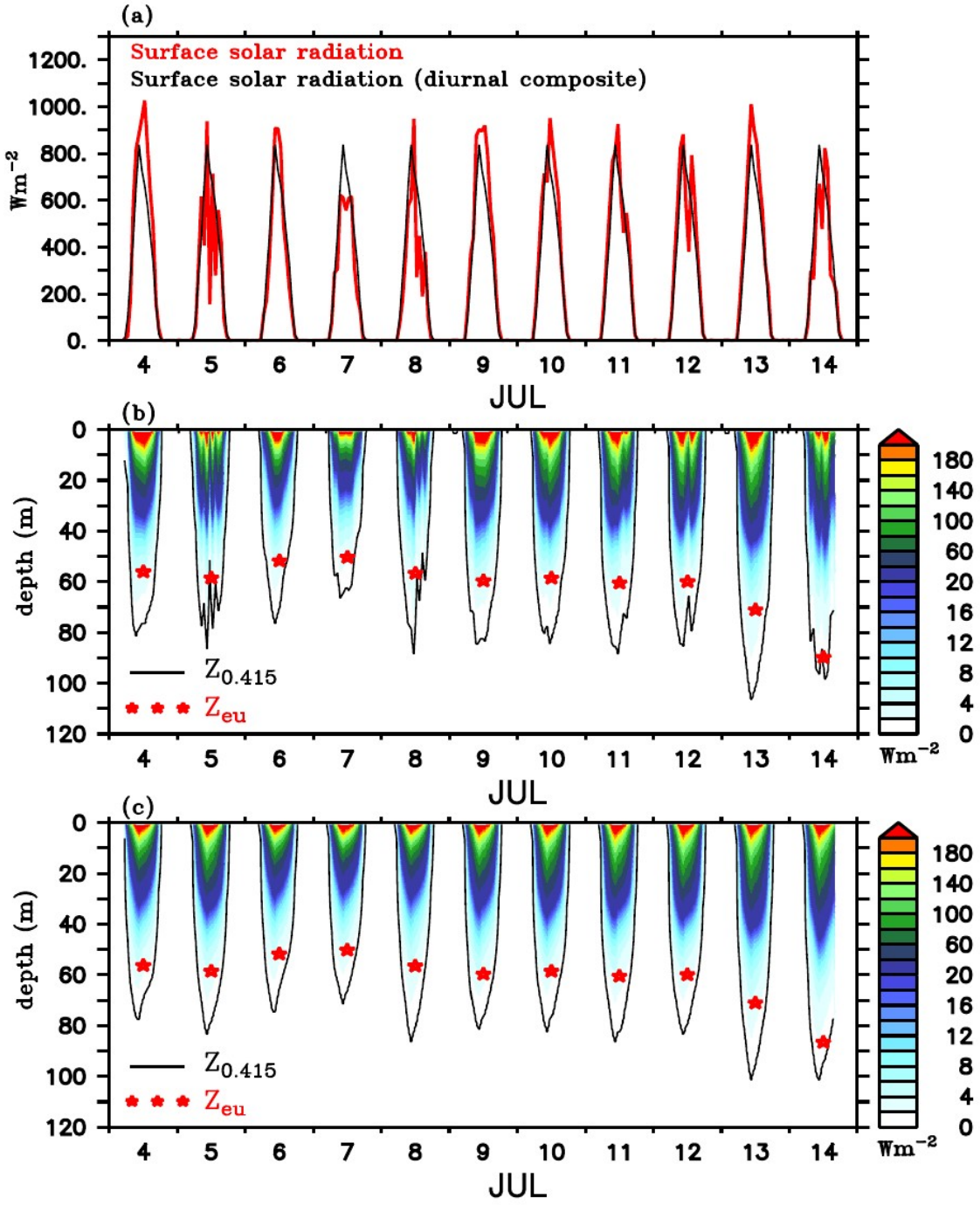

Figure R2. (a) Surface solar radiation measured by the shipboard AWS at TSE from 04–14 July (red) and the corresponding diurnal composite (black) calculated for the same period. Penetrative shortwave radiation (W m^{-2}) calculated following Morel and Antoine (1994) and Manizza et al. (2005) scheme using (b) observed and (c) diurnal composite of radiation. Chlorophyll from SG620 is used for the calculations. PAR (E m^{-2} s^{-1}) was estimated from the calculated penetrative radiation in the visible range following Morel and Smith (1974). The red stars in b) and c) represent daily averaged depth of euphotic zone (Z_{eu}, m) which is taken as the depth at which light reduces to 1% of the surface PAR value. The black contours in b) and c) represent the depth of threshold isolume ($Z_{0.415,}$ m) taken as the depth at which PAR is 0.415 E m^{-2} day^{-1}.

Major modifications made in the manuscript following the reviewer's comments are listed below:

1. A detailed analysis on Ekman pumping in the region of the Sri Lanka Dome has been included. Figure 6 shows the Ekman vertical velocities calculated using ASCAT winds.

2. In additional to the above analysis, the model nitracline tendency was compared with the calculated Ekman vertical velocities and SLA during the evolution of the modelled Sri Lanka Dome (Figure 14). During the developing phase of the dome, the nitracline tendency followed the Ekman vertical velocities.

3. Role of remote forcing in controlling the evolution of the SLD and hence, the chlorophyll distribution is presented. The decaying phase of the dome coincides with the arrival of the westward propagating downwelling Rossby wave signals from the east. A time-longitude hovmoller diagram of SLA along 8N is included in Figure 6 to demostrate the role of remote effects.

4. The term 'bloom' is used in the present study to represent elevated chlorophyll concentrations (> 0.3 mg m^{-3}), clearly distinguishable in space and time with respect to the oligotrophic background state of the Bay of Bengal. This explanation has been added in the revised version.

5. Calculations of penetrative radiation in Section 3.2.3 has been modified. PAR was estimated using radiation obtained from the light model following the conversion factor given by Morel and Smith (1974). Depth of the euphotic zone (Z_{eu}) was calculated as the depth at which light reduces to 1% of the surface PAR value. Depth of the threshold isolume ($Z_{0.415}$), taken as the depth where PAR is 0.415 E m^{-2} day^{-1} below which light is insufficient to support photosynthesis, is also shown.

6. Figure 8 has been expanded by including the first freshening event and the associated barrier layer formation. Inhibition of surface blooms and the intensification of the DCM in the presence of surface salinity stratification can be observed during both the freshening events.

7. The importance of biological loss terms in determining the chlorophyll bloom evolution, and the model limitations in representing these loss terms are mentioned in the revised version.

The above mentioned modifications are incorporated in the Abstract and Conclusions as well. Details in the Abstract have been removed, but retained in the text.

The marked-up manuscript version showing the changes made with respect to the previous version is given below. Newly added text are given in blue and the deleted text in red.

Vertical distribution of chlorophyll in dynamically distinct regions of the southern Bay of Bengal

Venugopal Thushara[1], Puthenveettil Narayana Menon Vinayachandran[1], Adrian J. Matthews[2], Benjamin G. M. Webber[3], and Bastien Y. Queste[3]

[1]Centre for Atmospheric and Oceanic Sciences, Indian Institute of Science, Bangalore, India.
[2]Centre for Ocean and Atmospheric Sciences, School of Environmental Sciences and School of Mathematics, University of East Anglia, Norwich, UK
[3]Centre for Ocean and Atmospheric Sciences, School of Environmental Sciences, University of East Anglia, Norwich, UK

Correspondence to: P. N. Vinayachandran (vinay@iisc.ac.in)

Abstract.

The Bay of Bengal (BoB) generally exhibits surface oligotrophy, due to nutrient limitation induced by strong salinity stratification. Nevertheless, there are hot spots of ~~biological activity~~ high chlorophyll in the BoB where the monsoonal forcings are strong enough to break the stratification; one such region being the southern BoB, east of Sri Lanka. A recent field program conducted during the summer monsoon of 2016, as a part of the Bay of Bengal Boundary Layer Experiment (BoBBLE), provides a unique high-resolution dataset of the vertical distribution of chlorophyll in the southern BoB using ocean gliders along with shipboard CTD measurements. Observations were carried out for a duration of 12–20 days~~during a suppressed phase of the Boreal Summer Intraseasonal Oscillation (BSISO), along a longitudinal transect at 8° N, extending from 85.3–89° E~~, covering the dynamically active regions of the Sri Lanka Dome (SLD) and the Southwest Monsoon Current (SMC). Mixing and upwelling induced by the monsoonal wind forcing enhanced surface chlorophyll concentrations (0.3–0.7 mg m^{-3})~~in the surface layers. Observations reveal the presence of prominent~~ . Prominent deep chlorophyll maxima (DCM; 0.3–1.2 mg m^{-3}) existed at intermediate depths (20–50 m), ~~generally below the mixed layer and above the thermocline,~~ signifying the contribution of subsurface productivity on the biological carbon cycling in the BoB. The shape

of chlorophyll profiles varied in different dynamical regimes~~indicating that the mechanisms determining the vertical distribution of chlorophyll are intricate; upwelling favoured~~ ; upwelling was associated with sharp and intense DCM, whereas mixing resulted in a diffuse and weaker DCM. Within the SLD, ~~open ocean Ekman pumping and the doming of thermocline~~ open-ocean Ekman suction favoured a substantial increase in chlorophyll~~concentration~~. Farther east, where the thermocline was deeper~~and moderate surface blooms were triggered by~~ , enhanced surface chlorophyll was associated with intermittent mixing events. Remote forcing by the westward propagating Rossby waves influenced the upper ocean dynamics and chlorophyll distribution in the southern BoB. Stabilising surface freshening events and barrier layer formation ~~were often observed to inhibit the surface blooms~~often inhibited the generation of surface chlorophyll. The pathway of the SMC intrusion was marked by a distinct band of chlorophyll, indicating the advective effect of biologically rich Arabian Sea waters. The region of monsoon current exhibits the strongest DCM as well as the highest column-integrated chlorophyll. Observations suggest that the persistence of DCM in the southern BoB is promoted by surface oligotrophy ~~, which reduces the self-shading effect of phytoplankton~~ and shallow mixed layers~~, which prevent the vertical redistribution of subsurface phytoplankton~~. Results from a coupled physical-ecosystem model substantiate the dominant role of mixed layer processes associated with the monsoon in controlling the nutrient distribution and biological productivity in the southern BoB. The present study provides new insights into the vertical distribution of chlorophyll in the BoB, ~~which is not captured in satellite measurements,~~ emphasizing the need for extensive in situ sampling and ecosystem model-based efforts for a better understanding of the ~~monsoonal~~ bio-physical interactions and the potential climatic feedbacks.

1 Introduction

The Bay of Bengal (BoB) is fascinating with its unique upper ocean features strongly linked to the Indian Summer Monsoon (ISM) variability (Gadgil et al., 1984; Vecchi and Harrison, 2002; Shankar et al., 2007). The upper layer of the BoB, especially the northern BoB, is highly stable, owing to strong near-surface salinity stratification in the presence of abundant freshwater influx from precipitation and rivers. The low salinity cap in the surface layers of the BoB leads to the formation of a shallow mixed layer and a barrier layer beneath (Vinayachandran et al., 2002; Wijesekera et al., 2016a), controlling air-sea interactions and the upper ocean heat budget (Shenoi et al., 2002). In addition, monsoonal winds are relatively weak over the BoB, leading to a sluggish upper ocean, where vertical overturning and mixing processes are weak (Shetye et al., 1991; Madhupratap et al., 1996; Kumar et al., 2002; McCreary et al., 2009; Wiggert et al., 2009). ~~Hence, destabilisation of salinity stratification is difficult, controlled by the competing effects of winds and freshwater influx.~~ This dynamical set up imparts strong nutrient limitation on phytoplankton growth, leading to weak biological productivity in the BoB (Gomes et al., 2000; Kumar et al., 2002; Madhupratap et al., 2003). Compared to the highly productive Arabian sea, chlorophyll distribution in the BoB is often light limited, despite being located in the same tropical band, due to large cloud cover during the active phase of the monsoon (Kumar et al., 2010). In addition, the presence of suspended sediments in the vicinity of discharge from major rivers reduces the light availability for photosynthesis (Gomes et al., 2000; Kumar et al., 2004).

Though the basin averaged productivity is weak in the BoB, satellite and in situ observations reveal the presence of intense regional chlorophyll blooms (Vinayachandran and Mathew, 2003; Kumar et al., 2004; Kumar et al., 2007). These blooms are clearly distinguishable in space and time, exhibiting elevated

levels of chlorophyll (> 0.3 mg m^{-3}) with respect to the oligotrophic background state of the BoB. The evolution of chlorophyll blooms in the ocean is controlled by the ecosystem balance between the growth and loss rates, as well as the physiological adaptations of the phytoplankton (Cullen, 2015 ; Behrenfeld and Boss, 2017). In the northern BoB where stratification is strong, surface chlorophyll ~~blooms are rarely observed, except those associated~~ levels are generally weak, except in association with coastal processes and eddy activity. The northwestern BoB is characterised by seasonal ~~blooms~~ increase in chlorophyll in the presence of strong coastal upwelling induced by the alongshore winds during the summer monsoon (Shetye et al., 1991), which enriches the previously nutrient-limited euphotic zone (Thushara and Vinayachandran, 2016). In addition, nutrients supplied through the monsoonal river discharge support ~~intense bloom activity~~ enhanced chlorophyll concentrations in the nearby coastal oceans (Kumar et al., 2004; Kumar et al., 2007). The occurrence of mesoscale eddies is an additional forcing, favouring biological productivity through the vertical supply of nutrients (Kumar et al., 2007; Nuncio and Kumar, 2013). Productivity in the BoB is mostly confined to the coastal ocean and dynamical regions of the open ocean, such as the southern BoB, where the freshwater effects are relatively weaker (Vinayachandran and Mathew, 2003).

The southern BoB, characterised by strong currents, intense mixing and upwelling, is one of the most dynamically active regions of the northern Indian Ocean (Murty et al., 1992; Schott et al., 1994; McCreary et al., 1996; Vinayachandran and Yamagata, 1998; Vinayachandran et al., 1999; Shankar et al., 2002; Lee et al., 2016; Wijesekera et al., 2016b). Unlike the northern BoB, salinity stratification is relatively weak in the south, resulting in a deeper mixed layer. Prominent chlorophyll blooms are observed in the coastal and open ocean regions of the southern BoB, closely linked to monsoon circulation (Vinayachandran,

2009). The region off the south coast of Sri Lanka is characterised by ~~intense summerblooms~~ high chlorophyll levels in summer, triggerred by the coastal upwelling of nutrients (Vinayachandran et al., 2004). Cyclonic wind stress curl east of Sri Lanka during the summer monsoon leads to the formation of the Sri Lanka Dome (SLD; Vinayachandran and Yamagata, 1998), where ~~open ocean Ekman pumping~~ open-ocean Ekman suction of nutrients triggers chlorophyll bloom generation (Vinayachandran et al., 2004). The Southwest Monsoon Current (SMC) intruding into the southern BoB (Vinayachandran and Yamagata, 1998; Vinayachandran et al., 2013; Jensen, 2001) carries biologically rich waters from the Indian and Sri Lankan coasts, supporting ~~bloom activity~~ elevated levels of chlorophyll all along its path (Vinayachandran et al., 2004). After finding its way into the BoB, the SMC bifurcates into several branches and the associated cold-core eddies are observed to enhance chlorophyll concentrations (Jyothibabu et al., 2015). During the winter monsoon, satellite observations and ecosystem models reveal the presence of moderate blooms triggered by open ocean upwelling in the southwestern BoB (Vinayachandran and Mathew, 2003; Vinayachandran et al., 2005). In addition to the seasonal forcings, frequent occurrence of tropical cyclones favour short-lived isolated patches of intense blooms (Madhu et al., 2002; Vinayachandran and Mathew, 2003; Rao et al., 2006).

The ~~biogeochemistry of the BoB has~~ biophysical interactions in the BoB have not been well explored and ~~its biophysical interactions have received even lesser attention. Our~~ our present understanding of the mechanisms determining the spatial and temporal distribution of productivity in the BoB is limited, owing to the scarcity of observational data and model simulations. Ocean colour retrievals by satellites are widely affected by the presence of cloud cover during monsoon, the period when the ~~bloom activity~~ surface chlorophyll levels are the highest in the BoB~~is at its peak~~. Past observational stud-

ies (Vinayachandran and Mathew, 2003; Vinayachandran et al., 2004; Kumar et al., 2004; Kumar et al., 2007; Jyothibabu et al., 2015) have contributed to our understanding of the biological productivity in the BoB, suggesting that ~~its bloom dynamics~~ the dynamics controlling the chlorophyll distribution are complex, determined by the competing effects of winds (local as well as remote) and freshwater flux on the mixed layer processes. However, the spatial and temporal coverage of observations is insufficient to obtain a complete picture of the chlorophyll distribution. We also lack estimates of subsurface chlorophyll, and hence, its contribution to the column integrated productivity (Kumar et al., 2009) has received little attention.

Until now, the paucity of previous chlorophyll measurements precluded a detailed investigation of the bio-physical feedbacks and the possible controls on the surface properties, and air-sea heat and gas exchanges of the BoB. The present study is aimed at documenting the observed chlorophyll distribution of the southern bay, obtained from four ocean gliders and conductivity-temperature-depth (CTD) measurements, taken during the Bay of Bengal Boundary Layer Experiment (BoBBLE; Vinayachandran et al., 2018) field program. ~~Surface bloom events~~ Enhanced levels of surface chlorophyll were observed at all glider locations, in response to the monsoonal forcings at seasonal and synoptic timescales~~were observed at all glider locations~~. The BoBBLE data reveal the presence of prominent ~~bloom activity at the subsurface of~~ deep chlorophyll maxima in the BoB, which is rarely captured by satellites. Results from a coupled physical-ecosystem model are incorporated to evaluate the model performance in reproducing the summer blooms in the BoB and to analyse in detail the associated bio-physical interactions. Section 2 describes the observational data and the ecosystem model; Section 3 examines the vertical distribution of chlorophyll

in the southern bay, colimited by light and nutrients, in response to the monsoonal wind and freshwater forcings. Summary and conclusions are given in the last section.

2 Observations and modelling

Observations were carried out in the region to the east coast of Sri Lanka, on-board ~~ORV Sindhu Sadhana~~*ORV Sindhu Sadhana*, which sailed from Chennai on 24 June 2016 and returned on 23 July 2016 (Fig. 1). The present analyses are based on the data along 8°N, extending from 85.3°E (hereafter referred to as TSW) to 89°E (hereafter referred to as TSE), including a 10–day CTD time series station at TSE. Shipboard measurements were taken back and forth along this longitudinal transect; the ship sailed from TSW to TSE during 29 June to 03 July, stayed at TSE from 03–15 July and returned back to TSW on 20 July. The longitudinal transect runs across the productive regions of the SLD and SMC covering a distance of about 400 km.

2.1 In situ measurements of chlorophyll

~~Vertical~~ The vertical distribution of chlorophyll fluorescence was measured along the cruise track using ocean gliders and a shipboard CTD. Ocean gliders are buoyancy driven autonomous underwater vehicles designed to dive from the surface to the deep ocean and back following a sawtooth pattern, collecting vertical profiles of oceanographic properties (Eriksen et al., 2001). Four gliders (SG579, SG534, SG532 and SG620) with biophysical sensors were deployed along the transect at 8°N (Fig. 1). They were positioned at specified locations, hence the measurements made can be considered as time series data (but note that SG579 shifted almost 60 km westwards during the observational period, but stayed within the

SLD). The gliders provided high-resolution measurements of biophysical properties, both in space (~~atleast~~ at least 0.5 m in vertical) and time (4–7 profiles a day). Data collection starts within the top 1m of the upper ocean, enabling better sampling of surface properties compared with conventional measurement techniques. Each glider was equipped with a SeaBird Electronics CTD package, a global positioning system (GPS), and Wetlabs Triplet ECOPuck sensors. All ECOPucks had at least one fluorescence channel, measuring chlorophyll, and were accompanied by one to two backscatter channels. In total, 405 dives were performed by the four gliders, including shallow (∼700 m) and deep (∼1000 m) profiles, where each dive lasted 3–5 hours. The typical speed of the gliders was about 0.25 m s^{-1} and vertical velocities ranged between 0.10–0.15 m s^{-1}. The shipboard CTD was equipped with auxiliary sensors for fluorescence, which are factory calibrated. In addition to the gliders, the CTD collected a total number of 147 profiles along the cruise track. The CTD data used for the present analysis is smoothed in time and depth spaces by 3 hours and 3 m respectively.

After quality control, the data from each glider were optimally interpolated (Bretherton et al., 1976) onto a two-dimensional (time-depth) equally spaced grid, following Matthews et al. (2014). First, a background gridded field was constructed from a weighted average of the observations. A two-dimensional Gaussian weighting function, with e-folding scales of 2 m for depth and 3 h for time, was used to map each observation onto the depth-time grid. An optimal interpolation increment was then calculated, again using the Gaussian weighting function, to calculate the final gridded field. The longitudinal positions of the gliders were then used to create a single glider data set. The two dimensional (depth-time) optimally interpolated fields from each of the four gliders were combined into a single three-dimensional (longitude-depth-time) gridded dataset, by linearly interpolating over longitude.

Observed fluorescence from gliders was corrected for non-photochemical quenching during daylight hours using chlorophyll-to-backscatter ratios during night-time (Thomalla et al., 2018). The glider chlorophyll values exhibited an offset~~(Webber et al., 2014)~~, similar to that found by Webber et al. (2014) , with higher concentrations compared to the concurrent observations from the shipboard CTD. However, the glider data is reliable to explain the processes underlying the bloom evolution since the spatial and temporal variability of chlorophyll were consistent with the CTD observations. For the present analysis, the glider data corrected for non-photochemical quenching was scaled to represent in situ chlorophyll value using the CTD data. An independent scale factor was calculated for each glider's ECOPuck using linear regression with the available nearby CTD profiles, where the distance between the ship and glider is not more than a quarter degree and the time difference is not more than an hour.

2.2 Coupled physical-ecosystem model

A coupled physical-ecosystem model was employed to study the observed chlorophyll distribution in the southern BoB during the BoBBLE field program. The physical model is based on the Geophysical Fluid Dynamics Laboratory (GFDL) Modular Ocean Model Version 4 (MOM4p1, Griffies et al., 2004), configured for the Indian Ocean region extending from 30°E to 120°E and 30°N to 30°S (Kurian and Vinayachandran, 2007; Behara and Vinayachandran, 2016). Horizontal resolution of the model is 0.25° and the vertical grid spacing is 5 m in the upper 60 m, increasing to 10 m at 100 m depth, 20 m at 200 m depth, and 700 m at 5000 m depth, altogether forming 40 levels. The ETOPO5 dataset with 5 min resolution is used to set up the model topography, with the minimum depth of the ocean fixed at 30 m. A no-flux condition is applied across the model boundaries. Additionally, a no-slip condition is applied on the closed western and north-

ern boundaries. The open southern and eastern boundaries consist of sponge layers where temperature and salinity fields are relaxed to climatology (Conkright et al., 1998) with a time scale of 30 days. The model mixing schemes are based on Large et al. (1994) and Chassignet and Garraffo (2001). Turbulent fluxes and upwelling longwave radiation are calculated using the bulk formula (Large and Yeager, 2004) and the penetrative shortwave radiation is parameterised based on Morel and Antoine (1994).

The ecosystem model used in this study is the Tracers of Phytoplankton with Allometric Zooplankton (TOPAZ) model (Dunne et al., 2010) consisting of 25 tracers including micro- and macro-nutrients, carbon, oxygen and lithogenic materials. The biogeochemical cycles are calculated with flexible nutrient stoichiometry. The phytoplankton class consists of three groups: small, large and diazotrophs. The small group represents the nanoplankton, which are weakly limited by nutrients and strongly limited by grazing. The large group represents the microplankton, which are strongly limited by nutrients and weakly limited by grazing, with the ability to store iron internally. Diazotrophs (nitrogen fixers) form a relatively small fraction of the total biomass (Gnanadesikan et al., 2011). The model also includes dissolved organic matter and heterotrophic biomass. The biogeochemical mechanisms consist of nitrogen fixation, denitrification, gas exchange, atmospheric decomposition, scavenging and sediment processes. Co-limitation by light and nutrients controls the phytoplankton physiology and growth (Geider et al., 1997), with a temperature dependency (Eppley, 1972). Grazing is parameterized using a size-based relationship (Dunne et al., 2005), in which the large (small) phytoplankton group dominates the ecosystem at high (low) growth rates and biomass. Detritus production is temperature dependent and calculated as a fraction of phytoplankton (Dunne et al., 2005). Nitrification is inhibited by light (Ward et al., 1982). A detailed technical description of the ecosystem model is available in Dunne et al. (2010).

The model configuration used in the present analysis is similar to that in Thushara and Vinayachandran (2016). The physical model was spun up for a period of 10 years, starting from a state of rest using climatological initial fields for temperature and salinity (Conkright et al., 1998). This was followed by a coupled spin up for another 10 years, after switching on the ecosystem model. ~~The succeeding interannual run was performed~~ A stable annual cycle was obtained for both physical and biological fields after the spin up and this was followed by an interannual run from 01 April 2015 to 31 December 2016. Nutrients for initialising the ecosystem model were obtained from the World Ocean Atlas (WOA09) and no-flux conditions applied at the open boundaries. The model forcing fields include air temperature, specific humidity, surface pressure, downward shortwave and longwave ~~radiations~~radiation fluxes, at hourly frequency from Goddard Earth Observing System (GEOS) Modern Era Retrospective-analysis for Research and Applications, Version 2 (MERRA-2 ; Rienecker et al., 2011). Wind speed and wind stress forcings were obtained from Advanced Scatterometer (ASCAT; Figa-Saldaña et al., 2002). The model freshwater forcings include daily precipitation from Tropical Rainfall Measuring Mission (TRMM; Huffman et al., 2007) and monthly climatological river runoff from the Centre for Sustainability and the Global Environment (SAGE; Vörösmarty et al., 1996). Weekly chlorophyll from Sea-Viewing Wide Field-of-View Sensor (SeaWiFS; Sweeney et al., 2005) was used for the calculation of penetrative shortwave radiation.

3 Results and Discussion

The BoBBLE field program coincided with a suppressed phase of the Boreal Summer Intraseasonal Oscillation (BSISO), when the convective activity was weak over the southern BoB (see Figure 4 of Vinayachandran et al. (2018)). Precipitation was minimal during most of the observational period, un-

til the establishment of the succeeding active phase of the BSISO by the end of the program. Surplus insolation associated with reduced atmospheric convection suggests that light availability only played a minor role in limiting the ~~chlorophyll distribution, which makes the observational period ideal to study the bloom dynamics. Prior to the BoBBLE period, the region was characterised by increased~~ surface chlorophyll distribution. In the presence of heavy cloud cover associated with the ~~preceding active phase of the BSISO. Winds were stronger but solar insolation was lower, indicating significant light limitation on bloom generation during this period. Similar conditions re-established by the end of the BoBBLE period, in relation to the succeeding active phase.~~ monsoon, light availability is generally believed to limit the growth of phytoplankton in the Bay of Bengal. However, observational evidences also show that light is not an important limiting factor in the low latitudes (Laws, 2013 ; Behrenfeld and Boss, 2017), where the phytoplankton growth is mainly determined by nutrient availability (Moore et al., 2013). According to a recent study in the northern BoB by Jyothibabu et al. (2018) , high PAR conditions were associated with low surface chlorophyll, and during low PAR conditions chlorophyll levels increased considerably.

Monsoonal cloud cover, especially during the active phase of BSISO, limits the continuous sampling of ocean color from satellites, restricting the analysis of daily or weekly evolution of the ~~blooms. Monthly means of chlorophyll~~ chlorophyll blooms. Ocean color data obtained from European Space Agency (ESA) Ocean Colour Climate Change Initiative (OC-CCI v3.1) merged product reveal that the southern bay ~~was biologically active~~ exhibited high chlorophyll levels during the BoBBLE period. The mean chlorophyll concentration in the southern bay (82–92° E and 4–12° N) averaged for the month of July was about 0.2 mg m^{-3}, which is comparable to that of the previous years.

3.1 Hydrography

To provide a dynamical context for the chlorophyll distribution, the hydrography of the southern BoB during the BoBBLE period is briefly described here. Further details can be found in Vinayachandran et al. (2018) and Webber et al. (2018). In response to the prevailing atmospheric conditions, the upper ocean in the southern bay exhibited large spatial variability at seasonal and synoptic timescales. The climatological distribution of surface temperature shows cooler waters in the region of the SMC, creating an east-west contrast along 8°N (see Figure 1 of Vinayachandran et al. (2018)). Weaker winds and higher insolation, associated with the suppressed phase of BSISO during the observational period, resulted in high sea surface temperature (SST). The mean SST obtained from the Group for High Resolution Sea Surface Temperature (GHRSST; Chao et al., 2009) dataset, averaged for the observational period (27 June–21 July 2016), was ∼29.3 °C at TSW and ∼0.5 °C less at TSE~~(not shown)~~, deviating from the climatology. The mean sea surface salinity (SSS) from the Soil Moisture Active Passive (SMAP; Fore et al., 2016) mission was ∼33.3 psu at TSW and farther east at TSE, salinity was 0.8 psu higher~~(not shown).~~ .

A depth-longitude section of temperature and salinity recorded by gliders, averaged for the period 03–14 July, is shown in Fig. 2. Gliders in the west (SG579 and SG532) exhibited higher SST and lower SSS compared to those in the east (SG534 and SG620), consistent with the satellite observations. The thermocline, represented by the 20 °C isotherm (D20), ~~exhibits~~ exhibited an east-west dip along 8°N extending from TSW till 88°E, followed by a rise towards TSE (Fig. 2a). The western sector of the transect (TSW) lies within the SLD, where ~~open ocean Ekman pumping~~ open-ocean Ekman suction leads to the doming of the thermocline. At TSW, D20 ~~is~~ was located at a depth of about 80 m, as observed by SG579, and ~~deepens~~ deepened towards the east. In the region of the high salinity core of the SMC

intrusion (Fig. 2b), D20 ~~is~~ was much deeper, located at a depth of about 180 m (SG532). At the eastern end of the transect (TSE), D20 slightly ~~shoals~~ shoaled by about 40 m, as observed by SG620.

Circulation in the southern bay during the observational period is characterised by a strong cyclonic gyre in the region of the SLD and the monsoon current which flows north-eastward (Webber et al., 2018). During the beginning of the observational period, the SMC was strong with surface velocities ranging between 0.5-0.8 m s^{-1} (Fig. 3a-g). The region of the SLD ~~is~~ was characterised by strong negative sea level anomalies (SLA) of about ~~-20~~ −20 cm. By the end of the first week of July, the SMC weakened and shifted westward, reducing the zonal extent of the SLD (Fig. 3h-l). Farther east, towards the eastern edge of the monsoon current, the upper ocean was relatively less dynamic with weaker currents (0.1–0.3 m s^{-1}) and positive sea level anomalies (10–20 cm).

The spatial variability in the upper ocean dynamics of the BoB, determined by local and remote forcings associated with the monsoon, influence the ~~biological response~~ chlorophyll distribution as well, which is of interest in the present study. The following sections characterise the observed chlorophyll in the southern bay in terms of intensities and the vertical distribution, during the BoBBLE period. The associated mechanisms determining the chlorophyll distribution are analysed, combining hydrographical observations and results from an ecosystem model.

3.2 Observed chlorophyll distribution

3.2.1 Surface bloom events

The gliders cover an east-west transect across the regions of the SLD and SMC (Fig. 1), providing time series measurements of chlorophyll. Surface layers remained weakly productive during most of the ob-

servational period, however, events of enhanced chlorophyll were observed at all the four glider locations (Fig. 4a-d) as well as in the CTD data (Fig. 4e). Surface chlorophyll concentrations from gliders and the CTD are shown in Fig. 5. During the beginning of the observational period, concurrent occurrence of ~~surface blooms~~ elevated chlorophyll levels were observed within the SLD and along the path of SMC, as recorded by SG579, SG534 and SG532. At SG620 (TSE), two events were recorded with relatively weaker magnitudes of chlorophyll compared to the other glider locations. CTD measurements captured the surface ~~blooms~~ chlorophyll events in the region of SMC during 01–02 July and at TSE during 06–08 July, consistent with the glider observations. The ship and glider were about 10 km apart during most of the observational period at TSE and hence an exact agreement in chlorophyll time series is not expected.

Within the SLD: Summer chlorophyll blooms in the region of the SLD have been reported earlier using satellite images of ocean color (Vinayachandran et al., 2004). The daily evolution of SLA and currents from Archiving, Validation, and Interpretation of Satellite Oceanographic data (AVISO) show the intensification of the SLD during the early ~~phase~~ part (29 June–03 July) of the BoBBLE field program (Fig. 3). Observations from SG579, which falls right inside the dome, revealed the development of a surface chlorophyll bloom during the same period (Fig. 4a, 30 June–2 July). Chlorophyll concentration at the surface was $\sim$ 0.3 mg m^{-3} on 30 June, increased to $\sim$ 0.7 mg m^{-3} on 01 July and reduced to $\sim$ 0.4 mg m^{-3} on 02 July (Fig. 5~~a~~). CTD observations were available within the dome during 28–29 June, before the ship started moving eastwards from TSW. Until 29 June, surface chlorophyll values were much lower ($<$ 0.1 mg m^{-3}), with higher concentrations mostly confined to a depth of about 30–60 m (Fig. 4e). Hence, it can be inferred that the surface ~~blooms~~ chlorophyll bloom within the dome probably commenced on 30

June, peaked on 01 July and started decaying on 02 July. There were no glider observations of chlorophyll before 30 June to corroborate the CTD data.

The ~~region~~ observed increase in surface chlorophyll at SG579 coincided with the intensification of the SLD~~is~~ , characterised by negative SLA embedded within the cyclonic circulation to the east of Sri Lanka (Fig. 3). ~~The hydrodynamics of~~ Time series of minimum SLA in the region of the dome shows that the SLD attained its peak by the ~~region suggests that the triggering mechanism for bloom generation is open ocean Ekman pumping forced by positive wind stress curl (Vinayachandran et al., 2004 ; Wijesekera et al., 2016a), favouring vertical transport of nutrients to the surface sunlit layers. The doming of the thermocline indicates dynamical uplifting of the nutricline and enhanced nutrient concentrations in the euphotic zone (Wilson and Coles, 2005 ; Turk et al., 2001).~~ end of June (Fig. 6a). Sea level anomalies decreased to about −0.3 m on 30 June. The thermocline was shallow, located at a depth of about 70 m, during the peak phase of the surface chlorophyll bloom (01 July, Fig. 4). The doming of the thermocline indicates dynamical uplifting of the nutricline and enhanced nutrient concentrations in the euphotic zone (Wilson and Coles, 200 Turk et al., 2001). The chlorophyll bloom event was characterised by lower surface temperatures (28.6 °C) and higher surface salinities (33.95 psu) with upsloping isotherms and isohalines (not shown), compared to the period when the surface chlorophyll concentrations were weak. The decay of surface chlorophyll bloom after 02 July (Fig. 5) followed the weakening of the dome (Fig. ~~3~~6a). Surface temperature increased by 0.7 °C and surface salinity decreased by ∼1.5 psu on 03 July~~, indicating the weakening of upwelling~~. The weakening of the dome indicates reduced upwelling of the subsurface nutrients. Nutrient limitation restrains the growth of phytoplankton leading to the decay of surface blooms, when the biological loss terms dominate. CTD observations within the dome until 29 June, when the ship was at TSW, show

that the subsurface chlorophyll concentrations were weak (< 0.5 mg m^{-3}) just before the surface ~~bloom~~ chlorophyll event (Fig. 4e). This indicates that the surface chlorophyll bloom is not probably a result of the vertical redistribution of subsurface phytoplankton~~does not have significant contribution in enhancing the~~ . On the other hand, the vertical transport of subsurface nutrients to the near-surface layers can favour the growth of phytoplankton in the given time scales (Laws, 2013), leading to the intensification of surface chlorophyll. ~~The generation of surface blooms~~ Though the evolution of observed chlorophyll follows the dynamics of the study region, the concurrent role of biological loss terms including grazing, mortality and sinking rates cannot be ignored, which requires additional data sampling.

The southern BoB was characterised by cyclonic windstress curl, inducing Ekman suction during the field program. The vertical transport of nutrients to the surface sunlit layers through Ekman suction favours the generation of phytoplankton blooms (Vinayachandran et al., 2004 ; Wijesekera et al., 2016a). Spatial distribution of Ekman vertical velocities, calculated using ASCAT winds, averaged for the BoBBLE observational period (24 June – 23 July) indicates widespread upwelling in the southern BoB (Fig. 6b). Time series of Ekman vertical velocities in the location of SG579 shows that Ekman suction peaked to about 2–3 m day^{-1} by mid-June (Fig. 6a). Ekman vertical velocities remained to be upwelling favourable (0.4–0.7 m day^{-1}) during the period of surface bloom (30 June–02 July), though the magnitudes were relatively weaker. Strong upwelling in the second half of June, prior to the surface chlorophyll event, is presumed to ~~be dominantly controlled by the vertical transport of subsurface nutrients to the euphotic zone~~provide a favourable preconditioning by lifting the nitracline towards the surface.

During the decaying phase of the SLD in July, Ekman vertical velocities were positive, with peak values of about 2 m day^{-1} (Fig. 6a). This indicates the dominant influence of remote effects propagating from the

eastern boundary of the BoB (Vinayachandran and Yamagata, 1998 ; Shankar et al., 2002 ; Wijesekera et al., 2016a ; Burns et al., 2017 ; Webber et al., 2018). A time-longitude hovmoller diagram of SLA from AVISO during May-July along 8°N, between 80-100°E is shown in Fig. 6c. The decay period of the SLD coincides with the arrival of positive SLA from east, representing the westward propagation of downwelling Rossby waves (Webber et al., 2018). Rossby waves propagating from the eastern boundary of the BoB can influence the depth of thermocline (nitracline) in the study region. This shows that, despite the Ekman suction, remote forcings contributed to the weakening of the SLD and hence the chlorophyll distribution. As far as surface chlorophyll is concerned, the proximity of nutricline to the surface is of primary concern. Results from the ecosystem model have been used to identify the dominant forcings controlling the vertical displacement of nitracline (see section 3.3.1).

Along the path of SMC: Increased surface chlorophyll levels were observed at SG534 and SG532 during 1–2 July (Fig. 4b) and 2–4 July (Fig. 4c) respectively. Both gliders were located along the path of the SMC, with SG532 in the region of the subsurface high salinity core (Fig. 2b). Surface chlorophyll concentration ~~peaks at~~ peaked to about 0.35 mg m^{-3} and 0.4 mg m^{-3} at SG534 and SG532 respectively (Fig. 5). ~~The bloom events were~~ This increase in chlorophyll was associated with lower temperatures (28.7 °C and 29.1 °C for SG532 and SG534 respectively) and higher salinities (34.4 psu and 34 psu for SG532 and SG534 respectively) at the surface, compared to the period when the ~~surface blooms were absent~~chlorophyll levels were weak.

Along the path of the SMC, ~~the thermocline lies at deeper levels during the surface bloom events~~ when the surface chlorophyll levels were high, the thermocline was deep (∼100–130 m at SG534 and ∼160–

180 m at SG532), which is 40–100 m deeper than that in the region of the dome (Fig. 4a-c). The spatial variability of thermocline is evident from the CTD observations as well, showing a shallow thermocline during the beginning (27–30 June) and end (20–21 July) of the field program, when the ship was in the west, and a deeper thermocline farther east (02–18 July; Fig. 4e). A deeper thermocline generally indicates a deeper nitracline and stronger nutrient limitation in the surface layers. At the same time, the region of SMC is also subject to an additional supply of biologically rich waters advected from the coasts of India and Sri Lanka (Vinayachandran et al., 2004). In addition, the possibility of lateral advection of nutrients and chlorophyll generated within the SLD to the nearby glider locations cannot be ignored (see Section 3.3.2).

Mixing events: Chlorophyll distribution observed outside the dome, farther east at TSE, differed from that in the region of the SLD and SMC, in terms of intensity as well as the vertical structure. SG620 ~~shows~~ captured two events of ~~surface blooms~~enhanced surface chlorophyll; the first ~~event~~ on 03 July and the second during 06–08 July (Fig. 4d). The surface chlorophyll concentrations were $\sim$0.3 mg m^{-3} during ~~the bloom~~ both the events (Fig. 5)~~. Both bloom events were characterised by cool~~ , characterised by low surface temperatures and high surface salinities. The observed SST from SG620 was about 28.7 °C on 03 July and 28.8 °C on 06 July. Surface salinities were about 34.5 psu and 34.7 psu during 03 July and 06 July respectively. Temporal coverage of the first event is insufficient to explain its evolution since the ~~bloom decays~~ chlorophyll bloom decayed immediately after 03 July, when the sampling ~~begins~~began. Wind speed measured by the shipboard automatic weather station (AWS) was 5–9 m s^{-1} during 03 July (Fig. 7). A deeper mixed layer depth (MLD) of about 60 m during ~~the bloom event~~ this period indicates

that vertical mixing is presumably the primary factor which favoured the increase in surface chlorophyll. The second event was captured by the CTD measurements as well (Fig. 4e), consistent with the glider data. This event coincided with a phase of increasing wind speed of about 6–11 m s^{-1} (06–07 July; Fig. 7). Subsequent deepening of the mixed layer (∼70 m, Fig. 4d) suggests the role of mixing and entrainment in triggering the ~~surface blooms~~intensification of surface chlorophyll. Enhanced vertical processes favour intensification of surface chlorophyll by transporting nutrients to the euphotic zone and by redistributing the subsurface chlorophyll to the surface layers.

~~Intermittent occurrence of freshening events were observed at the surface, associated with local precipitation and lateral advection, the latter being prominent.~~ The decay period of the ~~bloom (08–10 July~~observed surface chlorophyll blooms (Fig. 5) coincided with the development of ~~a freshening event. Surface salinity decreased by about 0.8 psu from 06 July to 10~~ intermittent freshening events at the surface; the first during 04-05 July and the second during 07-10 July. The initial drop in surface salinity during the freshening events was ∼0.4 psu on 04 July and 07 July (Fig. 7)~~and the corresponding decrease in surface chlorophyll was about~~ . The surface chlorophyll decreased by about 0.3 mg m^{-3} and 0.27 mg m^{-3} during the first and second freshening events respectivey (Fig. 5). There was an overall reduction in total chlorophyll integrated over the mixed layer by about 20 mg m^{-2} during both the freshening events (Fig. 7). ~~Freshening could be attributed to the lateral advection of low saline waters from the nearby regions, since no local rainfall was observed during this period~~

The freshening events were characterised by the formation of barrier layers (Vinayachandran et al., 2018). Vertical profiles of temperature, salinity and chlorophyll from SG620 during different stages of

the surface bloom evolution are shown in Fig. 8~~a-c~~a-e. During the peak of the surface chlorophyll ~~bloom (~~blooms (03 and 06 July), the mixed layer was deep (~~55~~ 50–55 m), with an almost uniform distribution of bio-physical properties (Fig. 8a and c), and the isothermal layer ~~depth coincided with the MLD. The following days (~~was close to the mixed layer. The days following the peak in surface chlorophyll (04–05 July and 08–10 July) were characterised by strong salinity stratification with the arrival of freshwater in the surface layers. ~~The mixed layer shoaled to ~30 m~~ Surface salinity decreased by about 0.25 psu and 0.75 psu for the first and second events respectively (Fig. 8b and ~~c)~~e). The mixed layer shoaled to ~30 m, whereas the isothermal layer remained around the same depth (Fig. 8b, d and e). The associated development of ~~a barrier layer~~ barrier layers is noticeable, with a thickness of ~25–30 m. ~~CTD observations at TSE also captured this freshening event and the subsequent decay of the surface bloom (~~Following the salinity stratification and barrier layer formation, surface chlorophyll decreased by about 0.1 mg m^{-3} and 0.15 mg m^{-3} during the first and second events respectively. Vertical profiles obtained from CTD at TSE for the same period are given in Fig. 8~~d-f)~~f-j. With the arrival of freshwater, surface salinity ~~as recorded by~~ from the CTD decreased by about 0.25 psu and 0.5 psu during the first and second events respectively, and the corresponding decrease in surface chlorophyll was 0.1 mg m^{-3} and ~~the mixed layer~~ 0.15 mg m^{-3} respectively. The mixed layers shoaled by about ~~25~~ 25–30 m, creating ~~a strong barrier layer~~ strong barrier layers (Fig. 8~~f). The corresponding decrease in surface chlorophyll was ~0.15 mg m^{-3}.~~

~~Freshening and the barrier layer formation inhibit the development of phytoplankton blooms in the surface layers by restricting vertical transport of subsurface nutrients and chlorophyll~~g, i and j). Even though high wind speed (~10–12 m s^{-1}) conditions prevailed during the decay period of the bloom, freshwater induced stratification was strong enough to overcome the wind effect (Fig. 7). The observed

biological response to freshwater is similar to that in the northern bay, where ~~salinity stratification restrains the growth of phytoplankton by inducing nutrient limitation~~ stratification inhibit the development of phytoplankton blooms in the surface layers by restricting the vertical transport of subsurface nutrients and chlorophyll (Kumar et al., 2002).

3.2.2 Deep chlorophyll maxima

~~Chlorophyll maxima at the subsurface are indicative of active biological productivity beneath the surface layers of the ocean.~~ The formation of deep chlorophyll maxima (DCM) is determined by a variety of mechanisms including enhanced growth rate of phytoplankton colimited by light and nutrients at optimum depths, photoacclimation of pigment content, and physiologically controlled swimming behaviors and buoyancy regulation (Cullen, 2015). The BoB is reported to have prominent DCM (Murty et al., 2000; Madhu et al., 2006), which contribute to the column integrated productivity (Gomes et al., 2000; Madhupratap et al., 2003; Li et al., 2012) with magnitudes often comparable to the highly productive Arabian Sea (Kumar et al., 2009). However, little is known about the distribution of subsurface chlorophyll in the BoB and the associated processes, due to the lack of observations.

During the BoBBLE field program, both the glider and CTD observations revealed the presence of prominent DCM in the southern bay (Fig. 4 and Fig. 9a). The chlorophyll maxima were centered at a depth of about 20–50 m, mostly below the mixed layer and above the thermocline (Anderson, 1969). Similar depth ranges of DCM were reported previously by Gomes et al. (2000) and Kumar et al. (2009) in the BoB. Subsurface chlorophyll concentrations ~~range~~ ranged from 0.3–1.2 mg m^{-3} (Fig. 9a), which were ~~2–3~~ 2–3 times higher than the surface values (Fig. 5). DCM were prominent in the region of the SLD

and along the path of the SMC (Fig. 4a-c), whereas outside the dome, the subsurface concentrations were weaker (Fig. 4d).

Vertical profiles of chlorophyll from the gliders during events of enhanced surface chlorophyll are shown in Fig. 10. The mean DCM was intense, located at a depth of about 20–30 m, in the region of the SLD and the SMC (Fig. 10a-c). The DCM became weaker, diffused and slightly deeper (~~30-40~~ 30–40 m) at TSE (Fig. 10d and e). Intensification of DCM in the region of SLD can be related to the doming of thermocline~~, followed by~~ . The vertical transport of nutrients is affected by the changes in thermocline depth and hence, the variability of nutricline is found to be largely correlated with the variability of thermocline in the tropical oceans (Turk et al., 2001 ; Wilson and Adamec, 2002 ; Wilson and Coles, 2005). The shoaling of thermocline in the region of the SLD indicates an upward sloping of nutricline~~. A shallow nutricline enriches~~ , indicating nutrient enrichment in the euphotic zone ~~with limiting nutrients, enhancing the~~ and enhanced growth of phytoplankton. At TSE (SG620), where the thermocline was deeper, ~~indicating a deeper nutricline and stronger nutrient limitation in the euphotic zone. During the surface bloom events,~~ mixing often penetrated to deeper layers pushing the mixed layer towards the DCM (Fig. 4d and e). This favours the dilution of DCM and a decrease in phytoplankton concentration at the subsurface through mixing with the weakly productive surface layers, leaving a near homogeneous distribution of chlorophyll within the water column (Fig. 10d and e).

Subsurface chlorophyll concentrations were noticeably higher in the region of the SMC (Fig. 4c and Fig. 10c). Maximum intensities were recorded by SG532, with magnitudes ranging from 0.7–1.2 mg m^{-3} during 02–07 July (Fig. 9a). Column-integrated chlorophyll was also observed to be the highest at SG532 (04 July), with total chlorophyll in the top 100 m reaching as high as 35 mg m^{-2} (Fig. 9b), which is

comparable to the previously observed values in the BoB (Gomes et al., 2000; Madhupratap et al., 2003; Kumar et al., 2009; Li et al., 2012). The region of SMC is characterised by the advection of upwelled chlorophyll rich water from the west coast of India and the southern coast of Sri Lanka. An isolated maximum (1.2 mg m^{-3}) in the DCM was recorded by SG579 in the region of SLD in the later half of the observational period (15 July). However, in the absence of surface blooms, the corresponding column-integrated chlorophyll was lower (28 mg m^{-2}), compared to the region of the SMC.

The core subsurface intrusion of the SMC, below the low salinity surface waters of the southern bay was located around SG532 during the observational period (Vinayachandran et al., 2018; Webber et al., 2018). The vertical salinity structure reveals a high salinity core at 88°E, extending up to a depth of about 180 m, with salinity values as high as 35.8 psu (Fig. 2b). Arabian Sea water, which is rich in nutrients and chlorophyll sliding through the subsurface layers of the BoB, is presumed to be contributing to the intensification of the DCM at SG532, suggesting a key role of SMC intrusion in the biological budget of the southern bay. However, it may be noted that the location of the subsurface high salinity core was much deeper relative to the depth of DCM. Most of the high salinity intrusions at 88°E occured below 80 m, in the deeper layers of the euphotic zone. Dynamics behind the distribution of the DCM in the region of the high salinity core are intricate. Though the effect of lateral advection by the SMC on DCM cannot be ignored, the possible contribution of vertical processes in supplying the subsurface nutrients or chlorophyll needs to be examined in detail.

Subsurface chlorophyll concentrations were observed to intensify for shorter durations following the weakening of surface blooms (Fig. 4). Increases in DCM concentrations after the decay of surface blooms were about 0.13 mg m^{-3}, 0.37 mg m^{-3} and 0.25 mg m^{-3} at SG534, SG532 and SG620 respectively

(Fig. 9a). In the region of the SLD (SG579), the subsurface chlorophyll concentrations increased to ∼0.7 mg m^{-3} during the peak phase of the surface bloom (01 July). During the decaying phase of the surface bloom (02-05 July), these high chlorophyll levels (0.7 mg m^{-3}) were maintained at the subsurface and weakened afterwards (Fig. 9a). This indicates enhanced biological productivity at the subsurface, after the triggering mechanisms inducing the surface blooms have weakened. During the decaying phase of surface blooms, the upper layers of the water column became less turbulent or more stably stratified (Fig. 8), inhibiting the vertical transport of nutrients and chlorophyll. However, the subsurface layers still possess enough nutrients to support phytoplankton growth. For example, the surface bloom event at SG620 weakened in response to the freshening event on 08 July (Fig. 8b). Consequently, there was an increase in DCM, which lasted for a period of about ~~2-3~~ 2–3 days from 10–12 July (Fig. 9a). The observed intensification of DCM in the absence of surface chlorophyll can be explained in terms of changes in subsurface irradiance levels. During the decaying phase of the surface bloom, the self-shading effect of surface phytoplankton weakens, enhancing the light availability at the subsurface, which is examined in the following section.

3.2.3 Role of light limitation

Chlorophyll interactive penetrative radiation was calculated at TSE for the period 04-14 July, following Morel and Antoine (1994) and Manizza et al. (2005) scheme as given below,

$$I_{(z)} = I_{IR} \cdot e^{-k_{IR}z} + I_{RED(z-1)} \cdot e^{-k_{(RED)}\Delta z} + I_{BLUE(z-1)} \cdot e^{-k_{(BLUE)}\Delta z}$$

$I_{(z)}$ is the penetrative radiation at each depth level, $I_{IR} = I_0 \cdot (0.58)$ represents the infrared band, $I_{VIS} = I_0 \cdot (0.42)$ represents the visible band and $k_{IR} = 2.86$ m^{-1} is the light attenuation coefficient for the infrared

band. The self-shading effect of phytoplankton is taken into account so that at every vertical level (z), the available visible light is computed as a function of irradiance at the level just above (z-1). Δz is the thickness of each layer between two vertical levels, which is 1 m in the present glider data. Visible light is ~~splitted in~~ split into two averaged wavelength bands as given below,

$$I_{RED} = I_{BLUE} = \frac{I_{VIS}}{2},$$

where I_{RED} and I_{BLUE} are the irradiances in red and blue/green bands respectively.

The light attenuation coefficients for the two visible bands is calculated as a function of chlorophyll concentration ([Chl]) as follows,

$$k_{(RED)} = 0.225 + 0.037 \cdot [Chl]^{0.629}$$

$$k_{(BLUE)} = 0.0232 + 0.074 \cdot [Chl]^{0.674}$$

Surface irradiance (I_0) for the above calculations was obtained from shipboard AWS (Fig. 11a) and chlorophyll from SG620 (Fig. 4d). In order to exclude the effect of daily variation in surface irradiance, a diurnal composite of radiation (Fig. 11a) for the period 4–14 July is also used for the calculations. ~~Estimated penetrative radiation and~~ Photosynthetically active Radiation (PAR) at each vertical level (z) was estimated using the following expression,

$$PAR_{(z)} = I_{vis_{(z)}} \times \frac{2.5 \times 10^{18}}{6.023 \times 10^{23}}$$

where $I_{vis_{(z)}}$ is the penetrative radiation (W m^{-2}) in the visible range calculated using the light model and 2.5×10^{18} quanta s^{-1} W^{-1} is the conversion factor obtained from Morel and Smith (1974) . The depth of euphotic zone (Z_{eu}) was calculated as the depth at which light reduces to 1% of the surface PAR value. Considering the fact that phytoplankton sees the absolute light level and not the percentage (Banse, 2004), the depth of threshold isolume ($Z_{0.415}$) is taken as the depth where PAR is 0.415 E m^{-2} day^{-1} below

which light is insufficient to support photosynthesis (Letelier et al., 2004 ; Boss and Behrenfeld, 2010). An Einstein (E) is a mole of photons, i.e., 6.023×10^{23} photons.

Estimated penetrative radiation (W m^{-2}) using the ~~depth of the euphotic zone using~~ observed surface irradiance and the diurnal composite are shown in Fig. 11b and c respectively. The ~~depth of the euphotic zone is estimated as the depth where irradiance reduces to 1 W m^{-2} (Pastor et al., 2013)~~corresponding depths of euphotic zone and the threshold isolume obtained from the calculated PAR values are overlayed. Nearly 40–60 % of the radiation was absorbed in the top 1 m of the water column and 80–90 % in the top 30 m. Below the DCM, irradiance levels were substantially weaker (< 10 W m^{-2}). During the daylight hours of peak insolation, ~~the euphotic zone~~ $Z_{0.415}$ extended to 70–110 m, with a well defined diurnal cycle.

~~The depth of euphotic zone was least (~~During days of enhanced surface chlorophyll, $Z_{0.415}$ and Z_{eu} were shallow. $Z_{0.415}$ shoaled to a depth of about 70–80 m ~~) during the surface bloom event (~~and Z_{eu} was about ~50 m during the chlorophyll bloom event at the surface on 06–07 July~~), indicating enhanced~~ . The shoaling of the $Z_{0.415}$ and Z_{eu} indicates the self-shading effect of surface phytoplankton. Elevated levels of chlorophyll enhances the absorption of radiation in the surface layers (Fig. 11b). ~~Euphotic depth calculated~~ Calculations using the diurnal composite of irradiance also ~~shows a minimum during the same period~~ give similar results (Fig. 11c). ~~The shoaling of the euphotic zone during the bloom event indicates the self-shading effect of surface phytoplankton.~~ Enhanced attenuation of radiation by near-surface phytoplankton reduces the irradiance levels in the deeper layers and strengthens the light limitation on phytoplankton growth in the subsurface. As a result, bloom activity weakens in the subsurface layers, despite the availability of nutrients.

Following the decay of surface blooms owing to nutrient limitation, ~~the euphotic zone depth~~ $Z_{0.415}$ and Z_{eu} increased due to the penetration of radiation to deeper layers (Perry et al., 2008). ~~The deepening of the euphotic zone following the decay of the surface bloom was~~ $Z_{0.415}$ and Z_{eu} deepened by about 25 m and 10 m respectively on 08 July (Fig. 11b). Enhanced light availability in the subsurface layers favours the intensification of DCM (Fig. 4d,e and Fig. 8). It should be noted that the DCM may not represent a deep biomass maximum as photoacclimation (Cullen, 1982; Geider, 1987; Mateus et al., 2012) leads to changes in carbon to chlorophyll ratios. At the base of the euphotic layer, the cellular concentration of chlorophyll will increase as an adaptation to the lower irradiance levels (Cullen, 2015).

3.3 Model simulation

A coupled physical-ecosystem model, employed to study the aforementioned ~~bloom features~~ bio-physical interactions in the BoBBLE region, enabled further understanding of the three-dimensional mixed layer processes controlling the evolution of chlorophyll blooms. The role of horizontal advection by the SMC and dynamics of the SLD in determining the simulated distribution of nutrients and chlorophyll is analysed in detail. The model provides a fairly good representation of the bio-physical features in the BoB. The physical model reproduces the observed seasonal and intraseasonal features of the Indian Ocean, with a realistic representation of the mixed layer processes and the heat and freshwater budgets (Kurian and Vinayachandran, 2006; Kurian and Vinayachandran, 2007; Vinayachandran and Kurian, 2007; Behara and Vinayachandran, 2016). Basin-averaged SST in the BoB (80–100°E and 0–25°N) for the month of July is about 28.37 °C, with a cold bias of 0.85 °C compared to the GHRSST observations. The seasonal temperature distribution of the southern bay, including the cooling associated with upwelling off the coasts of India and Sri Lanka

and the development of the cold pool, is well represented. The model reproduces the low salinity plumes associated with freshwater influx in the northern bay and high salinity intrusions from the Arabian Sea into the southern bay. Mean surface salinity for the basin is about 32.59 psu for the month of July, which exceeds SMAP observations by about 0.6 psu. The intrusion of the SMC into the BoB and its bifurcation into several branches is reproduced by the model. The vertical distribution of salinity reveals intermittent occurrence of high salinity cores at deeper levels, associated with the subsurface intrusion of the SMC. The model reproduces a well-developed SLD, characterised by negative SLA (-10 cm) embedded within the cyclonic circulation east of Sri Lanka, consistent with the AVISO observations.

The TOPAZ ecosystem model simulates well the mean distribution of oceanic productivity (Sarmiento et al., 2010; Pastor et al., 2013; Marvasti et al., 2016) and the biophysical interactions associated with major climatic events including Indian Ocean Dipole, El Niño Southern Oscillation and Atlantic Multidecadal Oscillation (Park and Kug, 2014; Park et al., 2014; Gnanadesikan et al., 2014). The model provides a realistic representation of the monsoonal biophysical interactions in the Indian Ocean and has been used to explain the bloom dynamics of northwestern BoB during the summer monsoon (Thushara and Vinayachandran, 2016) and northeastern Arabian Sea during winter (Vijith et al., 2016).

For the present analysis, simulated surface chlorophyll is validated using monthly means obtained from the OC-CCI merged product. The observed spatial distribution of surface chlorophyll, averaged for the month of July, to be consistent with the BoBBLE period, is shown in Fig. 12a. Along the path of the SMC, a distinct band of ~~moderate blooms~~ chlorophyll is present with concentrations of about 0.3–0.6 mg m^{-3}. The band extends from the southern coast of Sri Lanka up to about 11°N and 89°E, indicating lateral transport of nutrients and chlorophyll carried by the SMC from the upwelling regions off the coasts of

India and Sri Lanka. Seasonal evolution of chlorophyll in the region of the SLD is not well captured by the satellites, probably because of gaps in the ocean colour retrieval during the peak phase of the dome (29 June to 02 July). Moderate ~~blooms~~ chlorophyll concentrations (0.2–0.3 mg m^{-3}) are observed in regions farther east and southeast of the monsoon current.

3.3.1 Simulated chlorophyll distribution

The observed spatial distribution of surface chlorophyll in the BoB is well represented by the model (Fig. 12b), with prominent chlorophyll blooms in the coastal ocean, northwestern bay and the southern bay (Vinayachandran, 2009). ~~Bloom intensities are~~ Chlorophyll concentrations are the highest along the coastal regions, with magnitudes exceeding 1 mg m^{-3}. The northwestern bay is characterised by the seasonal occurrence of upwelling blooms triggered by coastal Ekman ~~pumping~~ suction and advection towards the offshore regions (Thushara and Vinayachandran, 2016). The southern bay exhibits ~~an isolated patch~~ isolated patches of chlorophyll in the region of the SLD and ~~moderate blooms~~ along the path of the SMC. Surface ~~bloom~~ chlorophyll concentrations are about 0.6–0.7 mg m^{-3} and 0.3–0.4 mg m^{-3} in the region of the SLD and the SMC respectively. The model ~~blooms are~~ chlorophyll is generally weaker compared ~~with~~ to satellite observations. The bias can be attributed either to the deficiencies in external nutrient inputs in the model or the overestimation of coastal blooms by satellites in the presence of optically active constituents other than chlorophyll (Gregg and Casey, 2004; Blondeau-Patissier et al., 2014). The presence of DCM is well represented by the model, consistent with the glider and CTD observations. Realistic representation of the chlorophyll distribution indicates that the model is ~~good at simulating monsoonal bio-physical interactions in the BoB~~suitable for explaining the underlying mechanisms. It may

also be noted that the model parameterisations on different biological controls can lead to biases in the simulated fields and processes with respect to the actual observations. For example, the model includes implicit representation of grazing and hence, loss of phytoplankton though grazing is independent of the zooplankton biomass.

While the major seasonal features of the southern BoB are reproduced by the model, they are often not exactly at the observed locations. For example, the SLD is slightly shifted westward and the meandering of the SMC around Sri Lanka is weaker (Fig. 12c and d), probably due to the discrepancies in the model wind forcing or the simulated remote forcings. The eastward (northward) extension of surface chlorophyll associated with the SMC is overestimated (underestimated). These inaccuracies can be ignored while examining the large-scale seasonal features, but may be significant at mesoscales or smaller scales. Hence, the ecosystem model results are used to explain the biological response to seasonal features including the Sri Lanka dome and the monsoon current, in comparison with the concurrent observations from gliders (SG579, SG534 and SG532) and the shipboard CTD.

The model SLD develops around 85°E, 8°N, close to the sampling location of SG579. A longitudinal transect extending from 82°E to 92°E along 8°N is selected to examine the vertical distribution of temperature, salinity, nitrate and chlorophyll on 01 July, during the peak phase of the surface chlorophyll bloom in the region of the SLD (Fig. 13). The region is characterised by an intense chlorophyll bloom ($\sim$ 0.5–0.8 mg m^{-3}) at the surface and a prominent DCM ($\sim$ 0.5~~-1.2~~ –1.2 mg m^{-3}). The DCM lies below the mixed layer, centered at a depth of about ~~20-30 m(Fig. 13a), well below the mixed layer~~ 20–30 m, and is about 10–30 m shallower than the nearby regions (Fig. 13~~b~~a). Temperature profiles show upsloping isotherms, providing cooler (27 °C) waters to the surface layers (Fig. 13b). Similarly, the salinity distribution shows

increased surface salinity (33.5 psu) with isohalines shoaling to the surface (Fig. 13c). Doming of the thermocline (D20) is evident between 83–87°E along the transect (Fig. 13b). The thermocline rises to a depth of ∼60 m, which is about 80 m shallower than the nearby regions outside the dome.

The surface layers were enriched with high nitrate concentrations in excess of 10 μmol kg^{-1} (Fig. 13a). By the second week of July, cyclonic circulation in the region of dome weakened and shifted towards the northwest followed by the weakening of chlorophyll.

The dynamics of the SLD favour biological productivity through the vertical transport of nutrients ~~triggered~~ induced by open ocean upwelling (Vinayachandran et al., 2004; Vinayachandran, 2009). The ~~modelled~~ time series of minimum SLA in the region of the SLD shows that the modelled dome peaked on 28 June (Fig. 14), two days prior to the observed peak. The simulated chlorophyll bloom intensifies during the peak phase of the dome and decays with the weakening of the dome, consistent with the BoBBLE observations. The ~~nitracline shoals~~ developing phase of simulated SLD (14-28 July) was characterised by the shoaling of nitracline (Fig. ~~13a)along with the vertical displacement of isotherms and isohalines~~14). We prefer using the 2 μmol kg^{-1} nitrate isoline as the nitracline rather than the vertical gradient criterion, since the absolute concentration of nutrients available for phytoplankton uptake is more important for bloom generation than the gradients (Wilson and Coles, 2005). The ~~euphotic zone is enriched with high nitrate concentrations in excess of 10 μmol kg~~shoaling rate of the nitracline increased to about 1.0 m day^{-1} ~~. The DCM shoals to about 30 m, which is 10–30 m shallower than the nearby regions. By the second week of July, cyclonic circulation in the region of dome weakens and shifts towards the northwest. The subsequent reduction in Ekman pumping leads to the decay of the bloom due to nutrient limitation~~by mid-June and closely followed the Ekman vertical velocities. This shows that the vertical supply of nutrients to the

surface layers during the developing phase of the SLD can be largely attributed to Ekman suction. During the peak phase of the SLD, both Ekman suction and nitracline shoaling rates weakened. However, the larger shoaling rates during the preceeding week indicate a favourable pre-conditioning for the generation of chlorophyll blooms during the peak phase of the SLD. Ekman suction gradually increased during the decaying phase of the SLD. The corresponding deepening tendency of the nitracline was not consistent with the positive Ekman vertical velocities, indicating the influence of remote forcings.

Chlorophyll distribution in the region of the SMC is influenced by the horizontal advection of both nutrients and chlorophyll. Simulated surface nitrate shows enhanced concentrations along the path of the SMC, indicating the lateral advection of nutrient-rich waters from the Arabian Sea (Fig. 12d). Advection of ~~chlorophyll~~ phytoplankton from the upwelling regions off the coasts of India and Sri Lanka could further intensify the ~~bloom~~ chlorophyll concentration (Vinayachandran et al., 2004; Vinayachandran, 2009). The relative role of mixed layer processes in maintaining the ~~summer blooms~~ chlorophyll concentrations along the path of SMC is presented in Section 3.3.2.

The model DCM shows large spatial variability in terms of intensity and depth. The DCM is strong in the region of the SLD and along the path of the SMC (Fig. 15a), consistent with the glider observations (Fig. 4). Subsurface chlorophyll concentrations increase to about 1.2 μmol kg^{-1} within the dome, which is more than twice the concentrations outside the dome. At the same time, the depth of the DCM is minimum in the region of the SLD (Fig. 15c). The DCM shoals to $\sim$20 m within the dome and deepens to $\sim$70 m outside the dome. Productivity is closely correlated with SLA and the depth of the nitracline and thermocline (Signorini et al., 1999; Wilson and Coles, 2005; Sarma, 2006; Signorini et al., 2015). The strongest DCM (Fig. 15a) coincides with the shallowest nitracline (Fig. 15d). Ekman ~~pumping~~ suction

leads to the upsloping of nitracline, which increases the concentration of limiting nutrients in the euphotic zone. The column integrated chlorophyll is found to be maximum along the path of the SMC (Fig. 15b), with magnitudes ranging from 50-70 μmol kg^{-1}.

3.3.2 Mixed layer nutrient budget

The nutrient budget from the ecosystem model is examined to identify the relative roles of mixed layer processes in controlling the summer ~~blooms~~ chlorophyll distribution in the southern BoB. In the TOPAZ ecosystem model, the growth of phytoplankton is determined by a limiting nutrient, in a multinutrient environment. Here, inorganic nitrate (NO_3) concentration is used to represent the nutrient budget (Fig. 16), since the dominant role of nitrate in controlling the biological productivity of the BoB is well known (Kone et al., 2009). The observed nitrate distribution has been used in previous studies to explain phytoplankton distribution in the BoB (Kumar et al., 2002, 2004, 2007). The present simulation also shows that during the pre-monsoon period, productivity in the southern bay is largely limited by nitrate when mixed layer dynamics were less favourable for the vertical supply of nutrients to the surface sunlit layers. Hence NO_3 was preferred over PO_4 and Fe ~~(SiO_4 does not limit growth in TOPAZ)~~ to explain the nutrient distribution. In addition, the chlorophyll concentration in TOPAZ is proportional to the nitrogen in phytoplankton (Dunne et al., 2010). Total chlorophyll is calculated as,

$$Chl = C\colon N \cdot 12 \cdot 10^6 \cdot (\theta^{Sm} \cdot N^{Sm} + \theta^{Lg} \cdot N^{Lg} + \theta^{Di} \cdot N^{Di}),$$

where C$\colon$ N is the carbon to nitrogen ratio, $12 \cdot 10^6$ is the molecular mass of carbon in μg mol^{-1}, θ is the chlorophyll to carbon ratio (Chl$\colon$ C), and N is the phytoplankton nitrogen concentration in mol kg^{-1}.

Physical processes controlling the model nutrient distribution include horizontal advection and vertical processes (including vertical advection and mixing). The biological processes include a source term represented by nitrification and sink terms comprising denitrification and uptake by the phytoplankton. The time rate of change of nitrate is given by,

$\frac{\partial NO_3}{\partial t} = -\nabla \cdot \mathbf{u} NO_3 + \nabla K \nabla NO_3 + S_{NO_3}$,

where **u** is the velocity vector from the OGCM, K is the vertical diffusivity and S_{NO_3} represents the biological processes.

Weekly averages of the model nitrate budget terms averaged over the mixed layer from 24 June to 21 July, comprising the BoBBLE observational period are shown in Fig. 16. The model MLD is defined as the depth at which the buoyancy difference with respect to the surface is equal to 0.0003 m s^{-2}. Before the onset of the summer monsoon, the upper ocean of the southern BoB maintained oligotrophic conditions, where nutrient levels were weak, inhibiting the growth of phytoplankton (not shown). Mixed layer dynamics associated with the monsoonal forcings play a dominant role in controlling the nutrient distribution of the southern BoB. As the monsoon intensifies, the monsoon current becomes stronger and the cyclonic circulation off the east coast of Sri Lanka leads to the development of the Sri Lanka Dome (Fig. 12).

The last week of June, coinciding with the beginning phase of the BoBBLE observational period, was characterised by a developing phase of the SLD, with strong open ocean upwelling. Nitrate concentrations in the mixed layer increased (Fig. 16a) as a result of enhanced vertical transport (Fig. 16b). At the same time, these nutrients were transported away from the region of upwelling and redistributed to the nearby regions through horizontal advection (Fig. 16c). Along the southern tip of India and Sri Lanka, coastal upwelling driven by alongshore winds leads to the intensification of nitrate levels, as evident from the ver-

tical processes (Fig. 16b). Offshore transport of upwelled nutrients occurs at significant rates, enhancing the nitrate concentrations in regions away from the coast (Fig. 16c). Within the mixed layer, uptake by the phytoplankton is higher than nitrification, so that the sink term exceeds the source term. Hence, biological processes contribute to a reduction in total nitrate, mainly in the coastal ocean and the region of SLD, where phytoplankton concentrations are high (Fig. 16d).

During the first week of July, nitrate levels in the mixed layer reduced slightly compared to the previous week; this period was characterised by the gradual weakening of the SLD and a reduction in the vertical supply of nutrients (Fig. 16f), leading to a decline in nitrate levels. Consequently, the associated horizontal transport (Fig. 16g) to the nearby regions also reduced. The nitrate uptake reduced due to the reduction in phytoplankton concentration, which explains the weaker negative tendencies due to biological processes in the region of the dome (Fig. 16h). Upwelling along the coasts of India and Sri Lanka (Fig. 16f) and the offshore advection effects (Fig. 16g) were still prominent during this period.

During the second week of July, nitrate levels in the mixed layer were generally higher compared to the previous week, especially in the region of the SMC (Fig. 16i). The SLD slightly regained its strength till 10 July, and weakened immediately. The related vertical transport of nutrients intensified (Fig. 16j) and the upwelled nutrients were distributed to the nearby regions (Fig. 16k). Though the upwelling was not as strong as that in the preceding peak phase (during the last week of June), vertical supply of nitrate occurred at higher rates (Fig. 16b and j). As a result of strong upwelling in the preceeding peak phase of the SLD, the nitrate isolines became shallower (not shown). This preconditioning probably favoured enhanced vertical supply of nitrate to the surface layers during the second peak phase, though the strength of upwelling was weaker.

The simulated eastward velocities associated with the summer monsoon current off the southern coast of India and Sri Lanka strengthened during the second week of July in relation to increasing wind speeds. Along the path of SMC, a clear patch of increased nitrate levels was evident (Fig. 16i), which extended from the southern tip of India up to about 85° E. This indicates horizontal advection of coastally upwelled nutrients from the southern coasts of India and Sri Lanka (Fig. 16k) into the southern BoB by the SMC. Lateral supply of nutrients by the SMC supports the growth of phytoplankton along its path. Increased uptake of nitrate by the phytoplankton further enhanced the negative contribution of biological processes (Fig. 16l).

During the third week of July, nitrate levels along the path of the SMC decreased (Fig. 16m). Following a reduction in wind speed, the monsoon current off the southern coast of India weakened and so did the horizontal transport (Fig. 16o). Vertical supply of nutrients was maintained in the region of dome (Fig. 16n). Contribution by biological processes decreased as the nitrate uptake weakened following a reduction in phytoplankton concentration (Fig. 16p). In summary, the above analyses show that the distribution of nutrients and the biological productivity in the southern BoB is largely dependent on the mixed layer dynamics associated with the summer monsoon and the relative roles of vertical and horizontal processes vary spatially following the circulation features.

4 Summary and Conclusions

The BoB plays a major role in controlling the monsoon variability through its unique upper ocean properties (Gadgil et al., 1984; Vecchi and Harrison, 2002; Shankar et al., 2007). A deeper understanding of the bio-physical feedbacks in the BoB is of primary importance since oceanic productivity plays a major

role in modifying the air-sea heat and gas exchanges (Arrigo et al., 1999; Chisholm, 2000). Despite its climatic significance, estimates of chlorophyll distribution in the BoB are limited owing to the restrictions in spatio-temporal coverage of in situ ~~data sampling. Remote sensing of ocean color is widely affected by the monsoonal cloud cover and turbid nature of coastal waters~~and satellite observations. In the presence of salinity stratification, which imparts strong nutrient limitation in the surface layers, ~~intense bloom activity is~~ high chlorophyll concentrations are mostly confined to the subsurface layers of the BoB. Hence, satellite retrieval algorithms based on ocean color in the surface layers would lead to an underestimation of actual chlorophyll content in the water column. These limitations in data sampling imply the need for high resolution and sustained measurements of the vertical distribution of chlorophyll in the BoB.

In this paper, we document the observed vertical distribution of chlorophyll in the southern BoB during the BoBBLE field program conducted during the summer monsoon of 2016. High-resolution data sampling using gliders accompanied by shipboard CTD record ~~prominent bloom activity~~ high chlorophyll concentrations in the southern BoB, with persistent DCM at intermediate depths. Hydrographic features of the region suggest that the observed spatio-temporal distribution of chlorophyll is strongly linked to the competing effects of monsoonal wind and freshwater forcings, which control the light and nutrient limited growth rate of the phytoplankton. ~~Reduced atmospheric convection and surplus insolation during the observational period suggest that surface chlorophyll distribution is weakly limited by light and dominantly determined by the nutrient availability. On the other hand, subsurface chlorophyll distribution is controlled by the balance between light and nutrient limitations.~~

The present observations underline the previously reported (Vinayachandran et al., 2004; Vinayachandran, 2009; Jyothibabu et al., 2015) role of the SLD and the SMC as the major physical drivers determining the

biological productivity of the southern BoB. The region of the SLD is characterised by enhanced chlorophyll concentrations in the presence of a shallow thermocline~~(nitracline)~~. A distinct band of chlorophyll is observed all along the path of the SMC, highlighting the role of lateral advection of nutrient-rich waters from the Arabian Sea in enriching the oligotrophic upper ocean of the BoB. In addition to the seasonal forcings, intermittent mixing events induced by local wind forcing trigger surface chlorophyll blooms outside the dome. A coupled physical-ecosystem model simulates satisfactorily the aforementioned distribution of chlorophyll, with prominent chlorophyll blooms in the regions of SLD and SMC. Model nutrient budget analyses demonstrate the role of monsoon dynamics in controlling the spatial and temporal distribution of biological productivity in the southern BoB. ~~Open ocean Ekman pumping~~ Open-ocean Ekman suction of nutrients is identified ~~as the major factor trigerring the generation and maintenance of summer blooms~~ to favour the intensification of chlorophyll in the region of the SLD. On the other hand, ~~advection~~ a reduction in chlorophyll levels during the decaying phase of the SLD can be associated with the remote forcing by the westward propagating downwelling Rossby wave signals. Advection by the SMC supplies coastally upwelled nutrients along the southern coasts of India and Sri Lanka to the southern BoB, favouring enhanced bloom concentrations.

~~Prominent bloom activity is~~ High chlorophyll concentrations observed at the subsurface ~~indicating~~ indicate the contribution of DCM in the column-integrated productivity of the BoB, where the surface waters are generally oligotrophic. Intense DCM exist in the region of the SLD and the SMC, whereas outside the dome, subsurface ~~blooms are~~ chlorophyll is weaker. Spatial variability of DCM intensity indicates that the dynamic uplifting of the thermocline (nutricline) is more efficient in enriching the euphotic zone with nutrients compared with wind-induced mixing. Upwelling leads to a sharp and intense DCM,

whereas mixing results in a more diffuse and weaker DCM. The region of the subsurface intrusion of the SMC exhibits the strongest DCM among all the glider locations, suggesting the contribution of Arabian Sea water in the biological budget of the BoB.

Inhibition of surface blooms induced by the freshwater effect was often observed in the southern BoB during the study period, similar to that in the northern BoB. The intermittent occurrence of surface freshening events favour restratification of the upper ocean and formation of barrier layers. Stratification curtails the wind-induced vertical transport of nutrients and subsurface chlorophyll, leading to the decay of surface blooms. Meanwhile, freshening leads to an intensification of DCM, favoured by enhanced light penetration into deeper layers as the self-shading effect weakens in the absence of surface chlorophyll blooms. In addition, shoaling of the mixed layer induced by salinity stratification impedes the vertical redistribution of subsurface chlorophyll, thereby intensifying the DCM.

The shape of chlorophyll profiles in different dynamical regimes indicates that the processes determining the vertical distribution of chlorophyll are intricate, which needs to be explored in detail using comprehensive datasets. The observed contrast in the vertical profiles of chlorophyll is largely dependent on the spatial extent and strength of the SMC and the SLD, which is attributed to the combined effect of local and remote forcings. Circulation and sea level anomalies reveal that the location and intensity of SMC and SLD varied during the observational period. Using geostrophic velocities obtained from satellite data, Webber et al. (2018) showed that the SMC moved westward during the BoBBLE observational period. They related the westward shift of SMC to the westward propagation of downwelling Rossby waves from the eastern boundary of the BoB. The strength and spatial extend of the SLD also varied accordingly. The

decay period of the SLD coincided with the arrival of westward propagating high in sea level anomalies associated with the Rossby wave propagation.

Chlorophyll distribution in the ocean is determined by both physical and biological processes. The intensity and depth distribution of DCM depends on a wide range of factors including the hydrography of the upper ocean, biochemical nutrient cycling as well as the physiological adaptations of different phytoplankton communities. The deep chlorophyll maxima do not necessarily represent biomass maxima, since the chlorophyll-to-biomass ratio varies with different phytoplankton species as well as with nutrient and light availability at depths (Geider et al., 1997, 1998; Wang et al., 2009; Li et al., 2010). Other loss terms including grazing~~and mortality rates also~~ , mortality and sinking rates have to be taken into account for a complete description of the evolution of chlorophyll blooms. However, the lack of observationl evidence on the loss terms restricts a detailed investigation on their relative importance with respect to the physical controls during different stages of the chlorophyll bloom evolution.

Bio-physical interactions in the ocean have significant impacts on climate variability through the control on upper ocean dynamics (Morel, 1988; Sathyendranath et al., 1991; Murtugudde et al., 2002; Strutton and Chavez, 2004; Manizza et al., 2005). Understanding different aspects of oceanic productivity helps to determine the potential feedbacks on the climate system. Proper estimation of the vertical distribution of marine phytoplankton and the total chlorophyll content in the upper ocean will help to understand the strength of carbon cycling in the ocean. Apart from the climatic impacts, the global marine fisheries production is highly dependent on the seasonal distribution of phytoplanton in the major fishing zones. Advanced data sampling using gliders, designed to operate under adverse oceanic conditions can make significant contributions in the understanding of biogeochemical cycling of the ocean and its climatic impacts, implying the

need for expanding such observations for future research. Realistic simulation of monsoonal bio-physical interactions underlines the potential role of ecosystem models in exploring the vertical distribution of oceanic productivity, which is beyond the scope of satellites.

Data availability. The data sets analysed in this paper are available from the corresponding author upon reasonable request.

Author contributions. V. Thushara and P. N. Vinayachandran performed data analysis and manuscript preparation. Bastien Y. Queste, Benjamin G. M. Webber and Adrian J. Matthews performed the glider data correction and quality control. V. Thushara carried out the ecosystem model simulation. All the authors contributed ~~significantly~~ in data interpretation.

Competing interests. No competing interests are present.

Acknowledgements. BoBBLE is a joint MoES, India–NERC, UK program (MM/NERC-MOES-02/2014/002). The BoBBLE field experiment on board RV Sindhu Sadhana was funded by Ministry of Earth Sciences, Govt. of India under the Monsoon Mission program administered by Indian Institute of Tropical Meteorology, Pune. We are thankful to the captain, technicians and crew of RV Sindhu Sadhana for their support and co-operation. BGMW was supported by the NERC BoBBLE project (NE/L013827/1). Glider data were processed using the UEA glider toolbox (http://www.byqueste.com/toolbox.html). We thank Global Modeling and Assimilation Office (GMAO) and the Goddard Earth Sciences Data and Information Services Center (GES DISC) for providing MERRA reanalysis product (http://disc.sci.gsfc.nasa.gov/daac-bin/DataHoldings.pl), IFREMER (http://www.ifremer.fr/cersat/en/data/data.htm) for ASCAT winds, AVISO (http://www.aviso.altimetry.fr) for SLA, ESA OC-CCI v3.1 (http://www.esa-oceancolour-cci.org/) for chlorophyll, JPL PODAAC (https://podaac.jpl.nasa.gov) for SST and

SSS products, TRMM (http://daac.gsfc.nasa.gov/precipitation) for precipitation and SAGE (http://www.sage.wisc.edu/riverdata/) for river discharge. Thanks to GFDL for providing the source code of the coupled physical-ecosystem model (MOM4P1-TOPAZ). We thank Dr. Jenson V. George for the helpful discussions. Computations were carried out at the Super Computer Education and Research Centre, Indian Institute of Science, Bangalore. Ferret has been used for data analysis and graphics.

References

Anderson, G. C.: Subsurface chlorophyll maximum in the northeast Pacific Ocean., Limnol. Oceanogr., 14, 386–391, 1969.

Arrigo, K. R., Robinson, D. H., Worthen, D. L., Dunbar, R. B., DiTullio, G. R., VanWoert, M., and Lizotte, M. P.: Phytoplankton Community Structure and the Drawdown of Nutrients and CO2 in the Southern Ocean, Science, 283, 365–367, 1999.

Behara, A. and Vinayachandran, P. N.: An OGCM study of the impact of Rain and River Water Forcing on the Bay of Bengal, Journal of Geophysical Research, https://doi.org/10.1002/2015JC011325, 2016.

Behrenfeld, M. J. and Boss, E. S.: Student's tutorial on bloom hypotheses in the context ofphytoplankton annual cycles, Glob. Change Biol., 24, 55–77, https://doi.org/DOI: 10.1111/gcb.13858, 2017.

Blondeau-Patissier, D., Gower, J. F., Dekker, A. G., Phinn, S. R., and Brando, V. E.: A review of ocean color remote sensing methods and statistical techniques for the detection, mapping and analysis of phytoplankton blooms in coastal and open oceans, Progress in Oceanography, 123, 123–144, 2014.

Boss, E. and Behrenfeld, M.: In situ evaluation of the initiation of the North Atlantic phytoplankton bloom, Geophysical Research Letters, 37, https://doi.org/doi:10.1029/2010GL044174, 2010.

Bretherton, F. P., Davis, R. E., and Fandry, C. B.: A technique for objective analysis and design of oceanographic experiments applied to MODE-73, Deep-Sea Res. Oceanogr. Abstr., 23, 559–582, https://doi.org/10.1016/0011-7471(76)90001-2, 1976.

Burns, J., Subrahmanyam, M. B., and Murty, V. S. N.: On the dynamics of the Sri Lanka Dome in the Bay of Bengal, Journal of Geophysical Research: Oceans, 122, 7737–7750, https://doi.org/10.1002/2017JC012986, 2017.

Chao, Y., Li, Z., Farrara, J. D., and Huang, P.: Blended sea surface temperatures from multiple satellites and in-situ observations for coastal oceans, Journal of Atmospheric and Oceanic Technology, 26, 1435–1446, https://doi.org/10.1175/2009JTECHO592.1, 2009.

Chassignet, E. P. and Garraffo, Z. D.: Viscosity parameterization and the Gulf Stream separation, in *From Stirring to Mixing in a Stratified Ocean: Proceedings 'Aha Huliko'a Hawaiian Winter Workshop, University of Hawai'i at Mānoa, January 16-19, 2001*, edited by P. Muller and D. Henderson, pp. 37-41, Univ. of Hawai'i at Mānoa, Honolulu., 2001.

Chisholm, S. W.: Stirring times in the Southern Ocean, Nature, 407, 685–587, 2000.

Conkright, M. E., Levitus, S., O'Brein, T., Boyer, T. P., Antonov, J. J., and Stephens, C.: World Ocean Atlas 1998, [CD-ROM] *NODC Int. Rep. 15*, 16 pp., NOAA, Silver Spring, Md., 1998.

Cullen, J. J.: The deep chlorophyll maximum: Comparing vertical profiles of chlorophyll a, Can. J. Fish. Aquat. Sci, 39, 791–803, 1982.

Cullen, J. J.: Subsurface Chlorophyll Maximum Layers: Enduring Enigma or Mystery Solved?, Annu. Rev. Mar. Sci., 7, 207–239, 2015.

Dunne, J. P., Armstrong, R. A., Gnanadesikan, A., and Sarmiento, J. L.: Empirical and mechanistic models for the particle export ratio, Global Biogeochemical cycles, 19, GB4026, https://doi.org/10.1029/2004GB002390, 2005.

Dunne, J. P., Gnanadesikan, A., Sarmiento, J. L., and Slater, R. D.: Technical description of the prototype version (v0) of Tracers of Phytoplankton with Allometric Zooplankton (TOPAZ) ocean biogeochemical model as used in the Princeton IFMIP model, Biogeosciences, 7 (Suppl.), 3593, https://doi.org/10.5194/bg-7-3593-2010, 2010.

Eppley, R. W.: Temperature and Phytoplankton growth in the sea, Fishery Bulletin, 70, 1063–1085, 1972.

Eriksen, C. C., Osse, T. J., Light, R. D., Wen, T., Lehman, T. W., Sabin, P. L., Ballard, J. W., and Chiodi, A. M.: Seaglider: A Long-Range Autonomou s Underwater Vehicle for Oceanographic Research, IEEE Journal of Oceanic Engineering, 26, 424–436, 2001.

Figa-Saldaña, J., Wilson, J. J. W., Attema, E., Gelsthorpe, R., Drinkwater, M. R., and Stoffelen, A.: The advanced scatterometer (ASCAT) on the meteorological operational (MetOp) platform: A follow on for European wind scatterometers, Can. J. Remote Sensing, 28, 404–412, 2002.

Fore, A., S, H. Y., Tang, W., Stiles, B., and Hayashi, A.: Combined Active/Passive Retrievals of Ocean Vector Wind and Sea Surface Salinity With SMAP, IEEE Transactions on Geoscience and Remote Sensing, 54, 7396–7404, https://doi.org/10.1109/TGRS.2016.2601486, 2016.

Gadgil, S., Joseph, P. V., and Joshi, N. V.: Ocean atmosphere coupling over monsoon regions, Nature, 312, 141–143, https://doi.org/10.1038/312141a0, 1984.

Geider, R. J.: Light and temperature dependence of the carbon to chlorophyll a ratio in microalgae and cyanobacteria: implications for physiology and growth of phytoplankton, New Phytol., 106, 1–34, 1987.

Geider, R. J., Maclntyre, H. L., and Kana, T. M.: Dynamic model of phytoplankton growth and acclimation: responses of the balanced growth rate and the chlorophyll a:carbon ratio to light, nutrient-limitation and temperature, Marine Ecology, 148, 187–200, 1997.

Geider, R. J., Maclntyre, H. L., and Kana, T. M.: A dynamic regulatory model of phytoplanktonic acclimation to light, nutrients, and temperature , Limnol. Oceanogr., 43, 679–694, 1998.

Gnanadesikan, A., Dunne, J. P., and John, J.: What ocean biogeochemical models can tell us about bottom-up control of ecosystem variability, ICES Journal of Marine Science, 68, 1030–1044, https://doi.org/10.1093/icesjms/fsr068, 2011.

Gnanadesikan, A., Dunne, J. P., and Msadek, R.: Connecting Atlantic temperature variability and biological cycling in two earth system models, Journal of Marine Systems, 133, 39–54, https://doi.org///dx.doi.org/10.1016/j.jmarsys.2013.10.003, 2014.

Gomes, H. R., Goes, J. I., and Saino, T.: Influence of physical processes and freshwater discharge on the seasonality of phytoplankton regime in the Bay of Bengal, Continental Shelf Research, 20, 313–330, 2000.

Gregg, W. W. and Casey, N. W.: Global and regional evaluation of the SeaWiFS chlorophyll data set, Remote Sensing of Environment, 93, 463– 479, 2004.

Griffies, S. M., Harrison, M. J., Pacanowski, R. C., and Rosati, A.: A technical guide to MOM4, Tech. Rep. 5, Geophys. Fluid Dyn. Lab. Ocean Group, Princeton, N. J., 2004.

Huffman, G., Adler, R., Bolvin, D., Gu, G., Nelkin, E., Bowman, K., Hong, Y., Stocker, E., and Wolff, D.: The TRMM Multi-satellite Precipitation Analysis: Quasi-Global, Multi-Year, Combined-Sensor Precipitation Estimates at Fine Scale., J. Hydrometeor., 8, 38–55, 2007.

Jensen, T. G.: Arabian Sea and Bay of Bengal exchange of salt and tracers in an ocean model, Geophys. Res. Lett., 28, 3967–3970, 2001.

Jyothibabu, R., Vinayachandran, P. N., Madhu, N., Robin, R., Karnan, C., Jagadeesan, L., and Anjusha, A.: Phytoplankton size structure in the southern Bay of Bengal modified by the Summer Monsoon Current and associated eddies: Implications on the vertical biogenic flux, Journal of Marine Systems, 143, 98–119, https://doi.org///dx.doi.org/10.1016/j.jmarsys.2014.10.018, 2015.

Jyothibabu, R., Arunpandi, N., Jagadeesan, L., Karnan, C., Lallu, K. R., and Vinayachandran, P. N.: Response of phytoplankton to heavy cloud cover and turbidity in the northern Bay of Bengal, Scientific Reports, 8, 2018.

Kone, V., Aumont, O., Levy, M., and Resplandy, L.: Physical and Biogeochemical Controls of the Phytoplankton Seasonal Cycle in the Indian Ocean: A Modeling Study, Geophysical Monograph Series, 185, 147–166, https://doi.org/10.1029/2008GM000700, 2009.

Kumar, S. P., Muraleedharan, P. M., Prasad, T. G., Gauns, M., Ramaiah, N., de Souza, S. N., Sardesai, S., and Madhupratap, M.: Why is the Bay of Bengal less productive during summer monsoon compared to the Arabian Sea?, Geophys. Res. Lett, 29, 2235, https://doi.org/10.1029/2002GL016013, 2002.

Kumar, S. P., Nuncio, M., Narvekar, J., Kumar, A., Sardesai, S., de Souza, S. N., Gauns, M., Ramaiah, N., and Madhupratap, M.: Are eddies nature's trigger to enhance biological productivity in the Bay of Bengal?, Geophys. Res. Lett, 31, L07 309, https://doi.org/10.1029/2003GL019274, 2004, 2004.

Kumar, S. P., Nuncio, M., Ramaiah, N., Sardesai, S., Narvekar, J., Fernandes, V., and Paul, J. T.: Eddy-mediated biological productivity in the Bay of Bengal during fall and spring intermonsoons, Deep-Sea Research I, 54, 1619–1640, https://doi.org/10.1016/j.dsr.2007.06.002, 2007.

Kumar, S. P., Narvekar, J., Nuncio, M., Gauns, M., and Sardesai, S.: What drives the biological productivity of the northern Indian Ocean?, Geophys. Monogr. Ser, pp. 33–56, https://doi.org/10.1029/2008GM000757, 2009.

Kumar, S. P., Narvekar, J., Nuncio, M., Kumar, A., Ramaiah, N., Sardesai, S., Gauns, M., Fernandes, V., and Paul, J.: Is the biological productivity in the Bay of Bengal light limited?, Curr. Sci., 98, 1331–1339, 2010.

Kurian, J. and Vinayachandran, P. N.: Formation mechanisms of temperature inversions in the southeastern Arabian Sea, Geophys. Res. Lett., 33, L17 611, https://doi.org/10.1029/2006GL027280, 2006.

Kurian, J. and Vinayachandran, P. N.: Mechanisms of formation of the Arabian Sea mini warm pool in a high resolution OGCM, J. Geophys. Res., 112, C05 009, https://doi.org/10.1029/2006JC003631, 2007.

Large, W. G. and Yeager, S. G.: Diurnal to decadal global forcing for ocean and sea-ice models: the data sets and flux climatologies, Tech. rep. NCAR/TN-460+STR, Natl., Cent. for Atmos. Res., Boulder, Colo, 2004.

Large, W. G., McWilliams, J. C., and Doney, S. C.: Oceanic vertical mixing: A review and a model with a nonlocal boundary layer parameterization, Rev. Geophys, 32, 363–403, 1994.

Laws, E. A.: Evaluation of In Situ Phytoplankton Growth Rates: A Synthesis of Data from Varied Approaches, Annu. Rev. Mar. Sci., 5, 247–268, https://doi.org/10.1146/annurev-marine-121211-172258, 2013.

Lee, C. M., Jinadasa, S., Anutaliya, A., Centurioni, L. R., Fernando, H. J., Hormann, V., Lankhorst, M., Rainville, L., Send, U., and Wijesekera, H. W.: Collaborative Observations of Boundary Currents, Water Mass Variability, and Monsoon Response in the Southern Bay of Bengal, Oceanography, 29, 102—111, https://doi.org/http://dx.doi.org/10.5670/oceanog.2016.43, 2016.

Letelier, R. M., Karl, D. M., Abbott, M. R., and Bidigare, R. R.: Light driven seasonal patterns of chlorophyll and nitrate in the lower euphotic zone of the North Pacific Subtropical Gyre, Limnology and Oceanography, 49, 508–519, 2004.

Li, G., Lin, Q., Ni, G., Shen, P., Fan, Y., Huang, L., and Tan, Y.: Vertical Patterns of Early Summer Chlorophyll a Concentration in the Indian Ocean with Special Reference to the Variation of Deep Chlorophyll Maximum, Journal of Marine Biology, 2012, https://doi.org/10.1155/2012/801248, 2012.

Li, Q. P., Franks, P. J. S., Landry, M. R., Goericke, R., and Taylor, A. G.: Modeling phytoplankton growth rates and chlorophyll to carbon ratios in California coastal and pelagic ecosystems, Journal of Geophysical Research, 115, G04 003, https://doi.org/10.1029/2009JG001111, 2010.

Madhu, N., Jyothibabu, R., Maheswaran, P., Gerson, V. J., Gopalakrishnan, T., and Nair, K.: Lack of seasonality in phytoplankton standing stock (chlorophyll a) and production in the western Bay of Bengal, Continental Shelf Research, 26, 1868–1883, 2006.

Madhu, N. V., Maheswaran, P. A., Jyothibabu, R., Revichandran, C., Balasubramanian, T., Gopalakrishnan, T. C., and Nair, K. K. C.: Enhanced biological production off Chennai triggered by October 1999 super cyclone (Orissa), Curr. Sci., 82, 1472–1479, 2002.

Madhupratap, M., S., P., P.M.A., B., M., D., S., R., K.K.C., N., and N., R.: Mechanism of the biological response to winter cooling in the northeastern Arabian Sea, Nature, 384, 549–552, 1996.

Madhupratap, M., Gauns, M., Ramaiah, N., Kumar, S. P., Muraleedharan, P., de Sousa, S., Sardessai, S., and Muraleedharan, U.: Biogeochemistry of the Bay of Bengal: physical, chemical and primary productivity characteristics of the central and western Bay of Bengal during summer monsoon 2001, Deep-Sea Research II, 50, 881–896, https://doi.org/10.1016/S0967-0645(02)00611-2, 2003.

Manizza, M., Quere, C. L., Watson, A. J., and Buitenhuis, E. T.: Bio-optical feedbacks among phytoplankton, upper ocean physics and sea-ice in a global model, Geophys. Res. Lett, 32, L05 603, https://doi.org/10.1029/2004GL020778, 2005.

Marvasti, S. S., Gnanadesikan, A., Bidokhti, A. A., Dunne, J. P., and Ghader, S.: Challenges in modeling spatiotemporally varying phytoplankton blooms in the Northwestern Arabian Sea and Gulf of Oman, Biogeosciences, 13, 1049–1069, https://doi.org/10.5194/bg-13-1049-2016, 2016.

Mateus, M., Leitao, P., de Pablo, H., and Neves, R.: Is it relevant to explicitly parameterize chlorophyll synthesis in marine ecological models?, Journal of Marine Systems, 94, S23–S33, https://doi.org/10.1016/j.jmarsys.2011.11.007, 2012.

Matthews, A. J., Baranowski, D. B., Heywood, K. J., Flatau, P. J., and Schmidtko, S.: The Surface Diurnal Warm Layer in the Indian Ocean during CINDY/DYNAMO, J. Climate, 27, 9101–9122, https://doi.org/10.1175/JCLI-D-14-00222.1, 2014.

McCreary, J. P., Kohler, K. E., Hood, R. R., and Olson, D. B.: A four-component ecosystem model of biological activity in the Arabian Sea, Progress in Oceanography, 37, 193–240, 1996.

McCreary, J. P., Murtugudde, R., Vialard, J., Vinayachandran, P. N., Wiggert, J. D., Hood, R. R., Shankar, D., and Shetye, S.: Biophysical Processes in the Indian Ocean, pp. 9–32, American Geophysical Union, https://doi.org/10.1029/2008GM000768, http://dx.doi.org/10.1029/2008GM000768, 2009.

Moore, C. M., Mills, M. M., Arrigo, K. R., Berman-Frank, I., Bopp, L., Boyd, P. W., Galbraith, E. D., Geider, R. J., Guieu, C., Jaccard, S. L., Jickells, T. D., Roche, J. L., Lenton, T. M., Mahowald, N. M., Marañón, E., Marinov, I., Moore, J. K., Nakatsuka, T., Oschlies, A., Saito, M. A., Thingstad, T. F., Tsuda, A., and Ulloa, O.: Processes and patterns of oceanic nutrient limitation, Nature Geoscience, 6, 701–710, https://doi.org/10.1038/NGEO1765, 2013.

Morel, A.: Optical modeling of the upper ocean in relation to its biogenous matter content (case I waters), Journal of Geophysical Research, 93, 10 749–10 768, https://doi.org/10.1029/JC093iC09p10749, 1988.

Morel, A. and Antoine, D.: Heating rate within the upper ocean in relation to its bio-optical state, J. Phys. Oceanogr., 24, 1652–1665, 1994.

Morel, A. and Smith, R. C.: Relation between total quanta and total energy for aquatic photosynthesis, Limnology and Oceanography, 19, 591–600, 1974.

Murtugudde, R., Beauchamp, J., McClain, C. R., Lewis, M., and Busalacchi, A. J.: Effects of Penetrative Radiation on the Upper Tropical Ocean Circulation, Journal of Climate, 15, 470–486, 2002.

Murty, V., Sarma, M., and Tilvi, V.: Seasonal cyclogenesis and the role of near-surface stratified layer in the Bay of Bengal, paper presented at the Fifth Pacific Ocean Remote Sensing Conference, PORSEC, Goa, India, 2000.

Murty, V. S. N., Sarma, Y. V. B., Rao, D. P., and Murty, C. S.: Water characteristics, mixing and circulation in the Bay of Bengal during southwest monsoon, Journal of Marine Research, 50, 207–228, 1992.

Nuncio, M. and Kumar, S. P.: Evolution of cyclonic eddies and biogenic fluxes in the northern Bay of Bengal, Biogeosciences Discuss., 10, 16 213–16 236, https://doi.org/10.5194/bgd-10-16213-2013, 2013.

Park, J.-Y. and Kug, J.-S.: Marine biological feedback associated with Indian Ocean Dipole in a coupled ocean/biogeochemical model, Clim. Dyn., 42, 329–343, https://doi.org/DOI 10.1007/s00382-012-1640-5, 2014.

Park, J.-Y., Kug, J.-S., and Park, Y.-G.: An exploratory modeling study on bio-physical processes associated with ENSO, Progress in Oceanography, 124, 28–41, 2014.

Pastor, M. V., Palter, J. B., Pelegri, J. L., and Dunne, J. P.: Physical drivers of interannual chlorophyll variability in the eastern subtropical North Atlantic, Journal of Geophysical Research, 118, 1–16, https://doi.org/10.1002/jgrc.20254, 2013.

Perry, M. J., Sackmann, B. S., Eriksen, C. C., and Lee, C. M.: Seaglider observations of blooms and subsurface chlorophyll maxima off the Washington coast, Limnol. Oceanogr., 53, 2169–2179, 2008.

Rao, K. H., Smitha, A., and Ali, M. M.: A study on cyclone induced productivity in south-western Bay of Bengal during November-December 2000 using MODIS (SST and chlorophyll-a) and altimeter sea surface height observations, Indian J. Mar. Sci., 35, 153–160, 2006.

Rienecker, M. M., Suarez, M. J., Gelaro, R., Todling, R., Bacmeister, J., Liu, E., Bosilovich, M. G., Schubert, S. D., Takacs, L., Kim, G.-K., Bloom, S., Chen, J., Collins, D., Conaty, A., and A. da Silva, e. a.: MERRA - NASA's Modern-Era Retrospective Analysis for Research and Applications, J. Climate, 24, 3624–3648, https://doi.org/10.1175/JCLI-D-11-00015.1, 2011.

Sarma, V. V. S. S.: The influence of Indian Ocean Dipole (IOD) on biogeochemistry of carbon in the Arabian Sea during 1997–1998, J. Earth Syst. Sci., 115, 433–450, 2006.

Sarmiento, J. L., Slater, R. D., Dunne, J., Gnanadesikan, A., and Hiscock, M. R.: Efficiency of small scale carbon mitigation by patch iron fertilization, Biogeosciences, 7, 3593–3624, https://doi.org/doi:10.5194/bg-7-3593-2010, 2010.

Sathyendranath, S., Gouveia, A., Shetye, S., Ravindran, P., and Platt, T.: Biological control of surface temperature in the Arabian Sea, Nature, 349, 54–56, 1991.

Schott, F., Reppin, J., Fischer, J., and Quadfasel, D.: Currents and transports of the Monsoon Current south of Sri Lanka , Journal of Geophysical Research, 99, 25 127–25 141, https://doi.org/https://doi.org/10.1029/94JC02216, 1994.

Shankar, D., Vinayachandran, P., and Unnikrishnan, A.: The monsoon currents in the north Indian Ocean, Progress in Oceanography, 52, 63–120, 2002.

Shankar, D., Shetye, S. R., and Joseph, P. V.: Link between convection and meridional gradient of sea surface temperature in the Bay of Bengal, J. Earth Syst. Sci., 116, 385–406, 2007.

Shenoi, S. S. C., Shankar, D., and Shetye, S. R.: Differences in heat budgets of the near-surface Arabian Sea and Bay of Bengal: Implications for the summer monsoon, J. Geophys. Res., 107, https://doi.org/10.1029/2000JC000679, 2002.

Shetye, S., Shenoi, S., Gouveia, A., Michael, G., Sundar, D., and Nampoothiri, G.: Wind-driven coastal upwelling along the western boundary of the Bay of Bengal during the southwest monsoon, Continental Shelf Research, 11, 1397–1408, https://doi.org/10.1016/0278-4343(91)90042-5, 1991.

Signorini, S. R., Murtugudde, R. . G. ., McClain, C. R., Christian, J. R., Picaut, J. ., and Busalacchi, A. J.: Biological and phys ical signatures in the tropical and subtropical Atlantic, Journal of Geophysical Research, 104, 18,367–18,382, 1999.

Signorini, S. R., Franz, B. A., and McClain, C. R.: Chlorophyll Variability in the Oligotrophic Gyres: Mechanisms, Seasonality and Trends, Frontiers in Marine Science 2, https://doi.org/10.3389/fmars.2015.00001, 2015.

Strutton, P. and Chavez, F.: Biological Heating in the Equatorial Pacific: Observed Variability and Potential for Real-Time Calculation, Journal of Climate, 17, 1097–1109, 2004.

Sweeney, C., Gnanadesikan, A., Griffies, S. M., Harrison, M. J., Rosati, A. J., and Samuels, B. L.: Impacts of shortwave penetration depth on large–scale ocean circulation and heat transport, J. Phys. Oceanogr., 35, 1103–1119, 2005.

Thomalla, S. J., Moutier, W., Ryan-Keogh, T. J., Gregor, L., and Schutt, J.: An optimized method for correcting fluorescence quenching using optical backscattering on autonomous platforms, Limnol. Oceanogr.: Methods, 16, 132–144, https://doi.org/10.1002/lom3.10234, 2018.

Thushara, V. and Vinayachandran, P. N.: Formation of summer phytoplankton bloom in the northwestern Bay of Bengal in a coupled physical-ecosystem model, Journal of Geophysical Research, 121, 8535–8550, 2016.

Turk, D., McPhaden, M. J., Busalacchi, A. J., and Lewis, M. R.: Remotely sensed biological production in the equatorial Pacific, Science, 293, 471–474, 2001.

Vecchi, G. A. and Harrison, D. E.: Monsoon Breaks and Subseasonal Sea Surface Temperature Variability in the Bay of Bengal, J. Climate, 15, 1485–1493, 2002.

Vijith, V., Vinayachandran, P. N., Thushara, V., Amol, P., Shankar, D., and Anil, A. C.: Consequences of inhibition of mixed-layer deepening by the West India Coastal Current for winter phytoplankton bloom in the northeastern Arabian Sea, J. Geophys. Res. Oceans, 121, 6583–6603, https://doi.org/10.1002/2016JC012004, 2016.

Vinayachandran, P. N.: Impact of Physical Processes on Chlorophyll Distribution in the Bay of Bengal, pp. 71–86, American Geophysical Union, https://doi.org/10.1029/2008GM000705, http://dx.doi.org/10.1029/2008GM000705, 2009.

Vinayachandran, P. N. and Kurian, J.: Hydrographic observations and model simulation of the Bay of Bengal freshwater plume, Deep-Sea Res. Part I, 54, 471–486, 2007.

Vinayachandran, P. N. and Mathew, S.: Phytoplankton bloom in the Bay of Bengal during the northeast monsoon and its intensification by cyclones, Geophys. Res. Lett, 30, 1572, https://doi.org/10.1029/2002GL016717, 2003.

Vinayachandran, P. N. and Yamagata, T.: Monsoon Response of the Sea around Sri Lanka: Generation of Thermal Domes and Anticyclonic Vortices, J. Phys. Oceanogr., 28, 1946–1960, 1998.

Vinayachandran, P. N., Masumoto, Y., Mikawa, T., and Yamagata, T.: Intrusion of Southwest Monsoon current into Bay of Bengal, Geophys. Res. Lett, 104, 11,077–11,085, 1999.

Vinayachandran, P. N., Murthy, V. S. N., and Babu, V. R.: Observations of barrier layer formation in the Bay of Bengal during summer monsoon, J. Geophys. Res., 107, 8018, https://doi.org/10.1029/2001JC000831, 2002.

Vinayachandran, P. N., Chauhan, P., Mohan, M., and Nayak, S.: Biological response of the sea around Sri Lanka to summer monsoon, Geophysical Research Letters, 31, L01 302, https://doi.org/10.1029/2003GL018533, 2004.

Vinayachandran, P. N., Jr., J. P. M., Hood, R. R., and Kohler, K. E.: A numerical investigation of the phytoplankton bloom in the Bay of Bengal during Northeast Monsoon, J. Geophys. Res, 110, https://doi.org/doi:10.1029/2005JC002966, 2005.

Vinayachandran, P. N., Shankar, D., Vernekar, S., Sandeep, K. K., Amol, P., Neema, C. P., and Chatterjee, A.: A summer monsoon pump to keep the Bay of Bengal salty, Geophys. Res. Lett, 40, 1777–1782, https://doi.org/10.1002/grl.50274, 2013.

Vinayachandran, P. N., Matthews, A. J., Kumar, K. V., Sanchez-Franks, A., Thushara, V., George, J. V., Vijith, V., Webber, B. G. M., Queste, B. Y., Roy, R., Sarkar, A., Baranowski, D. B., Bhat, G. S., Klingaman, N. P., Parida, S. C. P. C., Heywood, K. J., Hall, R., Giddings, J.,

King, B., Kent, E. C., Nayak, A. A., Neema, C. P., Amol, P., Lotliker, A., Kankonkar, A., Gracias, D. G., Vernekar, S., D.Souza, A. C., Valluvan, G., Pargaonkar, S. M., and Dinesh, K.: BoBBLE (Bay of Bengal Boundary Layer Experiment): Ocean–atmosphere interaction and its impact on the South Asian monsoon, Bull. Am. Meteorol. Soc., 2018.

Vörösmarty, C. J., Fekete, B. M., and Tucker, B. A.: River Discharge Database, Version 1.0 (RivDIS v1.0), Volumes 0 through 6. A contribution to IHP–V Theme 1. Technical Documents in Hydrology Series, Tech. rep., UNESCO, Paris, 1996.

Wang, X. J., Behrenfeld, M., Borgne, R. L., Murtugudde, R., and Boss, E.: Regulation of phytoplankton carbon to chlorophyll ratio by light, nutrients and temperature in the Equatorial Pacific Ocean: a basin-scale model, Biogeosciences, 6, 391–404, 2009.

Ward, B. B., Olson, R. J., and Perry, M. J.: Microbial nitrification rates in the primary nitrite maximum off southern California, Deep-Sea Res., 29, 247–255, 1982.

Webber, B. G. M., Matthews, A. J., Heywood, K. J., Kaiser, J., and Schmidtko, S.: Seaglider observations of equatorial Indian Ocean Rossby waves associated with the Madden-Julian Oscillation, J. Geophys. Res. Oceans, 199, 3714–3731, https://doi.org/10.1002/2013JC009657, 2014.

Webber, B. G. M., Matthews, A. J., Vinayachandran, P. N., Neema, C. P., Sanchez-Franks, A., Vijith, V., Amol, P., and Baranowski, D. B.: The dynamics of the Southwest Monsoon current in 2016 from high-resolution in situ observations and models, submitted, 2018.

Wiggert, J. D., Hood, R. R., Naqvi, S. W. A., Brink, K. H., and Smith, S. L.: Introduction to Indian Ocean Biogeochemical Processes and Ecological Variability: Current Understanding and Emerging Perspectives, pp. 1–7, American Geophysical Union, https://doi.org/10.1029/2009GM000906, http://dx.doi.org/10.1029/2009GM000906, 2009.

Wijesekera, H. W., Shroyer, E., Tandon, A., Ravichandran, M., Sengupta, D., Jinadasa, S. U. P., Fernando, H. J. S., Agarwal, N., and Coauthors: "ASIRI: An Ocean–Atmosphere Initiative for Bay of Bengal", Bull. Am. Meteorol. Soc., 97, 1859–1884, https://doi.org/10.1175/BAMS-D-14-00197.1,, 2016a.

Wijesekera, H. W., Teague, W. J., Wang, D. W., Jarosz, E., and Jensen, T. G.: Low-Frequency Currents from Deep Moorings in the Southern Bay of Bengal, Journal of Physical Oceanography, 46, 3209–3238, https://doi.org/10.1175/JPO-D-16-0113.1, 2016b.

Wilson, C. and Adamec, D.: A global view of bio-physical coupling from SeaWiFS and TOPEX satellite data, 1997–2001, Geophysical Research Letters, 29, https://doi.org/10.1029/2001GL014063, 2002.

Wilson, C. and Coles, V. J.: Global climatological relationships between satellite biological and physical observations and upper ocean properties, Journal of Geophysical Research, 110, https://doi.org/10.1029/2004JC00272, 2005.

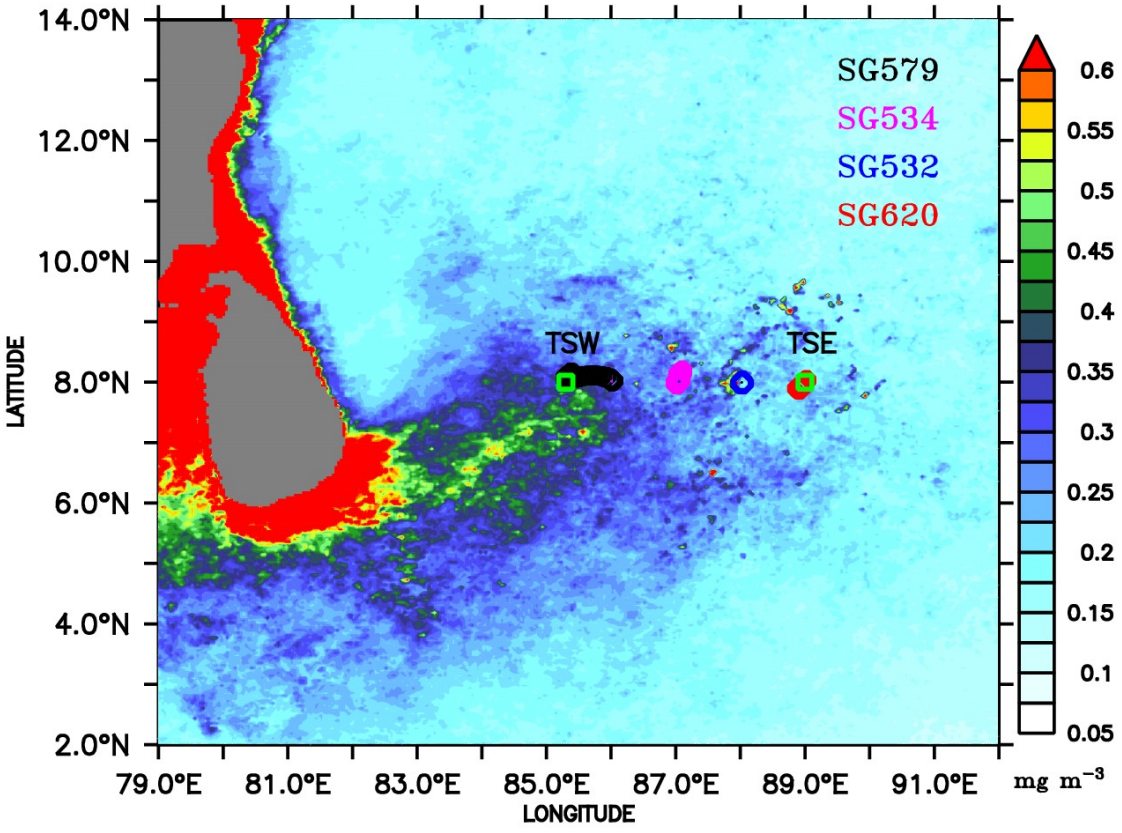

Figure 1. Chlorophyll (mg m^{-3}) climatology (2007–2016) for the month of July obtained from Ocean Colour Climate Change Initiative (OC–CCI) version 3.1. Ocean glider locations are marked as circles along 8°N, where the shipboard observations were performed. The glider deployment locations are (8°N, 86°E), (8°N, 87°E), (8°N, 88°E), and (8°N, 88°54′E) for SG579, SG534, SG532, and SG620 respectively. Observational period of gliders are 30 June–20 July, 01–17 July, 02–16 July, and 03–14 July of 2016 for SG579, SG534, SG532, and SG620 respectively. TSW and TSE (squares) are sampling locations at (8°N, 85.3°E) and (8°N, 89°E) respectively.

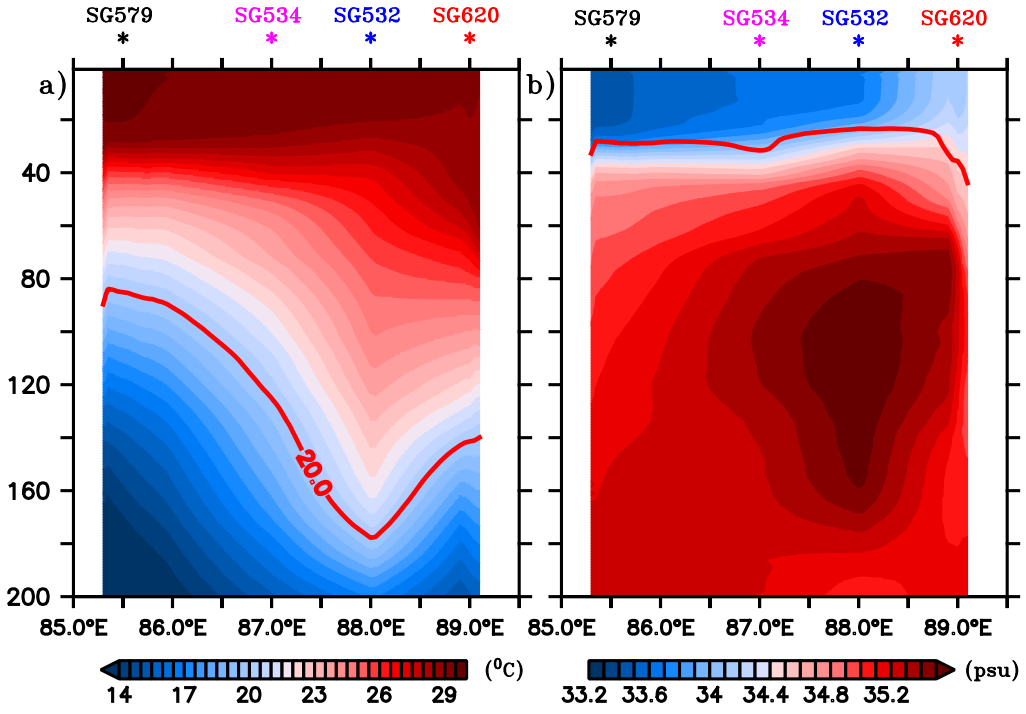

Figure 2. Depth-longitude sections of a) temperature (°C) and b) salinity (psu) obtained from ocean gliders averaged for 03–14 July, the common period when all the gliders performed data sampling. Mean glider locations are marked at the top of each panel. Red curves in a) and b) represent the thermocline and MLD respectively. The thermocline is represented by the 20 °C isotherm (D20). MLD is calculated as the depth where density is equal to the sea surface density plus an increase in density equivalent to a reduction in temperature of 0.8 °C.

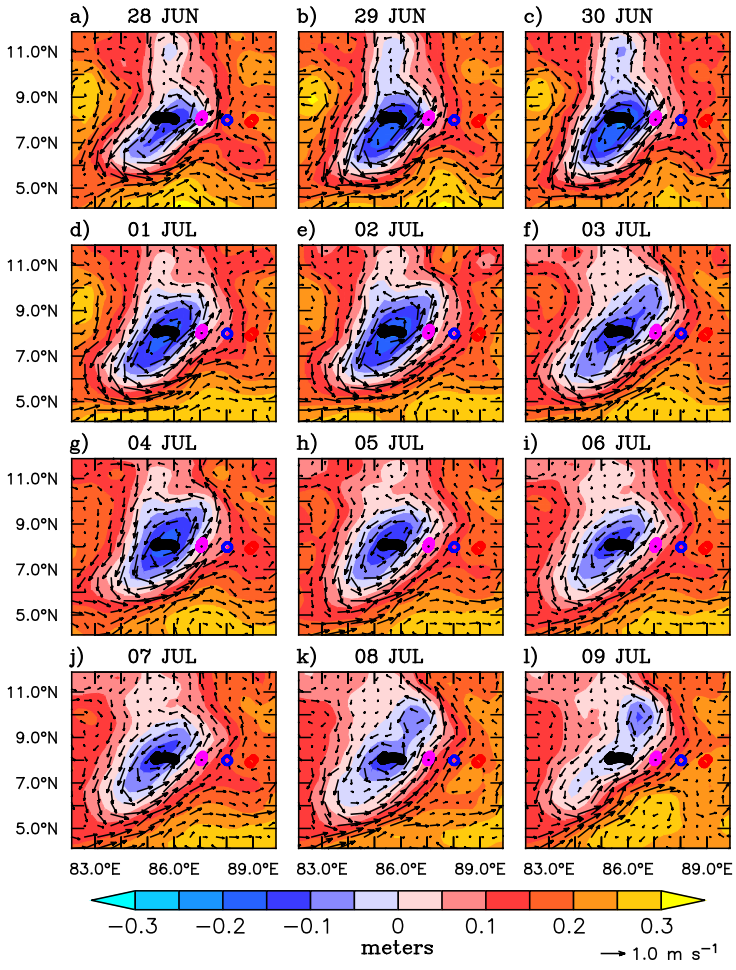

Figure 3. Sea level anomalies (SLA; m) and surface currents (m s^{-1}) from AVISO for the period 28 June 2016 to 09 July 2016. The glider locations are marked along 8°N (circles). Evolution of Sri Lanka dome (SLD) is represented by the negative SLA embedded within the cyclonic circulation.

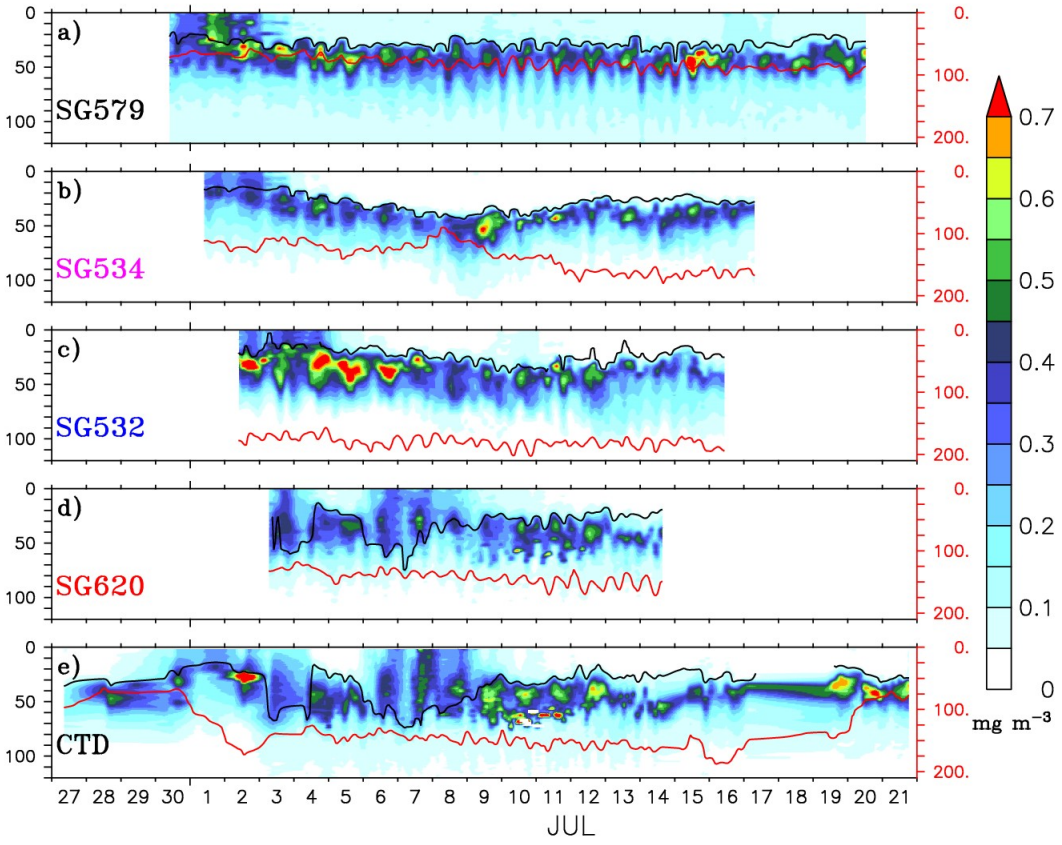

Figure 4. Time-depth sections of chlorophyll (mg m^{-3}) from ocean gliders (a-d) and CTD (e). The glider measurements are considered as time series data for the locations shown in Figure 1. CTD observations were collected at TSW (85.3°E, 8°N) from 27 June to 29 June, after which the ship sailed towards TSE (89°E, 8°N). From 03–15 July, time series measurements were made at TSE, after which the ship sailed back towards the west and reached TSW on 20 July. The black curve represents the mixed layer depth, which is calculated as the depth where density is equal to the sea surface density plus an increase in density equivalent to a reduction in temperature of 0.8 °C. The thermocline (red curve) is represented by the 20 °C isotherm (D20). Note that the y-axis at the right side has a different scale.

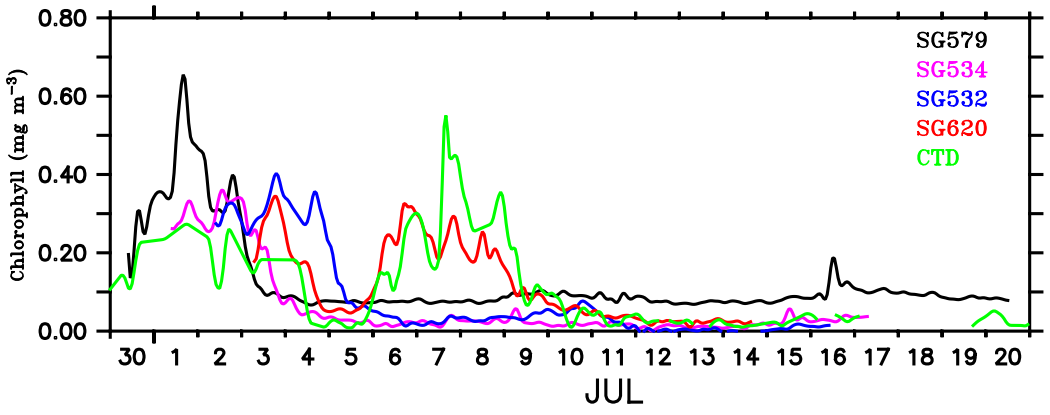

Figure 5. ~~a)~~ Surface chlorophyll concentration (mg m^{-3}) from ocean gliders (at 1 m) and the shipboard CTD (at 3 m). SG579 (black) falls within the region of SLD, SG534 (magenta) and SG532 (blue) along the path of SMC and SG620 (red) at the outer edge of SMC as shown in Figure 1. CTD (green) observations were collected along the 8°N section as described in Figure 4.

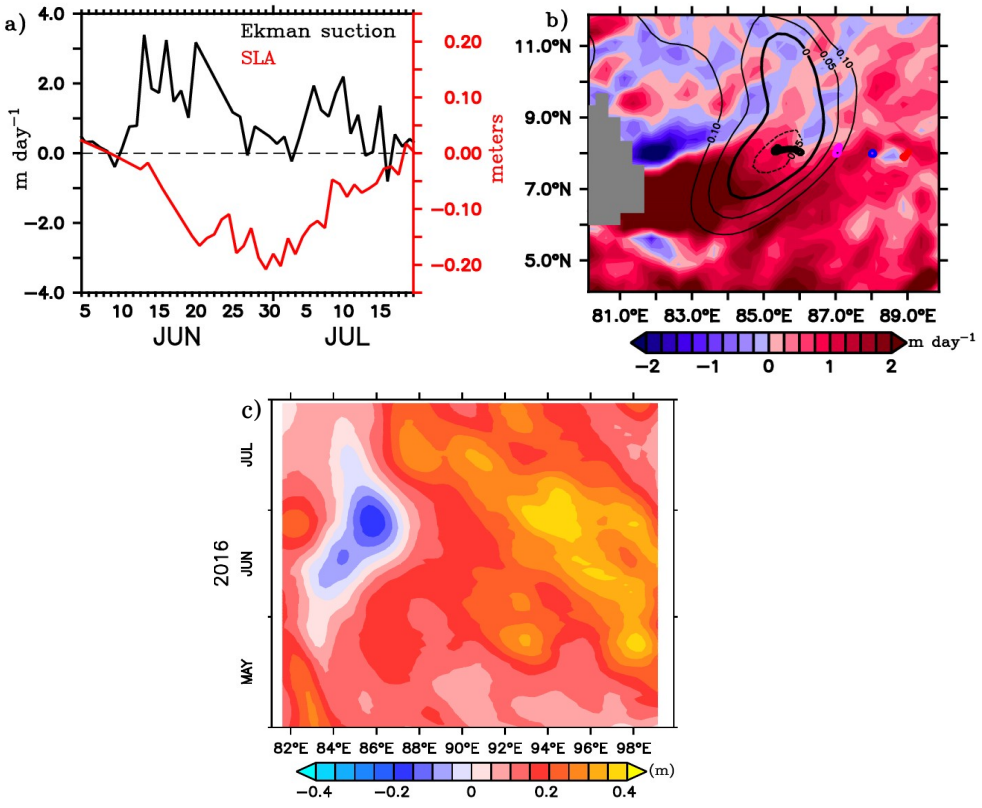

Figure 6. a) Time series of Ekman vertical velocity (m day^{-1}; black) around the location of SG579 (85-86°E, 7.5-8.5°N) and the minimum SLA (m; red) in the region of the Sri Lanka Dome (SLD) from 05 June to 20 July. b) Ekman vertical velocity averaged for the BoBBLE observational period (24 June – 23 July) in the southern BoB. Contours of SLA are overlayed. c) Time–longitude hovmoller diagram of SLA along 8°N between 81-100°E from May to July.

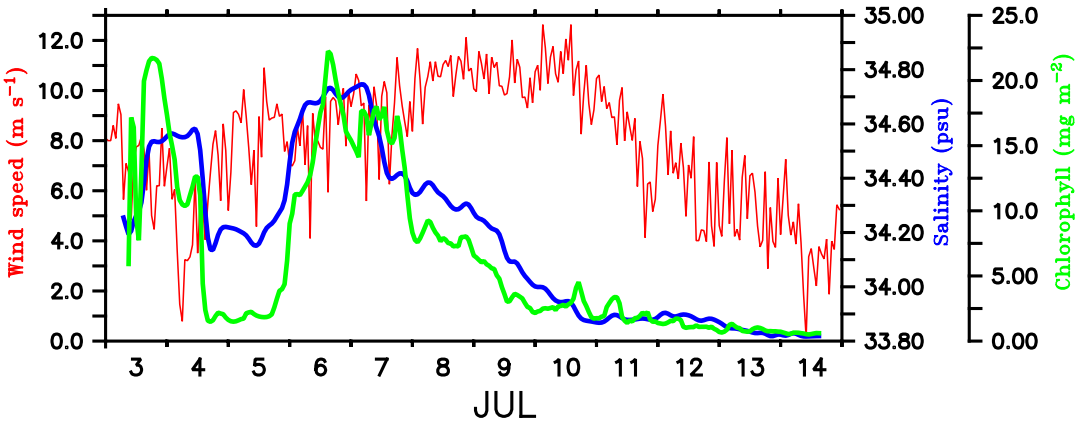

Figure 7. Time series of wind speed (m s^{-1}; red) from shipboard AWS at TSE (89°E, 8°N). Surface salinity (psu; blue) and total chlorophyll integrated over the mixed layer (mg m^{-2}; green) is from SG620 deployed at TSE. MLD is calculated as the depth where density is equal to the sea surface density plus an increase in density equivalent to a reduction in temperature of 0.8 °C.

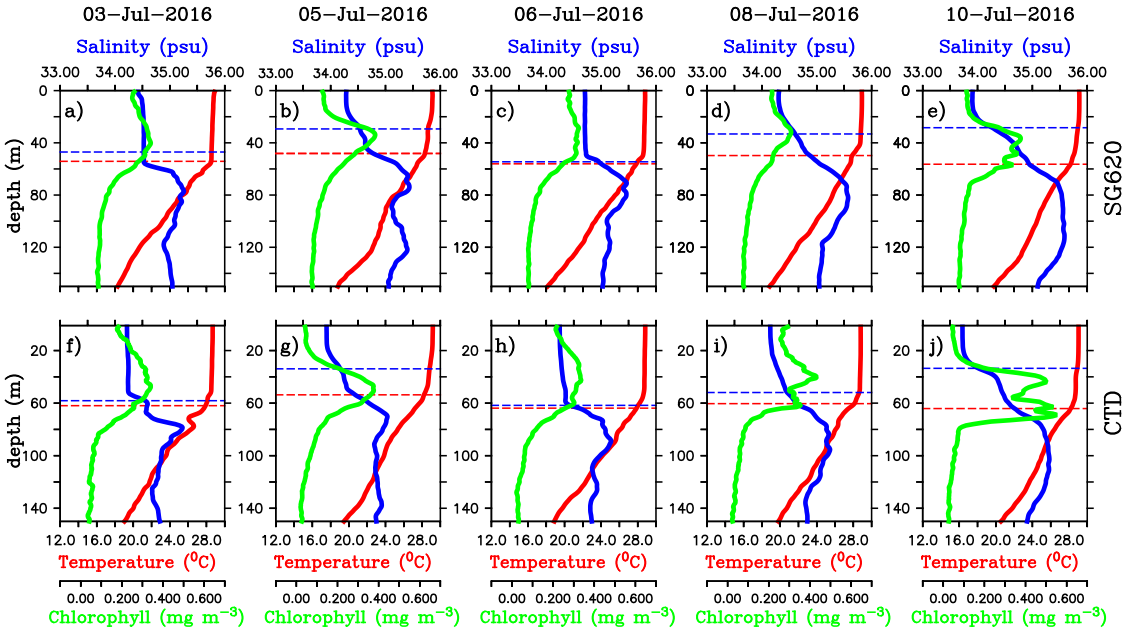

Figure 8. Daily mean vertical profiles of temperature (°C; red), salinity (psu; blue) and chlorophyll (mg m^{-3}; green) ~~during 06 July (left panels), 08 July (middle panels) and 10 July 2016 (right panels)~~ for selected days from ~~SG620 (top panels~~a-e) SG620 and ~~CTD (bottom panels~~f-j) CTD. The blue dashed line indicates the mixed layer depth, which is calculated as the depth where density is equal to the sea surface density plus an increase in density equivalent to a reduction in temperature of 0.8 °C. The red dashed line indicates isothermal layer depth (ILD) which is calculated as the depth where the temperature is cooler than SST by 0.8 °C. The region between the MLD and ILD represents the barrier layer.

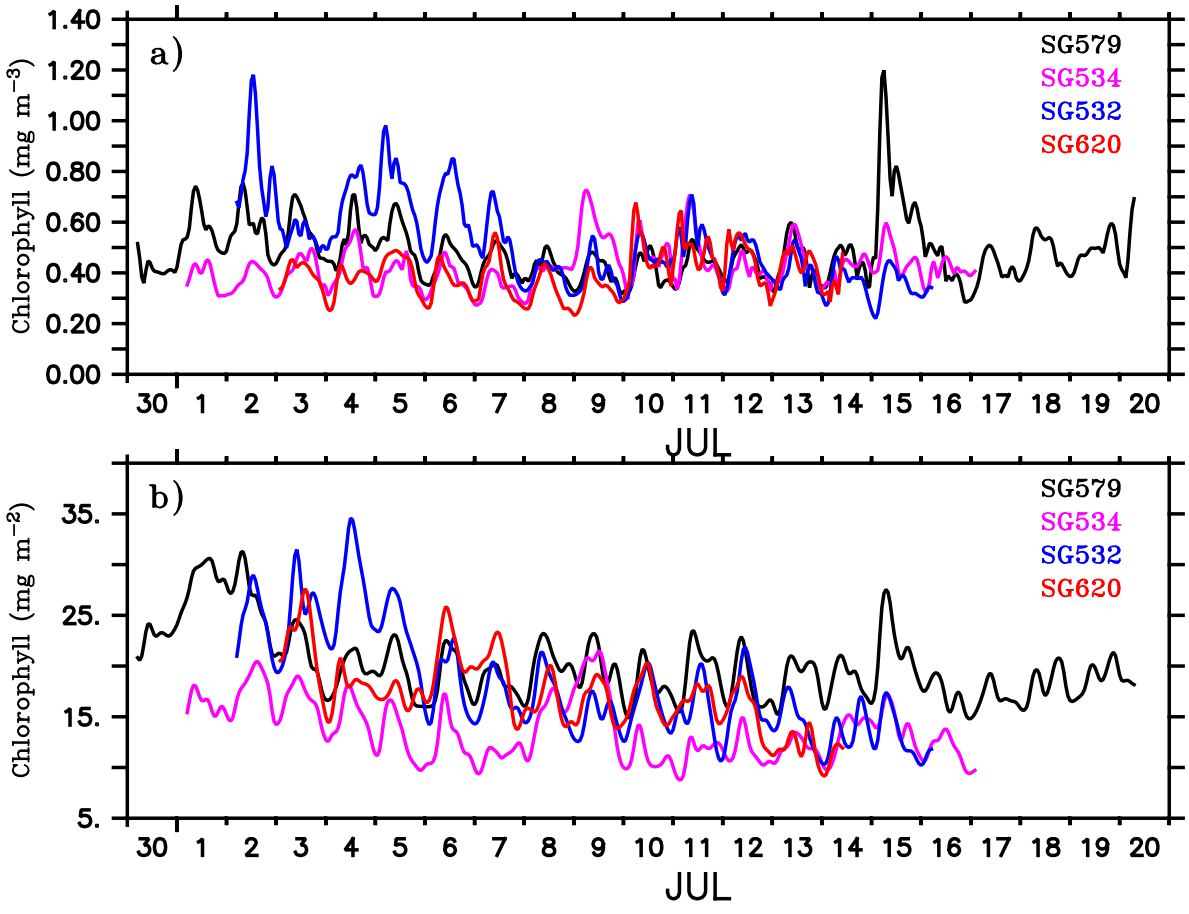

Figure 9. a) Concentration of deep chlorophyll maxima (mg m^{-3}) and b) depth-integrated (100 m) chlorophyll (mg m^{-2}) from ocean gliders; SG579 (black), SG534 (magenta), SG532 (blue) and SG620 (red).

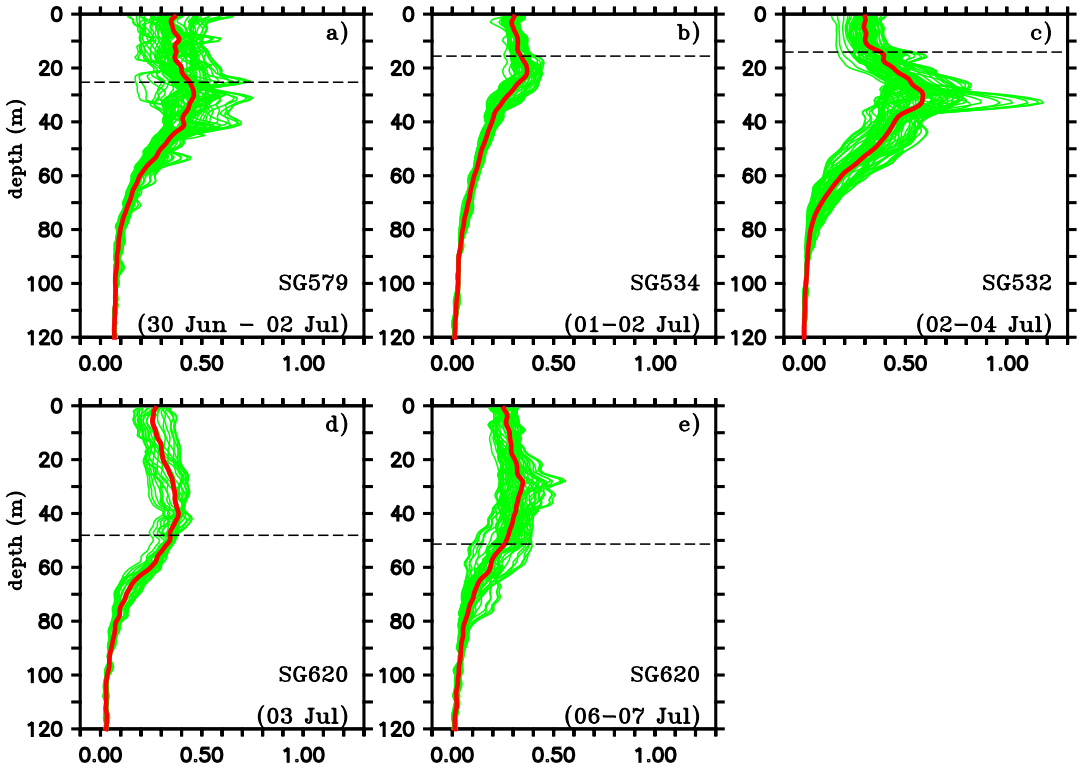

Figure 10. Vertical profiles of chlorophyll (mg m^{-3}) from ocean gliders during surface bloom events as shown in Fig. 5. Individual profiles are given in green and the corresponding mean profiles in red. Black dashed line represents the mixed layer depth, which is calculated as the depth where density is equal to the sea surface density plus an increase in density equivalent to a reduction in temperature of 0.8 °C.

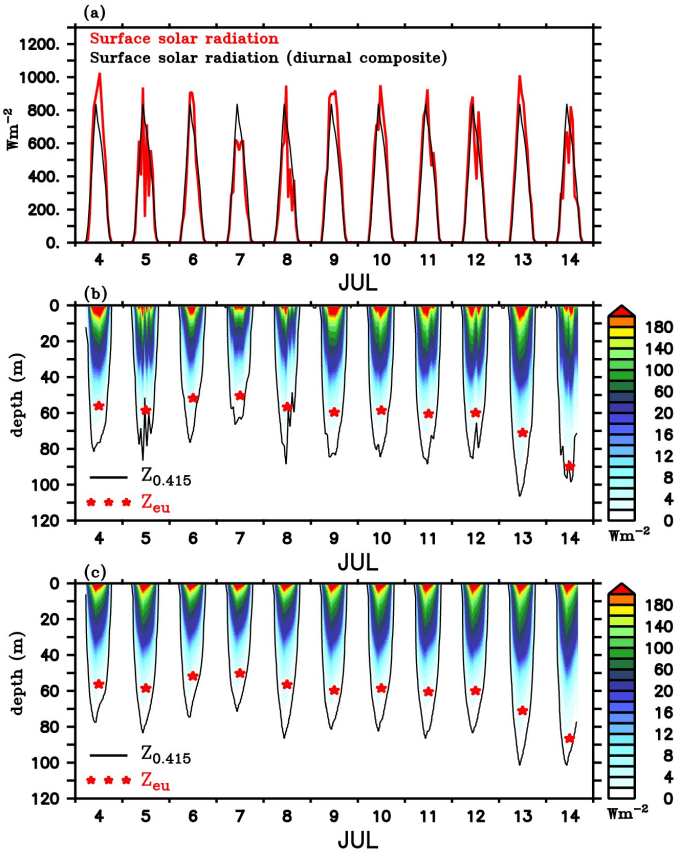

Figure 11. (a) Surface solar radiation measured by the shipboard AWS at TSE from 04–14 July (red) and the corresponding diurnal composite (black) calculated for the same period. Penetrative shortwave radiation (W m^{-2}) calculated following Morel and Antoine (1994) and Manizza et al. (2005) scheme using (b) observed and (c) diurnal composite of radiation. Chlorophyll from SG620 is used for the calculations. Phosynthetically active radiation (PAR; E m^{-2} s^{-1}) was estimated from the calculated penetrative radiation in the visible range following Morel and Smith (1974) . The red ~~curves~~ stars in b) and c) ~~represents the~~ represent daily averaged depth of euphotic zone (Z_{eu}, m) which is taken as the depth ~~of~~ at which light reduces to 1~~W~~ % of the surface PAR value. The black contours in b) and c) represent the depth of threshold isolume ($Z_{0.415}$, m) taken as the depth at which PAR is 0.415 E m^{-2} ~~irradiance~~s^{-1}.

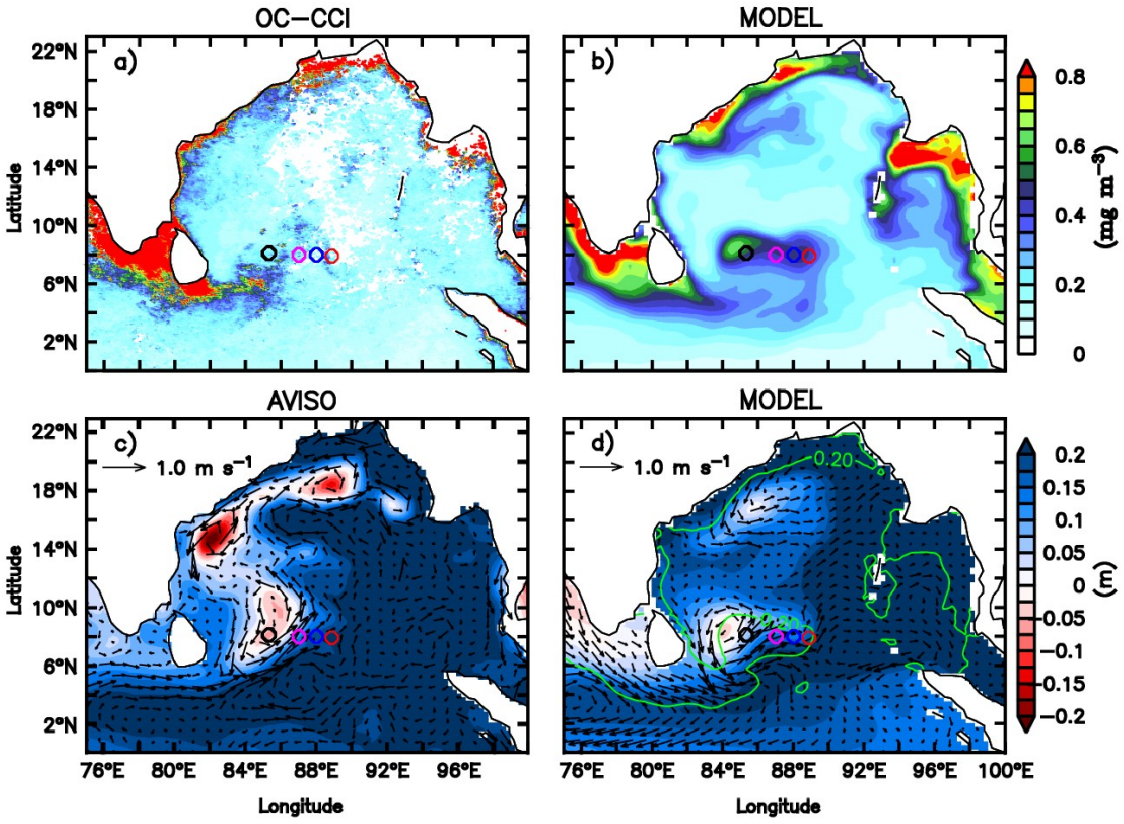

Figure 12. Comparision of the coupled physical-ecosystem model simulation with observations. Monthly mean surface chlorophyll concentrations (mg m^{-3}) for July 2016 from a) ESA OC-CCI merged product and b) model. Monthly mean SLA (m) are overlayed with surface current (m s^{-1}) vectors from c) AVISO and d) model. Green contour in panel d) represents 0.2 mmol kg^{-1} nitrate isolines. The glider locations are marked as circles in the study region along 8°N.

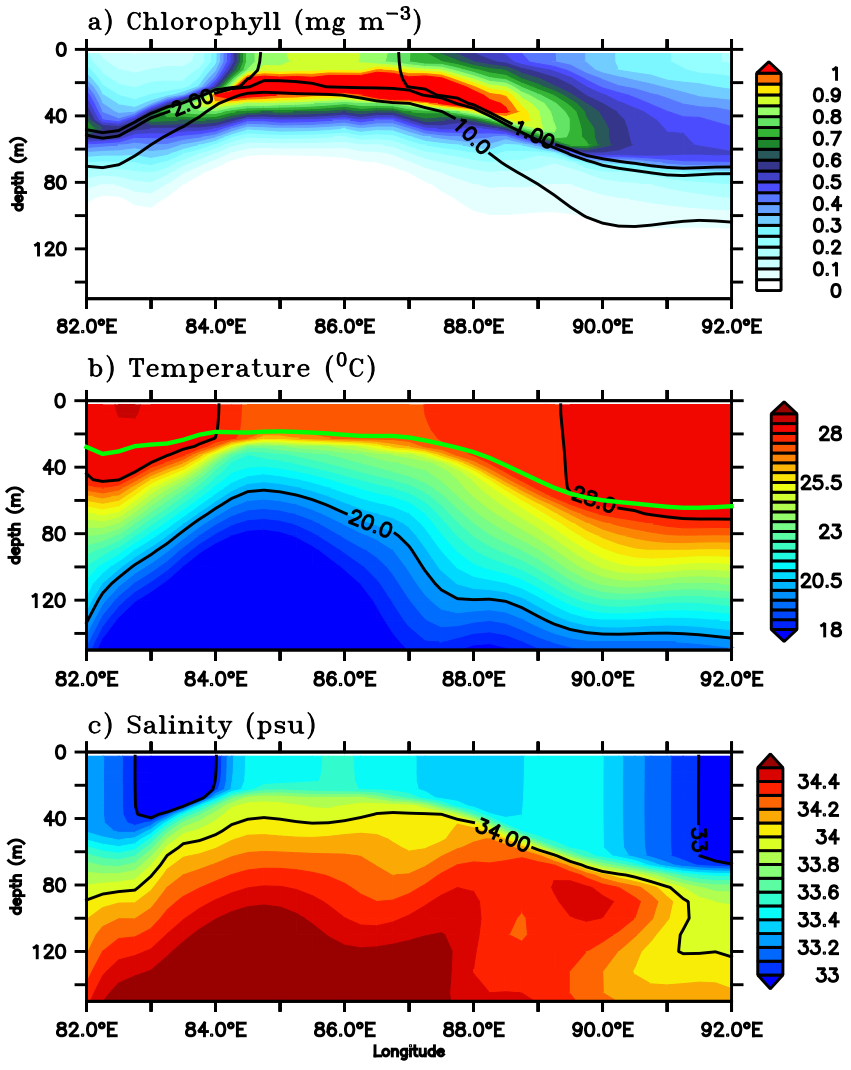

Figure 13. Depth-longitude sections of a) chlorophyll (mg m^{-3}), b) temperature ($^{\circ}$C) and c) salinity (psu) along 8°N for 01 July 2016 from the ecosystem model. Black contours in panels a), b) and c) represent nitrate (1 μmol kg $^{-1}$, 2 μmol kg $^{-1}$ and 10 μmol kg $^{-1}$), temperature (20 $^{\circ}$C and 28 $^{\circ}$C) and salinty (33 psu and 34 psu) respectively. Green curve in panel b) represents the model mixed layer depth.

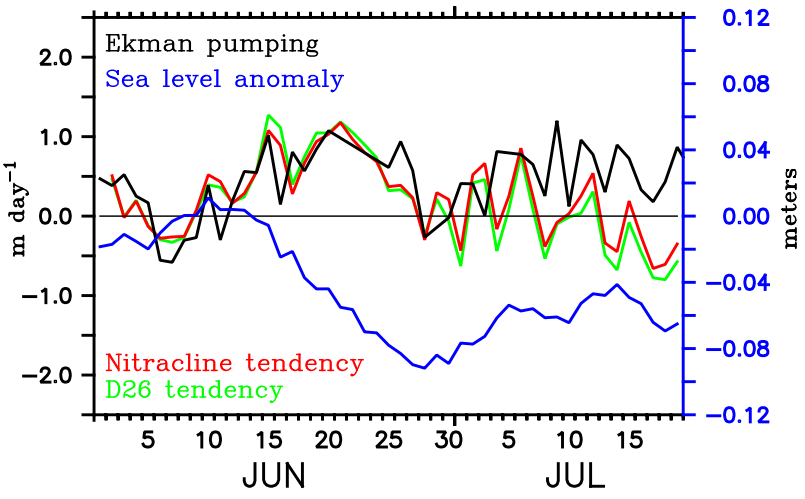

Figure 14. Ekman vertical velocity (m day^{-1}; black) and tendencies of nitracline (m day^{-1}; red) and D26 (m day^{-1}; green) averaged over the region of the modelled Sri Lanka Dome. Note that the tendency terms are reversed in sign so that positive (negative) values indicate shoaling (deepening). D26 is taken as the depth of the 26 °C isotherm. Nitracline is defined as the depth of 2 μmol kg $^{-1}$ nitrate isoline. Minimum sea level anomaly (m; blue) in the region of the SLD is overlayed.

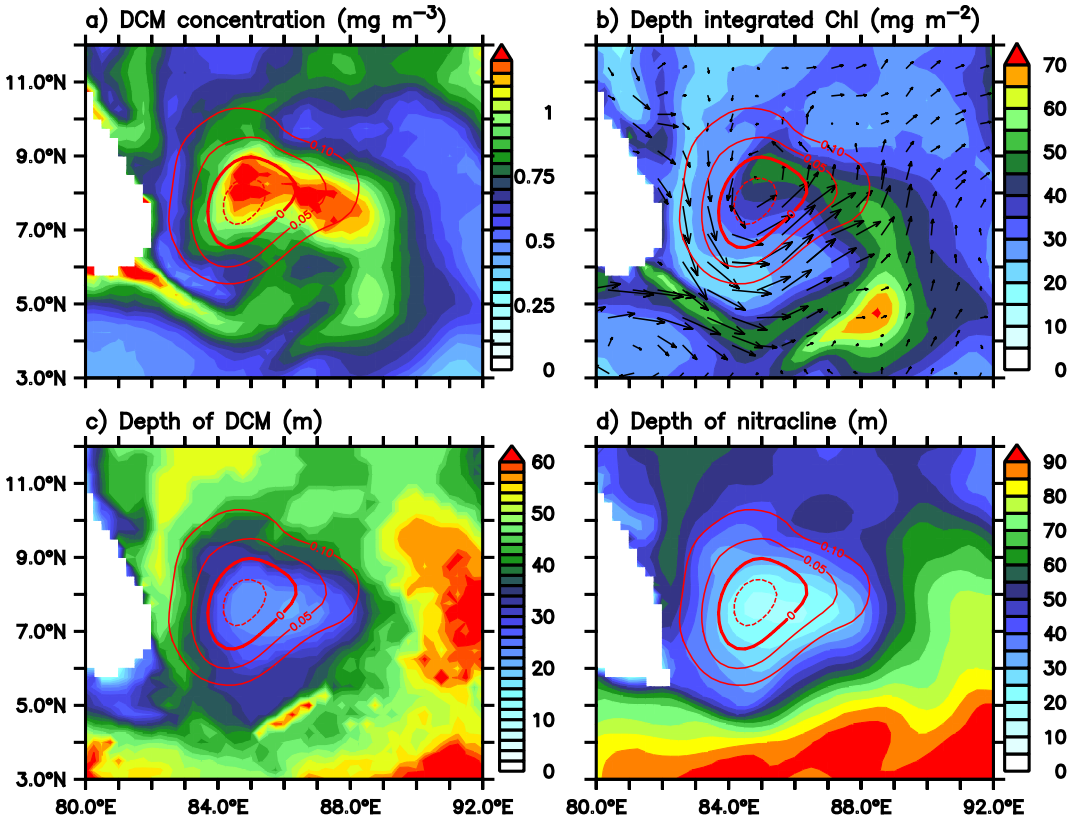

Figure 15. a) Intensity of deep chlorophyll maxima (DCM; mg m^{-3}), b) depth-integrated (100 m) chlorophyll (mg m^{-2}), c) depth of DCM (m), and d) the depth of nitracline (m) for 01 July 2016 from the ecosystem model. Nitracline is defined as the depth of 2 μmol kg^{-1} nitrate isoline. Red contours in all the panels represent SLA (m) in the region of the Sri Lanka dome.

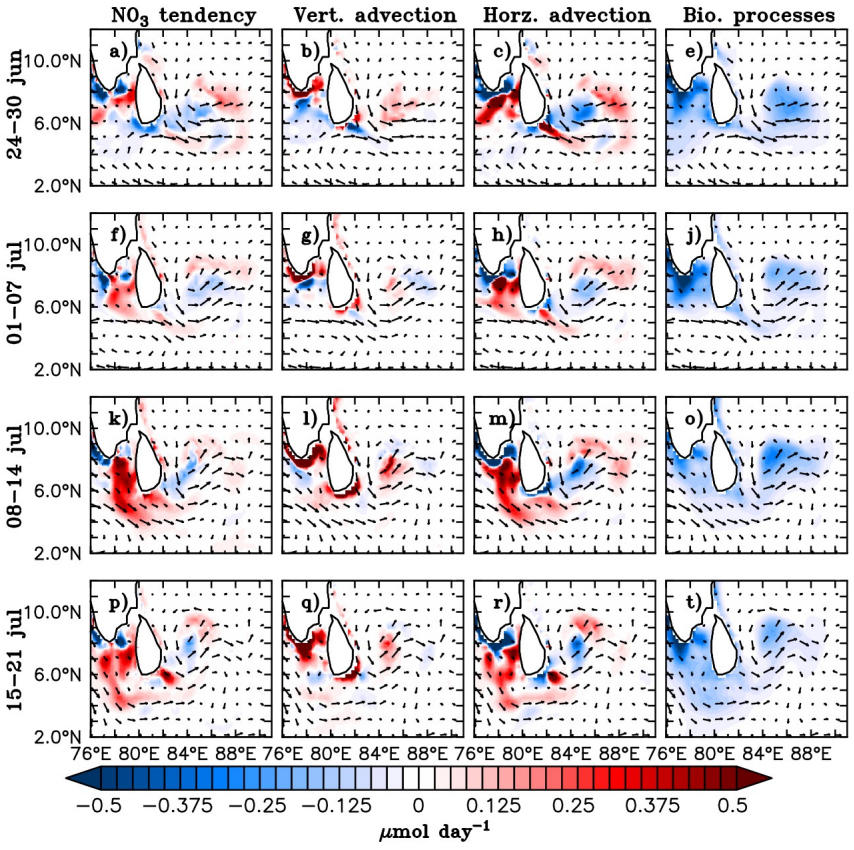

Figure 16. Model nitrate budget averaged over the mixed layer. Nitrate tendency (first column), vertical processes (second column), horizontal advection (third column) and the biological processes (fourth column) in μmol day^{-1} are shown for 7-day averages starting from 24 June to 21 July 2016, marked on the left side of the corresponding panels. Vertical processes include vertical advection and mixing, and biological processes include source (nitrification) and sink (denitrification and uptake by the phytoplankton) terms for the model nitrate. Surface current (m s^{-1}) vectors are overlayed.